UNIVERSIDADE DE BRASÍLIA
INSTITUTO DE GEOCIÊNCIAS

GEOLOGIA E PETROLOGIA DO PROSPECTO GT-34: EVIDÊNCIA DE METASSOMATISMO DE ALTA TEMPERATURA E BAIXA fO_2, PROVÍNCIA MINERAL CARAJÁS, BRASIL.

DISSERTAÇÃO DE MESTRADO

Autor: Lincoln Siepierski

Orientador: Prof. Dr. Cesar Fonseca Ferreira Filho
Co-Orientadora: Dra. Tereza Cristina Junqueira Brod

Brasília
2008

UNIVERSIDADE DE BRASÍLIA
INSTITUTO DE GEOCIÊNCIAS

Geologia e petrologia do Prospecto GT-34: evidências de metassomatismo de alta temperatura e baixa fO_2, Província Mineral de Carajás, Brasil.

Autor: Lincoln Siepierski

Examinadores:

Prof. Dr. Cesar Fonseca Ferreira Filho (Orientador)

Profa. Dra. Lydia Maria Lobato

Prof. Dr. Nilson Francisquini Botelho

Como requisito parcial à obtenção do Grau de Mestre em Ciências na área de Geologia Econômica e Prospecção

Brasília, abril de 2008

AGRADECIMENTOS

Ao professor Dr. Cesar Fonseca Ferreira Filho, pela orientação dedicada, apoio e comprometimento com este projeto de mestrado.

Ao Instituto de Geociências da Universidade de Brasília, pelo suporte na execução de todas as etapas do trabalho.

A Dra. Tereza Cristina Junqueira Brod, co-orientadora, pela orientação, apoio e importantes discussões durante todas as etapas deste projeto.

À VALE-Companhia Vale do Rio Doce, em especial ao Gerente Geral de Exploração Noevaldo Teixeira, pelo inestimável apoio na disponibilização dos dados de exploração mineral e custeio das análises laboratoriais.

Aos meus pais, por me ensinarem a ser perseverante e me mostrarem a importância do conhecimento.

À minha esposa e filhas, pelo estímulo, apoio irrestrito e pela compreenção durante os meus períodos de ausência do convívio.

ÍNDICE

ÍNDICE DE FIGURAS

ÍNDICE DE TABELAS

RESUMO

A área GT-34, localizada na Província Mineral de Carajás, encontra-se situada no domínio gnáissico-migmatítico do Complexo Xingu (Silva et al.,1974). Caracteriza-se por apresentar zonas ricas em sulfetos hospedadas em corpos irregulares constituídos por rochas brechadas e/ou litologias ricas em ortopiroxênio-anfibólio, que afloram entre rochas gnáissicas. As rochas brechadas são constituídas por abundantes fragmentos heterogêneos resultantes da alteração do gnaisse encaixante. Os corpos enriquecidos em sulfetos ocorrem ao longo de uma faixa com direção geral NE-SW de aproximadamente 1,5 km de comprimento, atingindo localmente 500 m de profundidade. Essas zonas ricas em sulfetos ocorrem intimamente associadas a rochas costituídas dominantemente de ortopiroxênio (ortopiroxenititos) e anfibólio, consideradas como formadas por metassomatismo.

As intersecções ricas em sulfetos variam de centimétricas a decamétricas. Ortopiroxenititos brechados com injeções de veios ricos em sulfetos são observados em vários pontos do GT-34. Nestas zonas observam-se brechação e substituição parcial do ortopiroxenitito por uma associação contendo sulfetos com proporções variadas de apatita, escapolita e hornblenda. Zonas enriquecidas em sulfetos ocorrem como vênulas discretas, como sistema de veios tipo "*stock-work*", ou como zonas brechadas, semi-maciças, contendo fragmentos de ortopiroxenitito parcialmente alterado. Apatita ocorre invariavelmente associada e pode alcançar até 25% em volume nas amostras com sulfetos semi-maciços e veios enriquecidos. A abundância de apatita nestas zonas enriquecidas em sulfetos resulta em alto conteúdo em P, alcançando até 7,9 % em peso e com vários resultados analíticos entre 1 e 5% em peso, evidenciando uma correlação geoquímica positiva entre P e S. As zonas sulfetadas são enriquecidas em Fe o que reflete a paragênese dos sulfetos dominada por pirrotita, com pirita, calcopirita e pentlandita associadas; contudo, as rochas metassomatizadas vizinhas a essas zonas sulfetadas não são enriquecidas em Fe. Os ortopiroxenititos são caracterizados pelo alto conteúdo de Mg (>3 % em peso) e estão associados às zonas sulfetadas porém, nem sempre, representam as rochas hospedeiras desses corpos.

A composição dos cristais de ortopiroxênio de diversas áreas do GT-34 é similar. O conteúdo de En nessas amostras varia de 68,0 a 77,5% e não mostra correlação significativa com o conteúdo de TiO_2, Cr_2O_3, CaO e Al_2O_3. Quando comparados a cristais de ortopiroxênio com conteúdo similar de En provenientes de intrusões acamadadas máficas-ultramáficas, os cristais de ortopiroxênio do GT-34 exibem invariavelmente baixo conteúdo de TiO_2, Cr_2O_3, CaO e Al_2O_3. Igualmente, os ortopiroxenititos possuem conteúdo extremamente baixo de Cr_2O_3 (< 0.01 % em peso; ou 22 a 71 ppm Cr) e TiO_2 (0.03 a 0.14 % em peso), confirmando o mesmo aspecto

composicional distinto quando comparado com ortopiroxenitos de origem magmática. Essas características sustentam a interpretação que os cristais de piroxênios, e por associação, os ortopiroxenititos do GT-34 foram originados por processos metassomáticos.

A evolução composicional dos ortopiroxenititos com ou sem sulfetos, e das rochas ricas em sulfetos sugere que a formação das zonas sulfetadas resulta da substituição moderada a extensiva das rochas ricas em ortopiroxênio. O conteúdo de ETR encontrado nas rochas ricas em sulfetos é diretamente correlacionável a abundância de apatita. Esta correlação é também observada no gráfico Ce x P_2O_5 que indica a substituição progressiva do ortopiroxenitito pelos termos mais ricos em apatita-sulfeto.

A interpretação dos dados disponíveis do GT-34, portanto, sugere que as rochas ricas a ortopiroxênio representem metassomatitos de alta temperatura desenvolvidos sobre rochas gnáissicas (Fase 1), seguido por evento posterior caracterizado por brechação, percolação de fluídos e deposição de sulfetos (Fase 2). As condições geológicas apropriadas para desenvolver um sistema metassomático equivalente ao observado no GT-34 (P>0,5 Kb), sugerem temperaturas superiores a 700°C, compatíveis com a cristalização de ortopiroxênio. A Fase 2 no sistema GT-34 consiste no desenvolvimento de brechação e venulação nos ortopiroxenititos e gnaisses, com cristalização de sulfeto e apatita. Este processo promoveu a concentração de diversos elementos (ex.: P, F, S, ETR, Fe, Cu, Co, Ni, etc). A associação espacial entre essas litologias sugere uma relação genética entre o processo de alteração inicial (Fase 1) e a sulfetação tardia (Fase 2). Apesar disso, observa-se que o enriquecimento e empobrecimento relativos de diversos elementos são distintos nas duas fases, indicando que os fluidos associados ao metassomatismo e/ou as condições físicas atuantes durante o processo de alteração foram significativamente diferentes. As zonas ricas em sulfetos possuem abundantes sulfetos portadores de ferro (pirrotita-pirita-calcopirita-pentlandita) e são desprovidas de óxidos de ferro (magnetita ou hematita). A cristalização de pirrotita e pirita na ausência de óxidos de Fe indica condições de alta fugacidade de enxofre (fS_2) e baixa fugacidade de oxigênio (fO_2). A temperatura de cristalização para as fases ricas em sulfetos pode ser inferida pela presença de hornblenda associada, sugerindo temperaturas superiores a 500°C, na ausência de ortopiroxênio (T < 700°C).

As características presentes no GT-34, quando comparadas com os depósitos de Cu-Au em Carajás, sugerem que o metassomatismo ocorreu em condições de alta temperatura e baixa fO_2. Esses aspectos permitem indicar que o metassomatismo e sulfetação desenvolvidos no GT-34 ocorreram em nível crustal relativamente mais profundo, representando possivelmente zonas hipogênicas do sistema IOCG regional, com idade 2.5 Ga, da Província Mineral de Carajás.

ABSTRACT

The GT-34 Prospect in the Carajás Mineral Province is located within older gneiss-migmatite terrains (Xingu Complex). Sulfide mineralization is hosted by irregular bodies of brecciated rocks and/or orthopyroxene-amphibole bearing rocks outcropping among gneissic rocks. Distribution of sulfide-rich intervals form an irregular NE trend of about 1.5 km-long and up to 500 meters deep. Breccias include highly heterogeneous fragmental rocks resulting from alteration of gneisses. Sulfide-rich zones are closely associated with rocks consisting mainly of orthopyroxene (orthopyroxenitite) and amphibole, considered to form by metasomatism.

Sulfide-rich intersections may be up to dozens of meters-thick or restricted to few centimeters-thick veins. Brecciation of orthopyroxenitites by sulfide-bearing veins is observed throughout the GT-34 Prospect. In these zones orthopyroxene is brecciated and partially replaced by an assemblage of sulfides associated with variable proportions of apatite, scapolite and hornblende. Enrichment in sulfides occurs in discrete veins, in veining systems developing net textured rocks or in semi-massive brecciated zones where partially altered fragments of orthopyroxenitites frequently occur. Apatite is ubiquitous and abundant (up to 25 vol. %) in brecciated semi-massive sulfides or sulfide-rich veins. Sulfide minerals consist mainly of pyrrhotite with associated pyrite, chalcopyrite and pentlandite. The abundance of apatite in the sulfide-rich samples results in their high P contents (up to 7.9 wt. % and several values between 1-5 wt. %) and good correlation with S values. Sulfide-rich zones are enriched in Fe, reflecting the abundance of Fe-bearing sulfides but metasomatic rocks closely associated with the sulfide-rich zones are not Fe-enriched. Higher Mg contents (> 3 wt. % Mg) characterizes the orthopyroxene-rich rocks (orthopyroxenitites). These rocks are closely associated with sulfide-rich zones but not neccessarily their host rocks.

Compositions of orthopyroxene crystals from orthopyroxenitites collected in different portions of the GT-34 Prospect are very similar. En contents for orthopyroxene from the GT-34 vary from 68.0 to 77.5 %. Variation in En content shows no correlation with contents of TiO_2, Cr_2O_3, CaO and Al_2O_3. When compared to orthopyroxene with similar En content of orthopyroxenites from mafic-ultramafic layered intrusions, orthopyroxene crystals from the GT-34 Prospect show lower contents for TiO_2, Cr_2O_3, CaO and Al_2O_3. Orthopyroxenitites have extremely low Cr_2O_3 (< 0.01 wt. %; or 22 to 71 ppm Cr) and TiO_2 (0.03 to 0.14 wt. %) contents, also indicating distinctive compositional features when compared to orthopyroxenites of magmatic origin. These compositional features support the interpretation that orthopyroxene crystals (and orthopyroxenitites) in the GT-34 Prospect are not magmatic, being originated by metasomatic processes.

Sulfide-rich rocks (S > 10 wt. %) have high total Fe_2O_3 (27.10 to 44.71 wt. %) and P_2O_5 (4.20 to 20.92 wt. %) contents, reflecting their abundance in Fe-sulfides (pyrrhotite, pyrite, chalcopyrite and pentlandite) and apatite. Compositional trends for orthopyroxenitites, sulfide-bearing orthopyroxenitites and sulfide-rich rocks suggest that sulfide-bearing rocks result from mild to extensive replacement of orthopyroxene-bearing rocks. REE contents in sulfide-bearing rocks are correlated with the abundance of apatite. This correlation is illustrated by the plot of Ce versus P_2O_5 contents for orthopyroxenitites, sulfide-bearing orthopyroxenitites and sulfide-rich rocks, indicating the progressive replacement of orthopyroxenitites by apatite-sulfide rich zones.

Interpretation of available data of the GT-34 Prospect suggests that high-temperature orthopyroxene-bearing metasomatic replacement bodies (Phase 1) developed within gneissic country rocks, followed by a late event of veining, brecciation and sulfide mineralization (Phase 2). Geological conditions appropriated to sustain the extensive high-temperature metasomatic system described in the GT-34 prospect (P > 0.5 Kb), suggest temperatures over 700°C for the crystallization of orthopyroxene. The second Phase in the GT-34 system consists of brecciation and veining of orthopyroxenitites and host gneisses, together with sulfide-apatite mineralization. This process involved the crystallization of significant amount of sulfides and apatite, thus promoting the concentration of a diverse range of elements (e.g. P, F, S, REE, Fe, Cu, Ni). The close spatial association suggests a genetic link between early alterarion (Phase 1) and later sulfidization (Phase 2). However, relative enrichment and depletion of elements are distinctively different in these two events indicating that fluids associated with metasomatism, and/or physical conditions prevailing during alteration, were highly different during these events. Sulfide-rich zones have abundant Fe-bearing sulfides (pyrrhotite, pyrite, chalcopyrite, pentlandite) and no associated oxides. Crystallization of pyrrhotite and pyrite without Fe-oxides (magnetite or hematite) indicates conditions of high sulfur fugacity (fS_2) and low oxygen fugacity (fO_2). The temperature of crystallization of sulfide-rich zones is constrained by associated hornblende, suggesting temperatures above 500°C, and the lack of orthopyroxene (e.g. T < 700°C).

Characteristics of the GT-34 Prospect suggest that metasomatism occurred under higher temperature and lower fO_2 conditions, compared to Cu-Au deposits in Carajás. These features possibly indicate that metasomatism and sulfidization of the GT-34 Prospect represent deep zones (e.g. deeper crustal level) of the regional 2.5 Ga Cu-Au ore-forming system of Carajás.

CONSIDERAÇÕES GERAIS

Introdução

A Provincia Mineral de Carajás é conhecida por hospedar diversos depósitos de classe mundial, sendo considerada como uma das mais importantes do mundo. Este aspecto tem motivado diversos estudos acadêmicos sobre as características e origens destes depósitos.

A presente dissertação de mestrado integra parte deste conhecimento e apresenta os resultados dos estudos sobre a área denominada GT-34, realizada sob a orientação dos Professores Cesar Fonseca Ferreira Filho (orientador) e Tereza Cristina Junqueira Brod (co-orientadora), e vinculada ao Programa de Pós-Graduação do Departamento de Geociências da Universidade de Brasília.

A área estudada faz parte da Província Mineral de Carajás, localizada no Estado do Pará. O Prospecto GT-34 foi descoberto no final dos anos 90 pela equipe de exploração da DOCEGEO (hoje VALE), representando uma ocorrência de sulfetos com características distintas dos depósitos de Cu-Au de Carajás. A sulfetação do GT-34 ocorre associada a rochas com ortopiroxênio e anfibólio abundantes, associadas a gnaisses do Complexo Xingu. Interpretações divergentes têm sido aventadas para explicar a origem das rochas encaixantes e da sulfetação do GT-34. Estas interpretações, reportadas como resultado dos trabalhos de exploração da VALE, incluem desde propostas de uma origem ortomagmática para o sistema (sulfetos segregados como líquidos imiscíveis à partir de um magma máfico-ultramáfico), passando por sugestões de que existiria superposição de processos hidrotermais em uma associação magmática de natureza máfica-ultramáfica, até propostas de uma origem epigenética para explicar tanto a gênese dos sulfetos como a de suas encaixantes. As controvérsias existentes no entendimento desta ocorrência e do seu enquadramento no contexto metalogenético da Província Mineral de Carajás motivaram o desenvolvimento deste estudo.

O escopo deste trabalho não envolve nenhum aspecto econômico do Prospecto GT-34. Esta restrição foi uma exigência da Gerência de Exploração da VALE para permitir o desenvolvimento dos estudos no GT-34 tendo sido acertado durante a definição do enfoque da dissertação de mestrado. Em vista disso o estudo não contempla resultados com implicação econômica (tonelagem, teores de metais, etc). Os resultados analíticos das rochas sulfetadas não incluem resultados para metais de valor econômico neste tipo de associação (Cu, Au, Ag, Ni, EGP, etc), não são reportadas análises químicas dos sulfetos, e as descrições petrográficas do sulfeto não contemplam composições modais quantitativas.

Localização e Fisiografia

O Prospecto GT-34 faz parte da Província Mineral de Carajás e está situado dentro dos limites do Município de Canaã dos Carajás, na porção sudeste do Estado do Pará. Está localizado a aproximadamente 35 km a oeste da sede do Município, nas seguintes coordenadas geográficas: 06°29'39"Sul-50°08'50"WGr. Canaã dos Carajás encontra-se a cerca de 720 km, por vias rodoviárias pavimentadas, da cidade de Belém (Figura 1A). O acesso pode ser feito fazendo-se uso das estradas BR-010 e BR-222, passando-se por Marabá, e pela PA-150 até Eldorado dos Carajás; a partir dessa localidade utiliza-se a rodovia PA-275 até a cidade de Parauapebas, e desse ponto até a cidade Canaã dos Carajás o acesso é feito pela rodovia PA-160. A partir de Canaã dos Carajás, o acesso é feito utilizando-se a estrada vicinal não pavimentada VS-52 para oeste, até o a área do GT-34. Localmente o acesso é feito por meio de estradas de terra em boas condições e trafegáveis o ano todo.

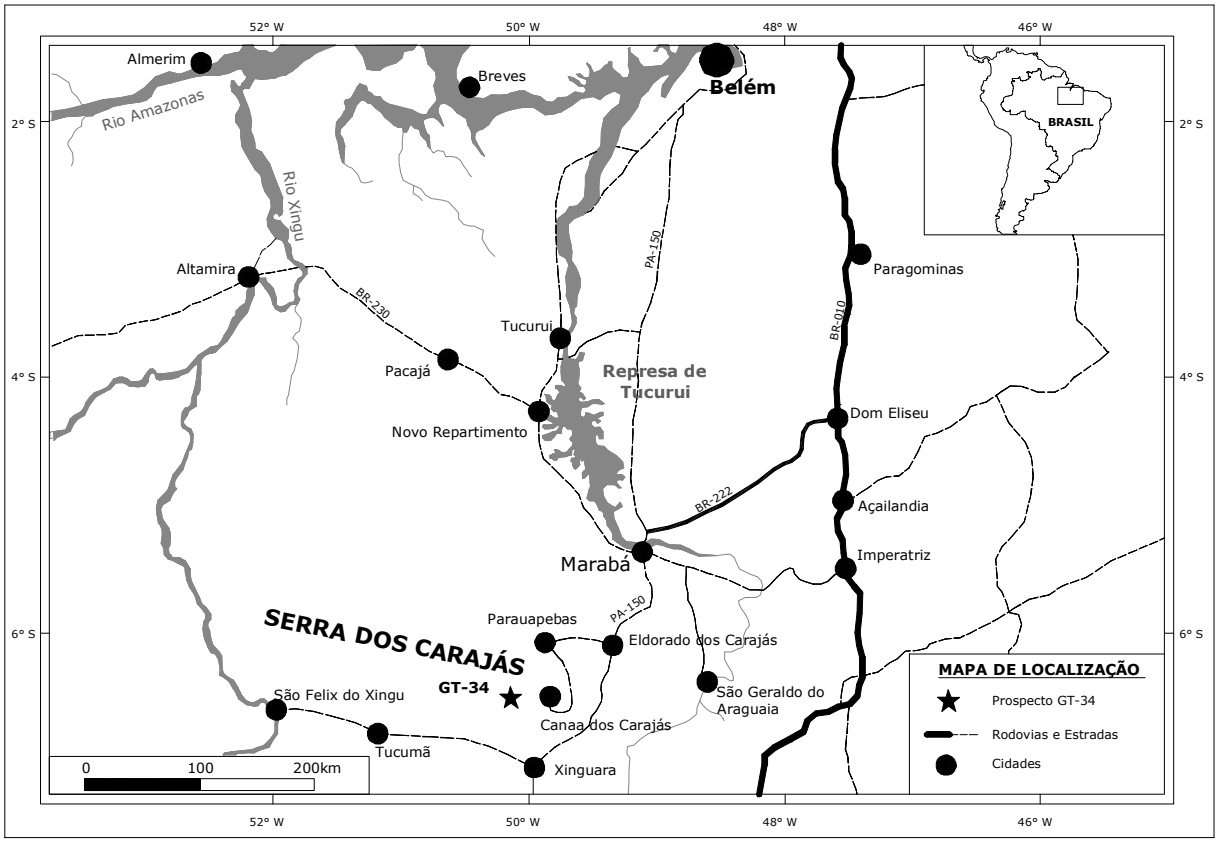

Figura 1A. Mapa de localização e acesso.

A região da Província Mineral de Carajás é dominada pela presença de duas principais unidades morfoestruturais, a saber: **(1)** o Planalto Dissecado do Sul do Pará é representado por maciços residuais de topo aplainado e conjuntos de cristas alinhadas e picos interpenetrados por terrenos rebaixados, com altitudes superiores a 500 m onde a principal feição da região é a Serra

dos Carajás com cristas sustentadas pelas formações ferríferas do Grupo Grão-Pará, onde foram verificadas cotas da ordem de 700 m (Beisiegel *et al.*, 1973), e que contrastam com os vales encaixados a exemplo do rio Itacaiúnas onde a cota é de 146 m. **(2)** a Depressão Periférica do Sul do Pará é caracterizada por vastas áreas arrasadas pelos processos erosivos pós-pliocênicos que circundam as duas porções residuais do Planalto Dissecado do Sul do Pará.

A área estudada é drenada por afluentes da margem esquerda do rio Parauapebas pertencente a sub-bacia do rio Itacaiúnas, principal afluente do rio Tocantins.

O clima da região enquadra-se como tropical com temperatura média anual variando entre 22,6^{o}C e 26,5^{o}C, sendo que nos meses de setembro a dezembro se eleva entre 26^{o}C a 28^{o}C, atingindo máximas absolutas de até 40^{o}C. Apresenta intensidade pluviométrica com médias anuais de 1.968 mm.

A vegetação original da área estudada foi, em grande parte, retirada, dando lugar a pastagens. Eventualmente ocorrem restos de mata secundária e a mata primária, quando preservada, é classificada como Floresta Tropical Densa em transição para Cerrados.

Histórico da Pesquisa DOCEGEO-CVRD

O alvo GT-34 foi descoberto a partir de anomalias eletromagnéticas definidas por levantamento aerogeofísico realizado durante os anos 90 com objetivo à prospecção de mineralizações de cobre e ouro. Os primeiros trabalhos de reconhecimento exploratório da anomalia aerogeofísica foram executados pela DOCEGEO (empresa de pesquisa do Grupo CVRD) nos anos de 1999-2000 e envolveram amostragem geoquímica, mapeamento geológico, levantamento geofísico terrestre (métodos eletromagnético e polarização induzida) e 8 furos de sondagem exploratória. Os resultados foram pouco animadores para mineralizações a cobre e ouro. Nessa época não foram encontradas evidências da continuidade lateral da mineralização e a integração das informações de sondagem e geologia de superfície indicavam ocorrências pouco extensas, o que fez com que os trabalhos de pesquisa fossem paralisados.

A partir do final de 2003 a CVRD retomou os trabalhos na área do GT-34. Nesta etapa os trabalhos consistiram em novo mapeamento geológico, amostragem de solo em área mais ampla, levantamentos geofísicos terrestres, com o objetivo do entendimento do comportamento da mineralização. As informações geológicas, geofísicas e geoquímicas foram progressivamente integradas, permitindo um melhor entendimento do alvo e de suas particularidades geológicas.

Justificativa e Objetivos

A evolução do conhecimento da Província Mineral dos Carajás vem acumulando, desde os anos 70, um saldo significativo de descobertas de diversas *commodities*, em especial Fe-Mn-Cu-Au-Ni. A zona sulfetada do GT-34, em função da sua associação com rochas que apresentam ortopiroxênio abundante, levantou questões importantes quanto a sua natureza e correlação com depósitos ortomagmáticos ou hidrotermais. Neste trabalho são apresentados os resultados de estudos desenvolvidos na área do GT-34 enfocando os seguintes aspectos:

- Apresentação do contexto geológico regional;
- Estudo da geologia e petrologia das rochas do GT-34, com uso de petrografia sistemática e análise química de mineral e rocha (testemunhos de sondagem);
- Discussão enfocando a origem das zonas sulfetadas e suas encaixantes.

Método

Para atingir estes objetivos foi efetuada revisão bibliográfica, inclusive de relatórios internos da CVRD. Na qualidade de geólogo-coordenador do Programa Níquel Carajás da CVRD, o autor participou dos trabalhos de prospecção desenvolvidos no Prospecto GT-34, incluindo mapeamento geológico, descrição sistemática dos testemunhos de sondagem e interpretação dos resultados. Para atender aos objetivos específicos da dissertação procedeu-se a descrição e amostragem para estudos petrográficos e químicos dos testemunhos de sondagem de sete furos selecionados.

Foram efetuados estudos petrográficos em 38 amostras selecionadas, o que permitiu o reconhecimento dos diversos litotipos que compõem o corpo do GT-34 e encaixante, assim como a seleção das amostras a serem analisadas por microssonda eletrônica.

As análises químicas de mineral via microssonda eletrônica foram realizadas no Laboratório de Microssonda Eletrônica da Universidade de Brasília, em equipamento Cameca SX-50. O tratamento dos dados foi feito por meio de planilha eletrônica Excel e os resultados analíticos encontram-se em ANEXO (Tabelas 1A a 4A).

Foram efetuadas análises litoquímicas em 33 amostras no laboratório ALS Chemex (Canadá). As análises para elementos maiores em rocha total (método: ME-XRF06), ICP-MS 47 elementos com abertura à 4 ácidos (método: ME-MS61) e Terras Raras (método: ME-MS82), os resultados analíticos encontram-se expressos na Tabela 3.

Escopo do Estudo

Conforme previsto no regulamento do Curso de Pós-graduação em Geologia da Universidade de Brasília e por sugestão do Orientador, esta dissertação de mestrado apresenta-se estruturada na forma de artigo intitulado "***Geology and petrology of the GT-34 Prospect: evidence for high-temperature and low fO_2 metasomatism in the Carajás Cu-Au belt, northern Brazil.***" à ser submetido para publicação em periódico com corpo editorial. O artigo é apresentado na forma que será submetido à revista *Economic Geology*, mantendo o estilo e o formato previstos no periódico.

Referências

Beisiegel, V.R., Bernardelli, A.L., Drummond, N.F., Ruff, A.W., e Tremaine, A. W., 1973, Geologia e Recursos Minerais da Serra dos Carajás: Revista Brasileira de Geociências, v. 3, p. 215-242.

Ferreira Filho, C.F., Cançado, F., Correa, C., Macambira, E.M.B., Siepierski, L., e Brod, T.C.J., 2007, Mineralizações estratiformes de EGP-Ni associadas a complexos acamadados em Carajás: os exemplos de Luanga e Serra da Onça: *in* Contribuições à Geologia da Amazônia, Sociedade Brasileira de Geologia - Núcleo Norte, v. 5, p. 01-14.

Lobato, L.M., Figueiredo e Silva, R.C., Rosière, C.A., Zucchetti, M., Baars, F.J., Seoane, J.C.S., Rios, F.J. e Monteiro, A.M., 2005, Hydrothermal origin for the iron mineralisation, Carajás province, Pará State, Brazil: *in* Proceedings Iron Ore 2005, The Australian Institute of Mining and Metallurgy, Publication Series No 8, p. 99-110.

Silva, G.G., Lima, M.I.C., Andrade, A.R.F., Issler, R.S., e Guimarães, G., 1974, Geologia das Folhas SB-22 Araguaia e parte da SC-22 Tocantins: *in* Levantamentos de Recursos Minerais, Projeto RADAM (Departamento Nacionalda Produção Mineral-DNPM e Companhia de Pesquisa e Recursos Minerais-CPRM), v.4, 455p.

GEOLOGY AND PETROLOGY OF THE GT-34 PROSPECT: EVIDENCE FOR HIGH-TEMPERATURE AND LOW O_2 METASOMATISM IN THE CARAJÁS Cu-Au BELT, NORTHERN BRAZIL.

LINCOLN SIEPIERSKI, CESAR FONSECA FERREIRA FILHO, TERESA JUNQUEIRA BROD.

A SER SUBMETIDO AO PERIÓDICO *ECONOMIC GEOLOGY*

Geology and petrology of the GT-34 Prospect: evidence for high-temperature and low fO_2 metasomatism in the Carajás Cu-Au belt, northern Brazil.

Lincoln Siepierski, Cesar Fonseca Ferreira Filho*, Tereza Cristina Junqueira Brod

Instituto de Geociências, Universidade de Brasília, Brasília, DF. 70910-900. Brazil.

* Corresponding author. Fax +55 61 3347 4062.

E-mail address: lincoln.siepierski@cvrd.com.br (L. Siepierski).

cesarf@unb.br (C.F. Ferreira Filho).

tcjbrod@unb.br (T.C.J. Brod)

Abstract

The GT-34 Prospect in the Carajás Mineral Province is located within older gneiss-migmatite terrains (Xingu Complex). Sulfide-rich zones are hosted by irregular bodies of brecciated rocks and/or orthopyroxene-amphibole bearing rocks outcropping among gneissic rocks. Distribution of sulfide-rich intervals form an irregular NE trend of about 1.5 km-long and up to 500 meters deep. Breccias include highly heterogeneous fragmental rocks resulting from alteration of gneisses. Sulfide-rich zones are closely associated with rocks consisting mainly of orthopyroxene (orthopyroxenitite) and amphibole, considered to form by metasomatism.

Sulfide-rich intersections may be up to dozens of meters-thick or restricted to few centimeters-thick veins. Brecciation of orthopyroxenitites by sulfide-bearing veins is observed throughout the GT-34 Prospect. In these zones orthopyroxene is brecciated and partially replaced by an assemblage of sulfides associated with variable proportions of apatite, scapolite and hornblende. Enrichment in sulfides occurs in discrete veins, in veining systems developing net textured rocks or in semi-massive brecciated zones where partially altered fragments of orthopyroxenitites frequently occur. Apatite is ubiquitous and abundant (up to 25 vol. %) in brecciated semi-massive sulfides or sulfide-rich veins. Sulfide minerals consist mainly of pyrrhotite with associated pyrite, chalcopyrite and pentlandite. The abundance of apatite in the sulfide-rich samples results in their high P contents (up to 7.9 wt. % and several values between 1-5 wt. %) and good correlation with S values. Sulfide-rich zones are enriched in Fe, reflecting the abundance of Fe-bearing sulfides but metasomatic rocks closely associated with the sulfide-rich zones are not Fe-enriched. Higher Mg contents (> 3 wt. % Mg) characterize the orthopyroxene-rich rocks (orthopyroxenitites). These rocks are closely associated with sulfide-rich zones but not neccessarily their host rocks.

Compositions of orthopyroxene crystals from orthopyroxenitites collected in different portions of the GT-34 Prospect are very similar. En contents for orthopyroxene from the GT-34 vary from 68.0 to 77.5 %. Variation in En content shows no correlation with contents of TiO_2, Cr_2O_3, CaO and Al_2O_3. When compared to orthopyroxene with similar En content of orthopyroxenites from mafic-ultramafic layered intrusions, orthopyroxene crystals from the GT-34 Prospect show lower contents for TiO_2, Cr_2O_3, CaO and Al_2O_3. Orthopyroxenitites have extremely low Cr_2O_3 (< 0.01 wt. %; or 22 to 71 ppm Cr) and TiO_2 (0.03 to 0.14 wt. %) contents, also indicating distinctive compositional features when compared to orthopyroxenites of magmatic origin. These compositional features support the interpretation that orthopyroxene crystals (and orthopyroxenitites) in the GT-34 Prospect are not magmatic, being originated by metasomatic processes.

Sulfide-rich rocks (S > 10 wt. %) have high total iron oxides (27.10 to 44.71 wt. %) and P_2O_5 (4.20 to 20.92 wt.%) contents, reflecting their abundance in Fe-sulfides (pyrrhotite, pyrite,

chalcopyrite and pentlandite) and apatite. Compositional trends for orthopyroxenitites, sulfide-bearing orthopyroxenitites and sulfide-rich rocks suggest that sulfide-bearing rocks result from mild to extensive replacement of orthopyroxene-bearing rocks. REE contents in sulfide-bearing rocks are correlated with the abundance of apatite. This correlation is illustrated by the plot of Ce versus P_2O_5 contents for orthopyroxenitites, sulfide-bearing orthopyroxenitites and sulfide-rich rocks, indicating the progressive replacement of orthopyroxenitites by apatite-sulfide rich zones.

Interpretation of available data of the GT-34 Prospect suggests that high-temperature orthopyroxene-bearing metasomatic replacement bodies (Phase 1) developed within gneissic country rocks, followed by a late event of veining, brecciation and sulfide mineralization (Phase 2). Geological conditions appropriated to sustain the extensive high-temperature metasomatic system described in the GT-34 prospect (P > 0.5 Kb), suggest temperatures over 700°C for the crystallization of orthopyroxene. The second Phase in the GT-34 system consists of brecciation and veining of orthopyroxenitites and host gneisses, together with sulfide-apatite mineralization. This process involved the crystallization of significant amount of sulfides and apatite, thus promoting the concentration of a diverse range of elements (e.g. P, F, S, REE, Fe, Cu, Ni). The close spatial association suggests a genetic link between early alterarion (Phase 1) and later sulfidization (Phase 2). However, relative enrichment and depletion of elements are distinctively different in these two events indicating that fluids associated with metasomatism, and/or physical conditions prevailing during alteration, were highly different during these events. Sulfide-rich zones have abundant Fe-bearing sulfides (pyrrhotite, pyrite, chalcopyrite, pentlandite) and no associated oxides. Crystallization of pyrrhotite and pyrite without Fe-oxides (magnetite or hematite) indicates conditions of high sulfur fugacity (fS_2) and low oxygen fugacity (fO_2). The temperature of crystallization of sulfide-rich zones is constrained by associated hornblende, suggesting temperatures above 500°C, and the lack of orthopyroxene (e.g. T < 700°C).

Characteristics of the GT-34 Prospect suggest that metasomatism occurred under higher temperature and lower fO_2 conditions, compared to Cu-Au deposits in Carajás. These features possibly indicate that metasomatism and sulfidization of the GT-34 Prospect represent deep zones (e.g. deeper crustal level) of the regional 2.5 Ga Cu-Au ore-forming system of Carajás.

Key words:
Carajás, metasomatism, alteration, IOCG, orthopyroxene, apatite, lithogeochemistry.

Introduction

Iron oxide-copper-gold (IOCG) deposits comprise a wide range of epigenetic mineralizations, including several world-class Cu-Au deposits (Olympic Dam, Ernest Henry, Salobo, Sossego and others). Since the formulation of the IOCG concept (Hitzman et al., 1992) this type of mineralization attracted considerable attention of exploration companies and academics. A large number of Cu-Au deposits around the world belong to this class of deposit, including, among many others, widely different deposits like Olympic Dam (Oreskes and Einaudi, 1990) and Ernest Henry (Mark and Crookes, 1999) in Australia; Candelaria in Chile (Marschik et al., 2000; Sillitoe, 2003); Kiruna-type deposits in northern Fennoscandia (Pollard, 2000); and Salobo in Carajás (Requia et al., 1999; Souza et al., 2000). Even though IOCG deposits form a well-recognized style of mineralization, our understanding of the genesis of this broad group of deposits became more controversial. The origin of the mineralizing fluids (magmatic vs nonmagmatic) and the type of intrusive activity (granitic, mafic, alkaline) associated with mineralized fluids for specific deposits, or districts, are still under scrutinity.

Carajás Mineral Province is characterized to be polimetalic and presents hydrothermal

deposits from different ages. Several Cu-Au deposits of the Carajás region are now considered to belong to the IOCG class of deposits (Tallarico et al., 2005; Grainger et al., 2007). Deposits such as Bahia-Alemão (Tazava, et al., 2000; Ronzé et al., 2000; Tallarico et al., 2004; 2005; Dreher at al., 2008), Salobo (Requia et al., 1999; 2000; 2003; Souza et al., 2000) and Sossego (Leveille et al, 2000; 2001; Marschik et al., 2003; Carvalho et al., 2005; Monteiro et al., 2005; 2008) share a number of characterisitcs suggesting that they are formed as part of a major hydrothermal system. They are characterized by: 1) intense Fe metasomatism resulting in the formation of abundant Fe-bearing silicates (garnet, grunerite, fayalite) and/or Fe oxides (magnetite and/or hematite); 2) associated K-Na alteration; 3) sulfur-poor ore paragenesis; 4) enrichment in LREE and U. Precise dating of hydrothermal minerals in the Bahia deposit (2,575 ±12 Ma; Tallarico et al., 2005) and Salobo (2,576 ±9 Ma; Requia et al., 2003) suggests a Neoarchean ages for the regional scale hydrothermal system and associated Cu-Au deposits.

In this paper we present the results of field and petrologic-geochemical studies of the GT-34 sulfide Prospect in Carajás. The style of metasomatic alteration here described is distinctively different from typical IOCG-type Cu-Au mineralizations in Carajás. The rocks formed by metasomatism in the GT-34 are not Fe-enriched, are free of iron oxides (magnetite and/or hematite), include abundant orthopyroxene-bearing metasomatic rocks (orthopyroxenitite) and have abundant pyrrhotite and pyrite in the sulfide assemblage. These characteristics suggest that alteration in the GT-34 occurred under high-temperature and low fO_2 conditions, possibly representing deep zones of the regional 2.5 Ga ore-forming system of Carajás.

Exploration Review

Sulfide mineralizations of the GT-34 were discovered by VALE (formerly known as CVRD-COMPANHIA VALE DO RIO DOCE) in 1999 during follow up of a GEOTEM anomaly. Follow up consisted of geological mapping, soil geochemistry, ground geophysic (EM and IP) and drilling; returning sulfide-bearing intersections. The best intersections consist of dozens of meters-thick semi-massive brecciated sulfide-rich zones (mainly pyrrhotite with associated pyrite, chalcopyrite and pentlandite). Exploration resumed in 2003 with geological re-interpretation followed by detailed ground geophysics (EM) and systematic drilling. Sulfide-rich intervals form an irregular NE trend of about 1.5 km-long and up to 500 meters deep. The GT-34 Prospect is currently under evaluation by VALE and geological resources and tenors are not available for publication.

Regional Geological Setting

The regional geology of the Carajás Mineral Province (Figure 1) is described by Hirata et al. (1982), Meireles et al. (1984), Docegeo (1988), Araújo and Maia (1991), Costa et al. (1995), Faraco et al. (1996) and Macambira and Vale (1997). The Carajás Province is best known for hosting several world-class deposits, including the largest iron ore resources in the world, as well as Cu-Au, Ni and Mn deposits. These deposits are all located within Neoarchean E-W trending volcano-sedimentary sequences or nearby basement rocks. These well-preserved volcano-sedimentary sequences are the most striking tectonic-geological feature of the region. However, mineral wealth and geological limits of what is known as the Carajás Province are not confined to these Neoarchean sequences.

The Carajás Province (Figure 1) lies in the eastern portion of the Amazon Craton, being bordered to the east by the Neoproterozoic Araguaia Belt and to the west by overlying Paleoproterozoic sequences of the Uatumã Supergroup (Docegeo, 1988; Araújo and Maia, 1991). Geological limits to the south, where typical granite-greenstone terrains occur, and to the north, where gneiss-migmatite-granulite terrains predominate, are not precisely defined.

The Xingu Complex consists mainly of gneiss, migmatite and granulites (Docegeo, 1988). U-Pb zircon dating of high-grade metamorphic rocks yielded Archean ages, 2,859±9 Ma for edembergites of the Pium Complex (Pidgeon et al., 2000) and 2,859±2 Ma for migmatites

(Machado et al., 1991). These are interpreted to represent ages of metamorphic recrystallization. These basement rocks experienced several episodes of reactivation during the Archean and Paleoproterozoic (Pinheiro and Holdsworth, 1997; Holdsworth and Pinheiro, 2000). The Andorinhas Supergroup consists of typical Archean (2,904 ± 29 Ma; Macambira and Lancelot, 1996) greenstone belts (Docegeo, 1988), including spinifex-textured komatiitc flows and pillowed basalts (Huhn et al., 1986).

The Itacaiúnas Supergroup includes several Archean (ca. 2.75 Ga; Machado et al., 1991; Trendall et al., 1998) volcano-sedimentary sequences (Docegeo, 1988). These include the large sequence of metabasalts of the Grão Pará Group, footwall to the jaspilite-hosted, giant iron deposits of Carajás (Figueiredo e Silva et al., 2008; Lobato et al., 2005). This extensive basaltic volcanism is usually considered to result of intra-plate rifting of older continental crust (Gibbs et al., 1986; Docegeo, 1988; Olszewski et al., 1989; Villas and Santos, 2001) but subduction-related environments have also been proposed (Dardenne et al., 1988; Teixeira and Eggler, 1994). According to Zucchetti (2007) and Zucchetti et al. (2007), the Grão Pará Group basalts have a calc-alkaline magmatic affinity, and Nb-negative and Th-positive anomalies that are consistent with a subduction zone signature. Trace-element enrichment (e.g., high Zr/Y and Nb/Yb ratios) suggests that they formed in a continental-arc environment (Zucchetti, 2007). Basalts (Olszewsky et al., 1989), and jaspilites with negative ε_{Nd} values (Lobato et al., 2005b) indicate crustal contamination of the Grão Pará sequence. Thus, the trace-element geochemistry characteristics suggest a back-arc-related tectonic setting on an attenuated continental crust (Zucchetti, 2007; Zucchetti et al., 2007).

The Águas Claras Formation (Araújo et al., 1988; Soares et al., 1994) comprises sandstone and siltstone formed in shallow marine to fluvial environment (Nogueira et al., 1994; 2000). This sequence of clastic sedimentary rocks covers different sequences of the Itacaiúnas Supergroup. A minimum age for the Águas Claras Formation was determined by Dias et al. (1996) from zircons obtained from cross cutting gabbroic dikes (2,645±12 Ma). The Gorotire Formation is a clastic immature sequence covering the Itacaiúnas Supergroup and Águas Claras Formation (Docegeo, 1988).

The Carajás Province was intruded by granititic magmas of distinct ages and compositions. These intrusions are mainly correlated to three distinct periods. Archean (ca. 2.74-2.76 Ga) intrusions include the Plaquê Suite, as well as the Planalto, Estrela and Serra do Rabo granites (Avelar et al., 1999; Huhn et al., 1999; Dall'Agnol et al., 1997; Barros et al., 2001). Younger (ca. 2.56 Ga) intrusions include alkaline granites like the Old Salobo (Machado et al., 1991) and Itacaiúnas intrusions (Souza et al., 1996). Paleoproterozoic (ca. 1.88 Ga) intrusions include several anorogenic granitic plutons (Machado et al., 1991) that belong to an extensive A-type Proterozoic province of the Amazon Craton (e.g. Santos et al., 2001).

Several mafic-ultramafic intrusions intrude the Xingu Complex or the Itacaiúnas Supergroup (Docegeo, 1988). These include large Ni-mineralized layered intrusions of the Cateté Suite and the PGE-mineralized Luanga Complex (Macambira and Valle, 1997; Ferreira Filho et al., 2007). The latter crystallized at 2,763±6 Ma (Machado et al., 1991) and is coeval with the extensive mafic magmatism of the Itacaiúnas Supergroup.

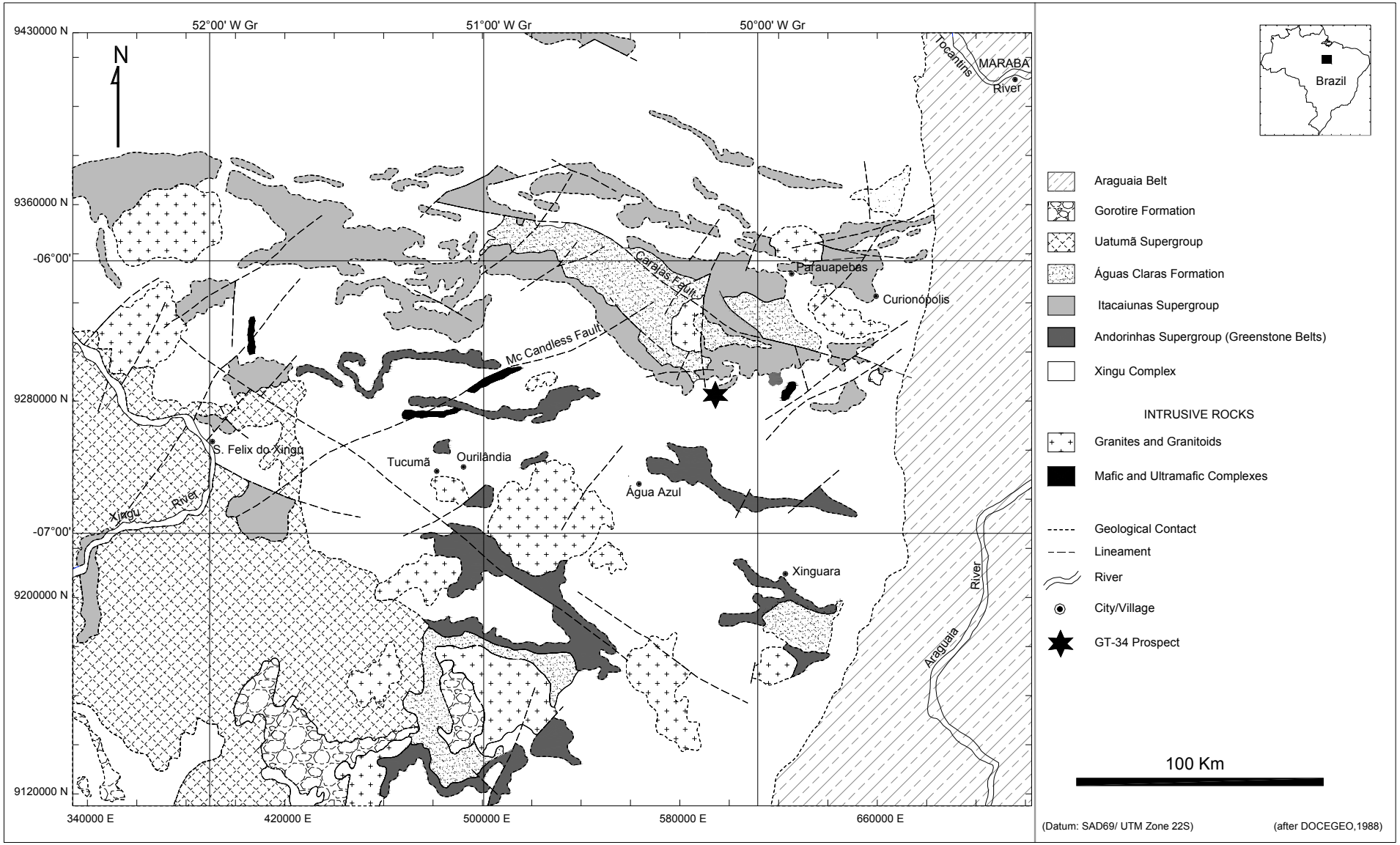

Figure 1. Main geotectonic units of Carajás Province. Modified from Docegeo (1988).

Geology of the GT-34 Prospect

The GT-34 Prospect is hosted by irregular bodies of brecciated rocks and/or orthopyroxene-amphibole-scapolite-rich rocks outcropping among basement gneissic rocks of the Xingu Complex (Figure 2 and 3). The region is mainly flat and outcrops are rare due to lateritic covers. Outcropping gneisses are partially to highly weathered and fresh samples are mainly restricted to drill core samples. Granodioritic gneisses show high K anomalies on GAMA surveys, helping to delineate domains of different gneissic rocks in the map.

Basement rocks include medium-grained banded biotite gneiss and coarse- to medium-grained granodioritic gneiss. The biotite gneiss has grey color and consists of centimeter-scale biotite- and quartz-rich bands alternated with quartz- and feldspar-rich bands (Table 1-Figure 4A). Granodioritic gneisses are quartz-feldspathic rocks consisting of diffuse centimeter-scale darker bands with up to 30-40% mafic minerals (greenish hornblende and biotite). Titanite, epidote, magnetite and zircon are acessory minerals in both types of gneissic rocks.

Brecciated rocks include highly heterogeneous fragmental rocks resulting from alteration of gneisses (Figure 4B). Fragments range from blocks of up to dozens of meters of granodioritic gneiss to centimeter-scale clasts of quartz feldspars. Due to protracted and pervasive alteration, fragments are frequently partially altered, developing diffuse and/or complex contacts with the matrix (like orthopyroxenitite, scapolitite, etc).

Sulfide-rich zones are closely associated with rocks consisting mainly of orthopyroxene, amphibole, scapolite and phlogopite, considered to be products of extensive alteration. Lithotypes vary from mainly monomineralic rocks (> 90% orthopyroxene, amphibole or scapolite) to rocks resulting from different proportions of these minerals (Table 1). Relations observed in drill core indicate that brecciated scapolite-rich rocks (scapolitite), usually closely associated with sulfides and apatite, cross cut orthopyroxene and-or amphibole-rich types (e.g. orthopyroxenitite, amphibolitite).

Coarse-grained dark grey-brownish rocks consisting of 80-100 vol. % orthopyroxene (orthopyroxenitite) with minor phlogopite and/or amphibole (< 20 vol %) are the most common rocks interpreted as product of metasomatism. Orthopyroxenitite forms irregular massive bodies or veins (Figure 4C and 4D), from few centimeters up to 300 meters-thick. Orthopyroxene crystals are up to few centimeters-long and form granoblastic aggregates with polygonal contacts and triple junctions (Figure 4E and 4F). Large orthopyroxene crystals are frequently bended and show undulatory extinction between crossed nicols. Recrystallization of large orthopyroxene crystals to fine-grained aggregates occurs in the edges or along irregular fractures (Figure 4G and 4H). The same optical and chemical (see microprobe analyses in the following section) features occur in large and fine-grained recrystallized orthopyroxene crystals. Recrystallization of orthopyroxene crystals is usually associated with brecciated zones and sulfide mineralization. Amphibole and phlogopite occur in cross cutting irregular veins (Figure 5B) or interstitial aggregates (Figure 5D) of different sizes (from less than one milimeter to metric). Phlogopite occurs in fine- to medium-grained pleochroic lamellae (light brownish yellow to colorless). Two distinct types of fine- to medium-grained amphiboles occur, distinctively pleochroic greenish crystals (hornblende) and colorless twinned crystals (from the grunerite-cummingtonite series). The first type is abundant while the latter is rare and restricted to small veins cross-cuting orthopyroxenitites. Low temperature alteration of orthopyroxenitite comprises talc and magnetite that partially replace orthopyroxene along fractures/borders or form orthopyroxene pseudomorphs.

Medium-grained greenish rocks (Figure 5A), consisting of 90-100 vol % hornblende (amphibolitite/hornblendite) with minor phlogopite, scapolite and/or plagioclase (< 10 vol %), are the second most common product of metasomatic alteration (Table 1). They occur in irregular massive bodies or veins (from few centimeters up to dozens of meters-thick). Hornblendites are mainly massive rocks with diablastic texture (Figure 5C). Foliated hornblendites with nematoblastic texture occur in restricted zones (usually less than one meter-thick) associated with the massive type. Fine-grained plagioclase and/or scapolite and minor sulfide occur associated with hornblende

in irregular patches.

Scapolite-rich rocks are fine- to medium-grained light-colored rocks with granoblastic texture (Figure 5E). These rocks are usually closely associated with brecciated zones and sulfide mineralization. Minerals associated with scapolite are quite variable including amphibole, apatite, quartz, orthopyroxene, plagioclase and epidote (Table 1).

Mafic dikes and small plugs cross cut all previously described lithotypes. These dark-colored rocks (black to dark grey) have fine-grained intergranular texture, consisting mainly of plagioclase, clinopyroxene and amphibole. Ubiquitous accessory minerals include ilmenite, magnetite, quartz and apatite (Table 1).

Table 1 – Rock types and Mineral Assemblege of the GT-34 Prospect.

Rock	Mineral Assemblage
Granodioritic gneiss	Quartz-plagioclase-K feldspar-hornblende ±biotite ±titanite ±epidote ±magnetite ±zircon
Biotite gneiss	Quartz-plagioclase-biotite
Orthopyroxenitite	Orthopyroxene ±hornblende ±phlogopite
Amphibolitite	Hornblende ±plagioclase ±phlogopite ±scapolite
Scapolitite	Scapolite ±sulfide ±apatite ±hornblende ±orthopyroxene ±plagioclase ±quartz ±epidote
Sulfide-rich rocks	Pyrrhotite-pyrite-apatite ±chalcopyrite ±pentlandite ±phlogopite ±hornblende ±scapolite
Mafic dikes	Plagioclase-clinopyroxene-amphibole ±ilmenite ±magnetite ±quartz ±apatite

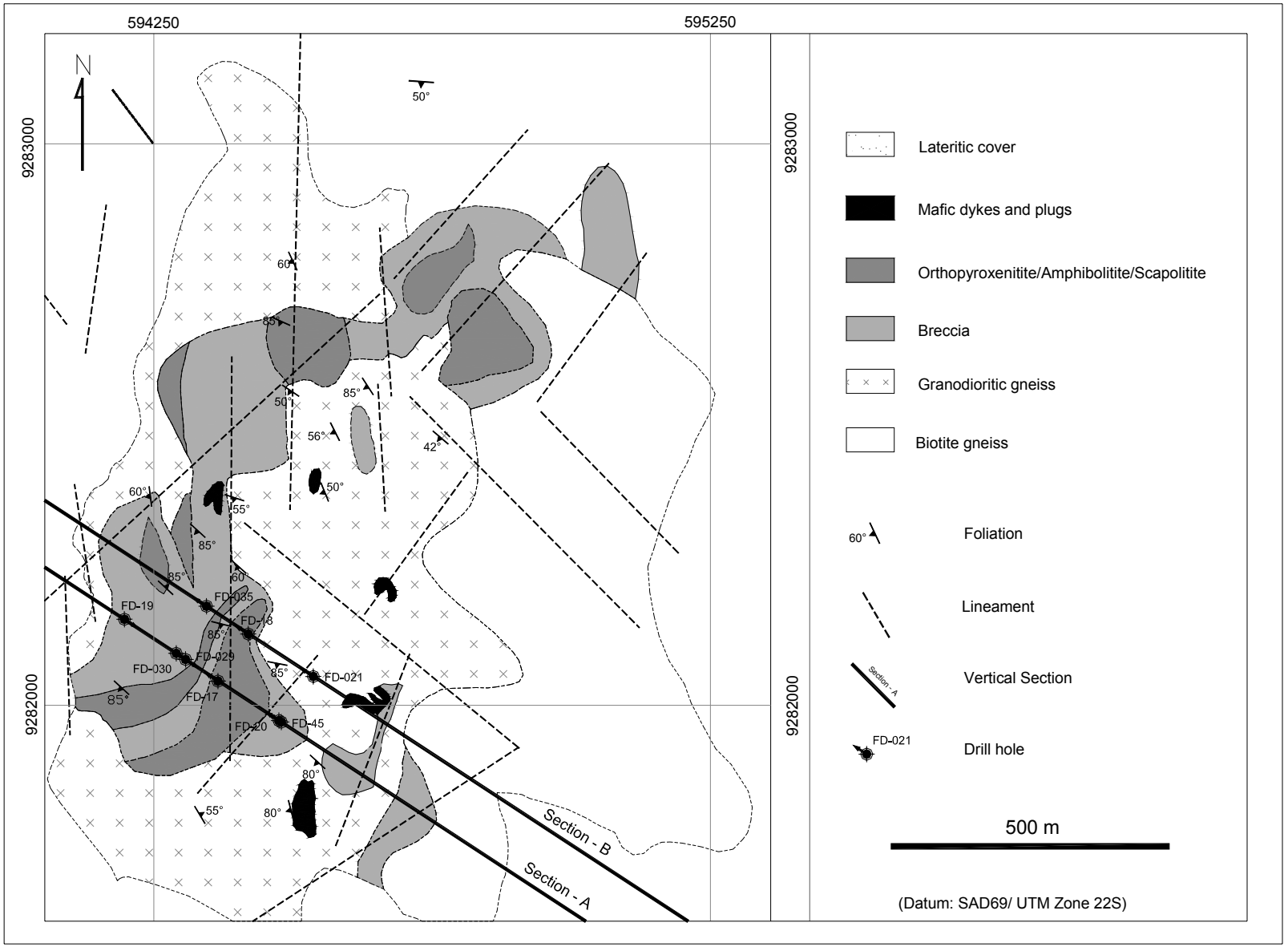

Figure 2. Geologic map of the GT-34 Prospect. Modified from unpublished report of VALE (2006).

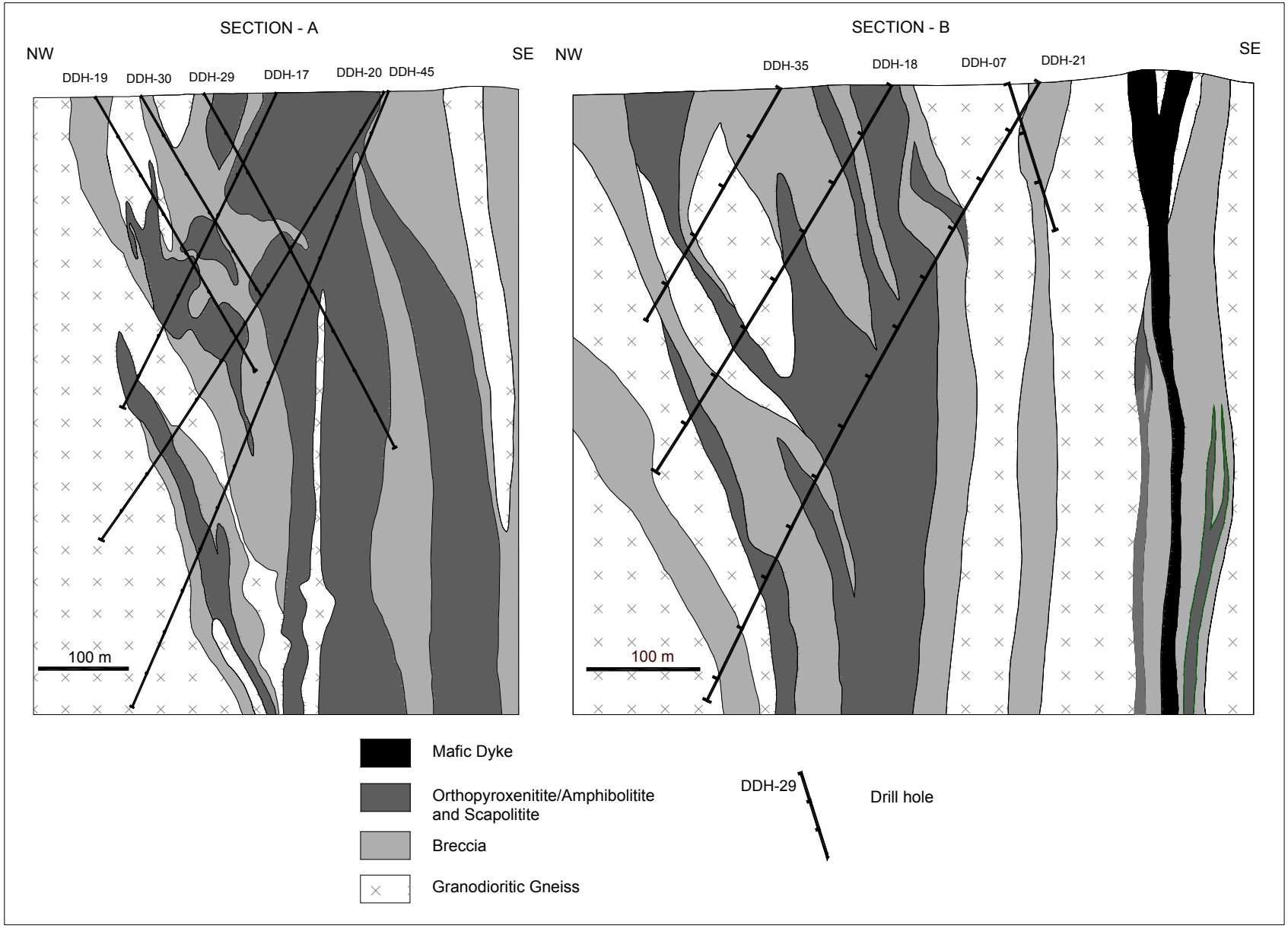

Figure 3. Geological sections "**A**" and "**B**". Modified from unpublished report of CVRD (2006).

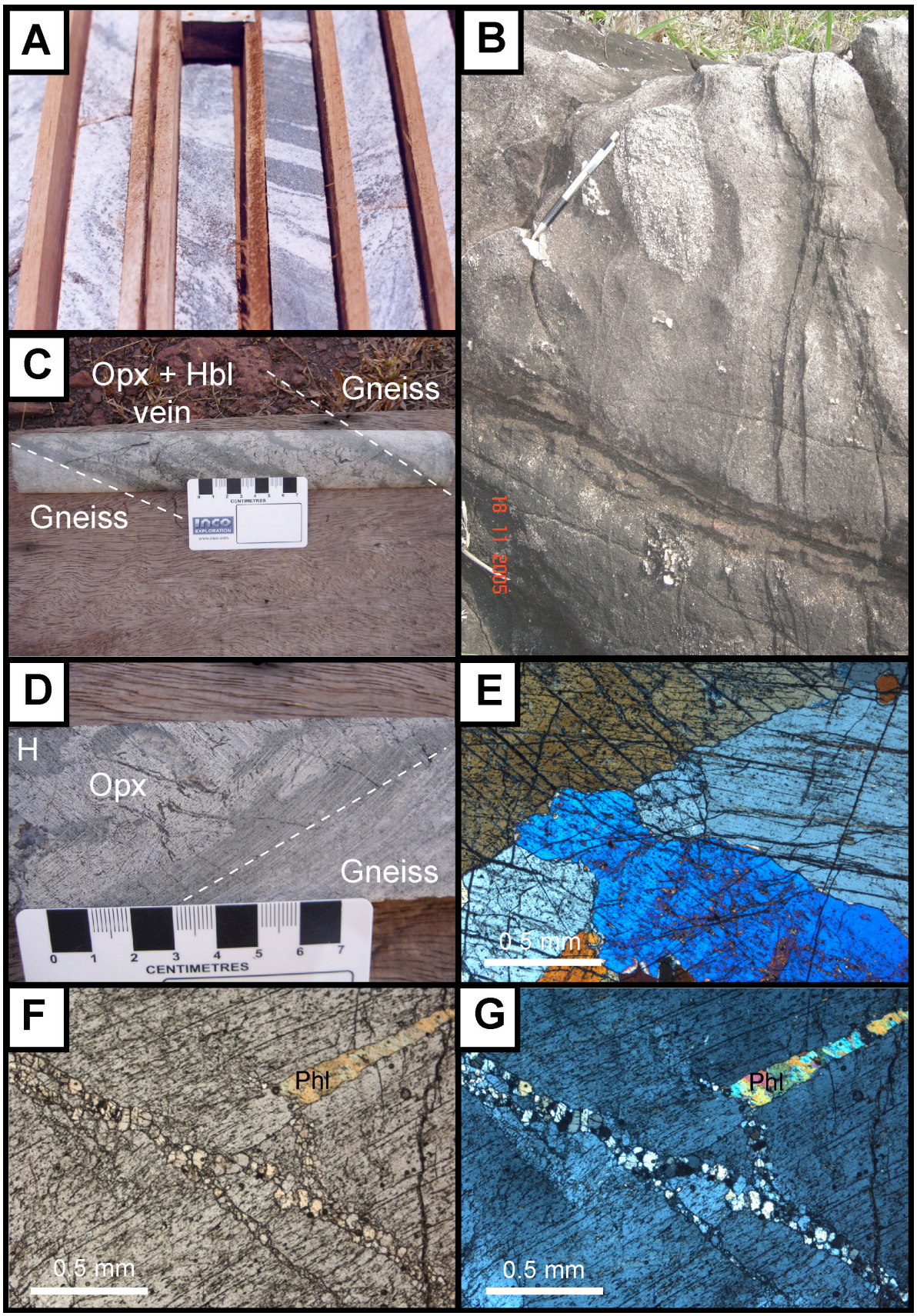

Figure 4. A) Banded biotite gneiss (FD01). B) Outcrop of altered brecciated gneiss. C) and D) Orthopyroxene and hornblende(H)-rich vein cross cutting gneiss (FD17_165,50m). E) Photomicrographs of orthopyroxenitite consisting of orthopyroxene crystals with granoblastic texture. View in cross-polarized light (XPL). F) and G) Orthopyroxenitite showing recrystallization of large crystals to fine-grained aggregates. View in plane-polarized light (PPL) and XPL. In addition to orthopyroxene there is a vein of fine- grained phlogopite (Phl).

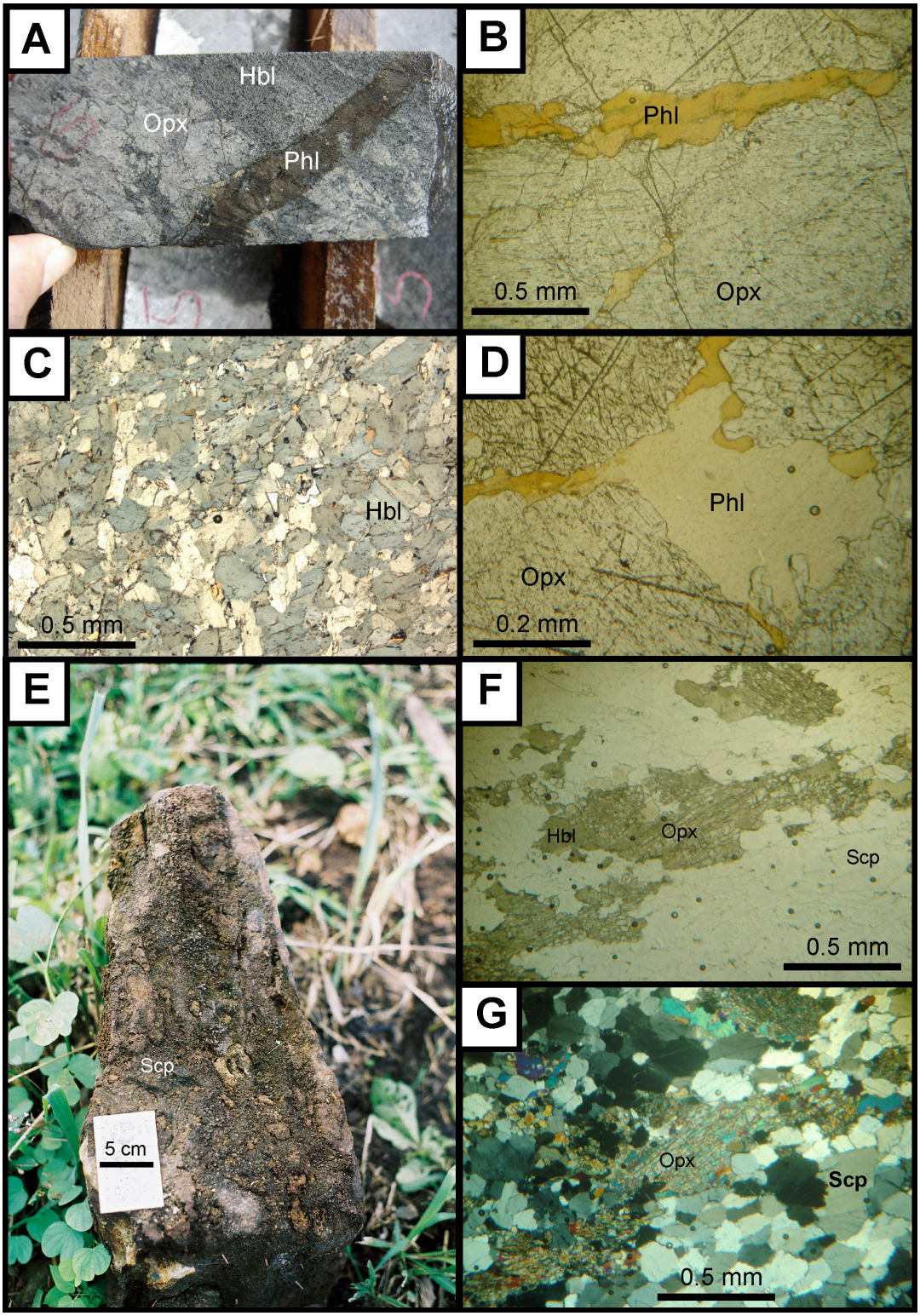

Figure 5. A) Closely associated orthopyroxenitite (Opx) and amphibolitite (Hbl) with cross-cutting vein of phlogopite (Phl). View in plane-polarized light (PPL). B) Orthopyroxenitite with coarse- to medium-grained orthopyroxene with cross-cutting phlogopite (PPL) C) Photomicrograph of diablastic texture in amphibolitite (PPL). The rock consists mainly of hornblende (Hbl) with minor phlogopite (yellowish color). D) Photomicrography of orthopyroxenitite with phlogopite in interstitial aggregates (PPL). E) Outcrop of brecciated scapolitite. This boulber shows irregular clusters of hornblende orthopyroxenititite (yellowish color) within fine-grained scapolitite. F) and G) Partially replaced orthopyroxene crystals within fine-grained granoblastic scapolitite. Orthopyroxene is partially replaced by hornblende (PPL and XPL).

Sulfide-rich Zones

Sulfide-rich intervals form an irregular NE trend of about 1.5 km-long and up to 500 meters deep. Sulfide-rich zones occur as irregular brecciated bodies and veins. Sulfide-rich brecciated zones and veins cross cut all other rocks with exception of mafic dikes and plugs. Sulfide enrichment is closely associated with brecciated gneisses and masses of orthopyroxenitite and/or amphibolitite, but also occurs cross cutting adjacent basement gneiss. Sulfide-rich intersections may be up to dozens of meters-thick or restricted to few centimeters-thick veins. Data on tonnage, metal contents, modal composition of sulfides and spacial distributions of the sulfide-rich bodies are not available for publication at the moment. Data and descriptions in this study are representative of the process leading to sulfide enrichment in breccias and veins of the GT-34 Prospect.

Brecciation of orthopyroxenitites by sulfide-bearing veins is observed throughout the GT-34 Prospect (Figure 6). In these zones orthopyroxene is brecciated and partially replaced by an assemblage of sulfides associated with variable proportions of apatite, scapolite and hornblende. Enrichment in sulfides occurs in discrete veins (Figure 6F), in veining systems developing net textured rocks (Figure 6D) or in semi-massive brecciated zones where partially altered fragments of orthopyroxenitites frequently occur (Figure 6E). Sulfides may be interstitial to orthopyroxene crystals (Figure 7A and 7B), occur in irregulat aggregates within zones where large orthopyroxene crystals were recrystallized to fine-grained aggregates (Figure 7C and 7D) or form massive to semi-massive aggregates mainly associated with apatite (Figure 6C, 7E). Massive to semi-massive apatite-sulfide masses are usually associated with scapolite (7G and 7H), hornblende and minor phogopite. Highly recrystallized and/or altered orthopyroxene crystals and/or orthopyroxenitites (Figure 7E and 7F) frequently occur in these sulfide-rich semi-massive zones.

Within large brecciated zones (Figures 6A, 6B and 6C) orthopyroxene disappears and gangue minerals consist mainly of apatite, hornblende and scapolite. These sulfide-rich assemblages usually have granoblastic texture with polygonal contacts between sulfides and gangue minerals. Apatite is ubiquitous and abundant (up to 25 vol. %) in brecciated semi-massive sulfides (Figure 6C, 6E, 8A, 8B) or sulfide-rich veins. It usually occurs in large (up to 1-2 centimeters) idiomorphic crystals within aggregates of sulfides. This close association of apatite and sulfides is a remarkable feature of the GT-34 prospect. Scapolite and hornblende are also frequently associated with sulfide-rich zones.

Sulfide minerals consist mainly of pyrrhotite with associated pyrite, chalcopyrite and pentlandite (Figures 8B, 8C and 8D). Ore mineralogy is the same throghout different mineralization zones of the GT-34. Pyrrhotite occurs mainly in medium- to coarse-grained (up to few centimeters) crystals, forming crystalline aggregates (Figure 8A). Pyrite and chalcopyrite (Figure 8C) occur in fine- to medium-grained anhedral to subhedral crystals unevenly distributed in hand sample scale. Chalcopyrite occasionally occurs in fine-grained intergrowth with pyrite. Pentlandite occurs mainly in medium-grained crystals, forming crystalline aggregates with pyrrhotite. Minor amounts of pentlandite also occur in exsolution lamellae hosted by pyrrhotite. These fine-grained (0.02-0.05 mm) ribbons (Figure 8D) or flame-type exsolutions are concentrated in or nearby the contact between pyrrhotite crystals.

The main geochemical characteristics of the sulfide-rich zones are illustrated by exploration data from Hole FD45 (Figure 9). Four significant sulfide-rich zones are intersected in Hole FD45. The abundance of apatite in the sulfide-rich samples results in their high P contents (up to 7.9 wt. % and several values between 1-5 wt. %) and good correlation with S values (Figure 9 and 10). The distribution of Mg, Fe and Cr in Bore Hole 45 is used to show some significant geochemical features of the mineralized interval and host rocks (Figures 9 and 10). Even though the sulfide zones are enriched in Fe, reflecting the abundance of Fe-bearing sulfides (pyrrhotite, pyrite, chalcopyrite and pentlandite), the metasomatic rocks closely associated with the sulfide-rich zones are not Fe-enriched. The overall Fe content of metasomatic rocks is lower or similar to Fe content of granodioritic gneisses, which correspond to the interval below 600 meters in Hole FD45 (Figure 9). Higher Mg contents (> 3 wt. % Mg) correspond to orthopyroxene-rich rocks

(orthopyroxenitites). These rocks are closely associated with sulfide-rich zones but not neccessarily their host rocks. This feature is well illustrated by the sulfide-rich zone between 200 and 300 meters in Hole FD45, which is limited by orthopyroxenitites (Figure 9), as well as by generally low Mg content for suldide-rich intervals (Figure 10). The distribution of Cr in Hole FD45 indicates that these sulfide-rich zones and their host rocks have contents generally below 150 ppm, which are similar to Cr contents of granodioritic gneisses. These data also indicate that Cr contents of Mg-rich rocks (orthopyroxenitites) are similar to Cr content of granodioritic gneisses.

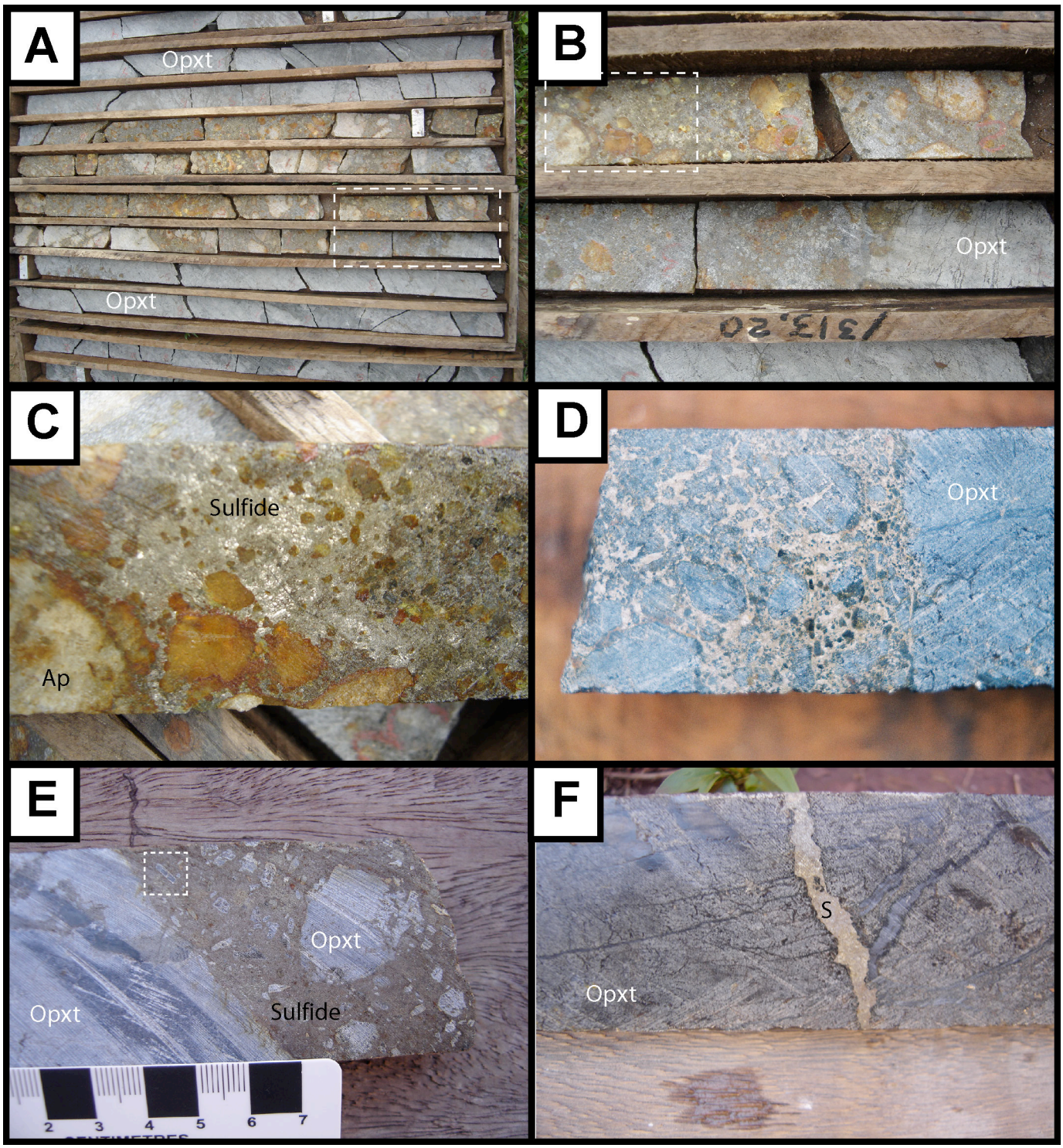

Figure 6. A) Sulfide-rich brecciated zone cross cutting orthopyroxenitite (core is 4.5 cm wide and boxes are 1 meter-long). B) Contact of the orthopyroxenitite (Opxt) and sulfide-rich breccia. This corresponds to the interval shown in the dashed rectangle in the previous photograph. C) Apatite- and sulfide-rich zone. This corresponds to the interval shown in the dashed rectangle in the previous photograph D) Orthopyroxenitite with interstitial sulfides. Black minerals associated with sulfides are hornblende. E) Brecciated orthopyroxenitite in sulfide-rich zone. Sulfides enclose several fragments of orthopyroxenitite and large euhedral apatite (see dashed square for prismatic apatite crystal). F) Sulfide-rich vein cross-cutting orthopyroxenitite.

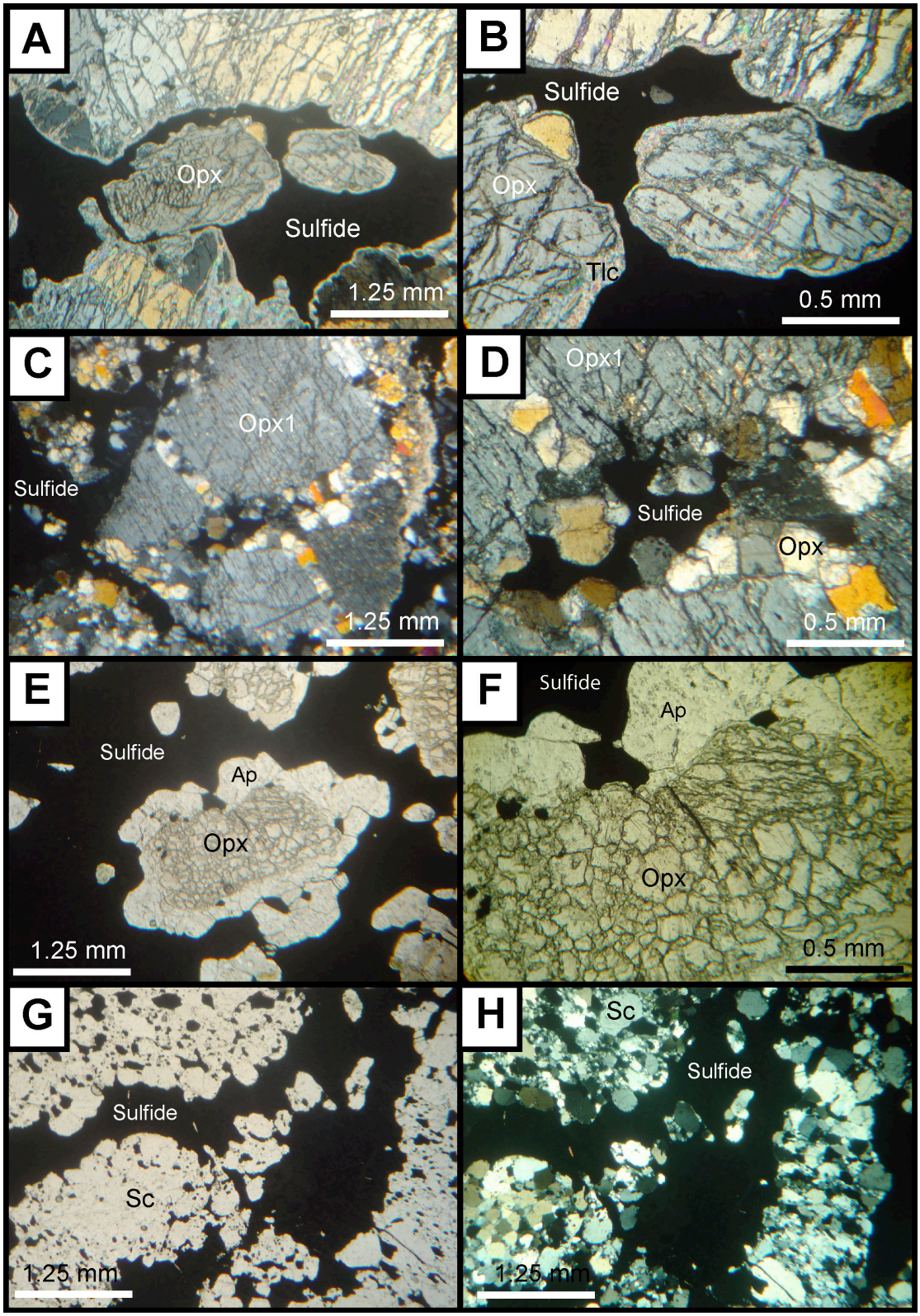

Figure 7. A and B) Photomicrograph of orthopyroxenitite with interstitial sulfides. Orthopyroxene (Opx) is partially altered to talc (Tlc) and serpentine along fractures and cleavages (XPL). C and D) Photomicrograph of sulfides associated with orthopyroxene (Opx1) crystals partially recrystallized to fine-grained aggregates of orthopyroxene (XPL). E and F) Fine-grained granoblastic aggregate of orthopyroxene (Opx) enclosed in sulfides and apatite (Ap). (PPL). G and H) Fine-grained aggregates of scapolite (Sc) enclosed in sulfides. Note granoblastic textures with polygonal contacts between scapolite and sulfides (PPL and XPL).

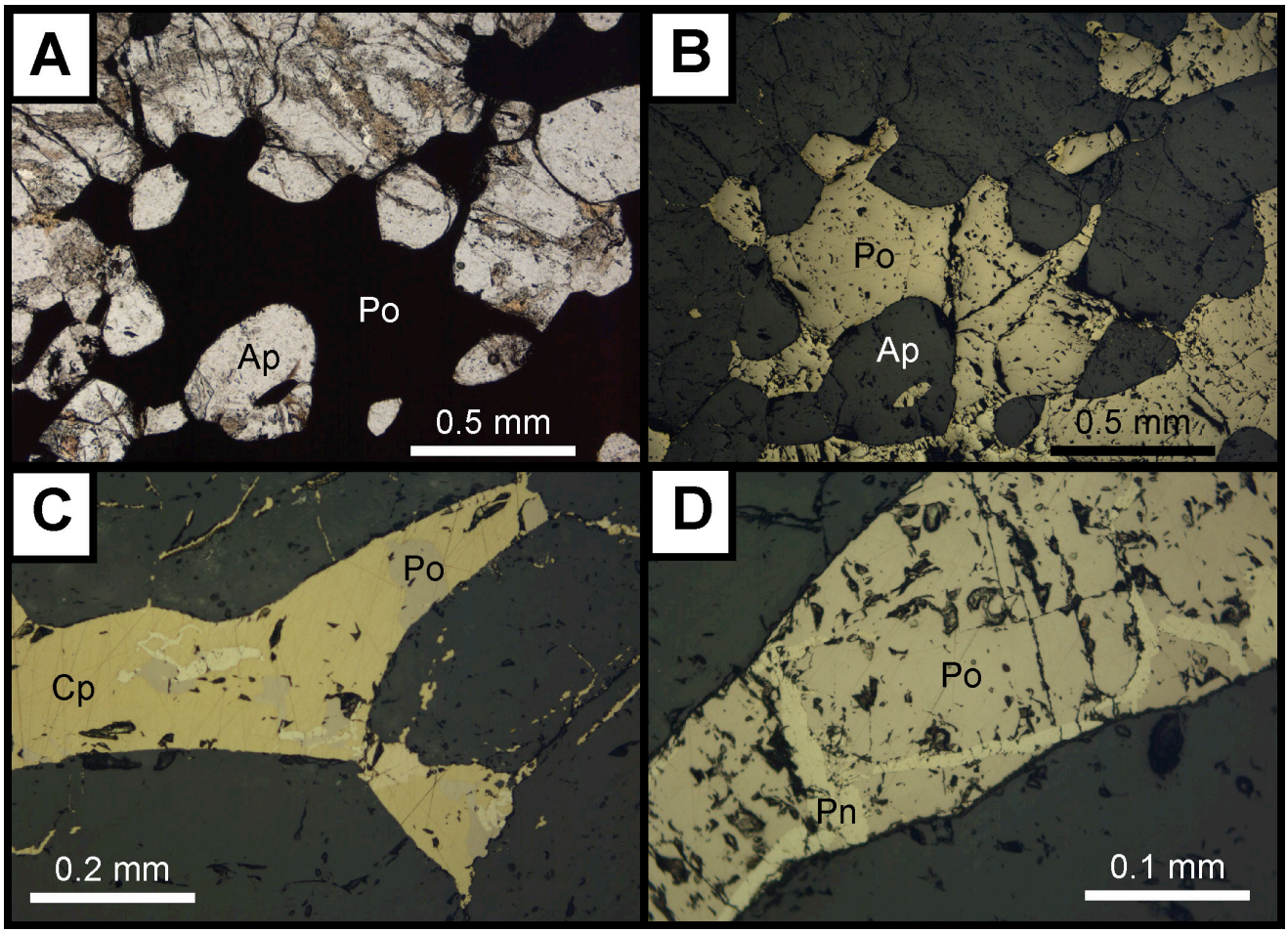

Figure 8. A) Photomicrograph of sulfides associated with apatite (PPL). B) Same field of view with observation under reflected light (PPL). Sulfides consist mainly of pyrrhotite (Po) and minor pyrite (light yellow color). C) Sulfides consisting mainly of chalcopyrite (Cp), pyrrhotite (Po) and pyrite (light yellow color). Observation under reflected light (PPL) D) Pyrrhotite (Po) crystals enclosing ribbons of pentlandite (Pn). Observation under reflected light (PPL).

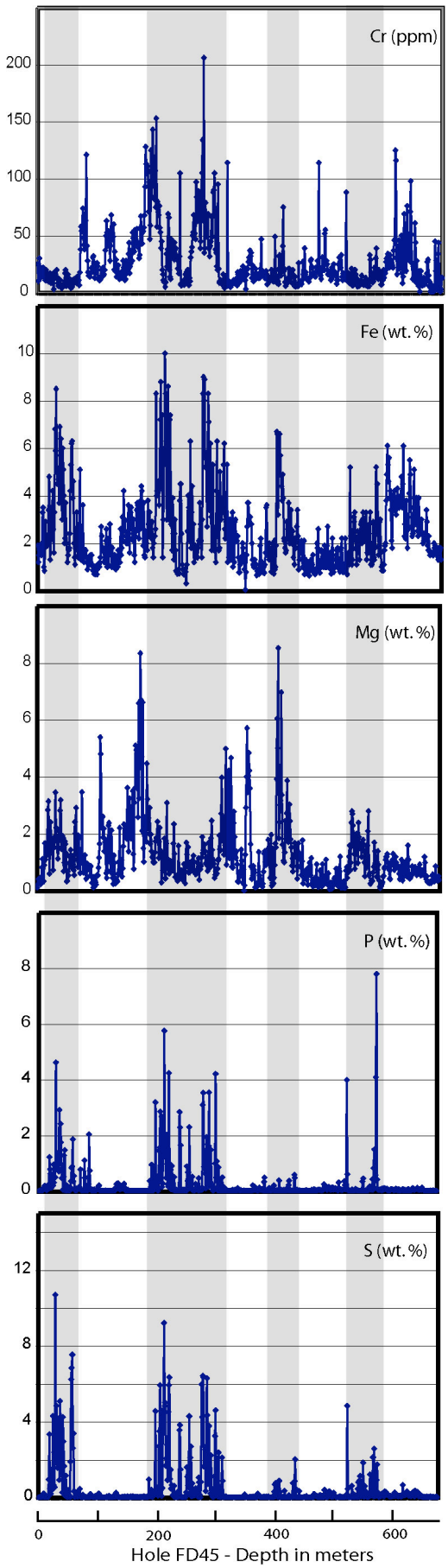

Figure 9. Distribution of Cr, Fe, Mg, P and S throughout borehole FD45. This figure is based upon exploration data, consisting of continuos analyses of core samples (1 meter interval). Samples were assayed at the ALS Chemex. Figure 3 has the geological section for borehole FD45.

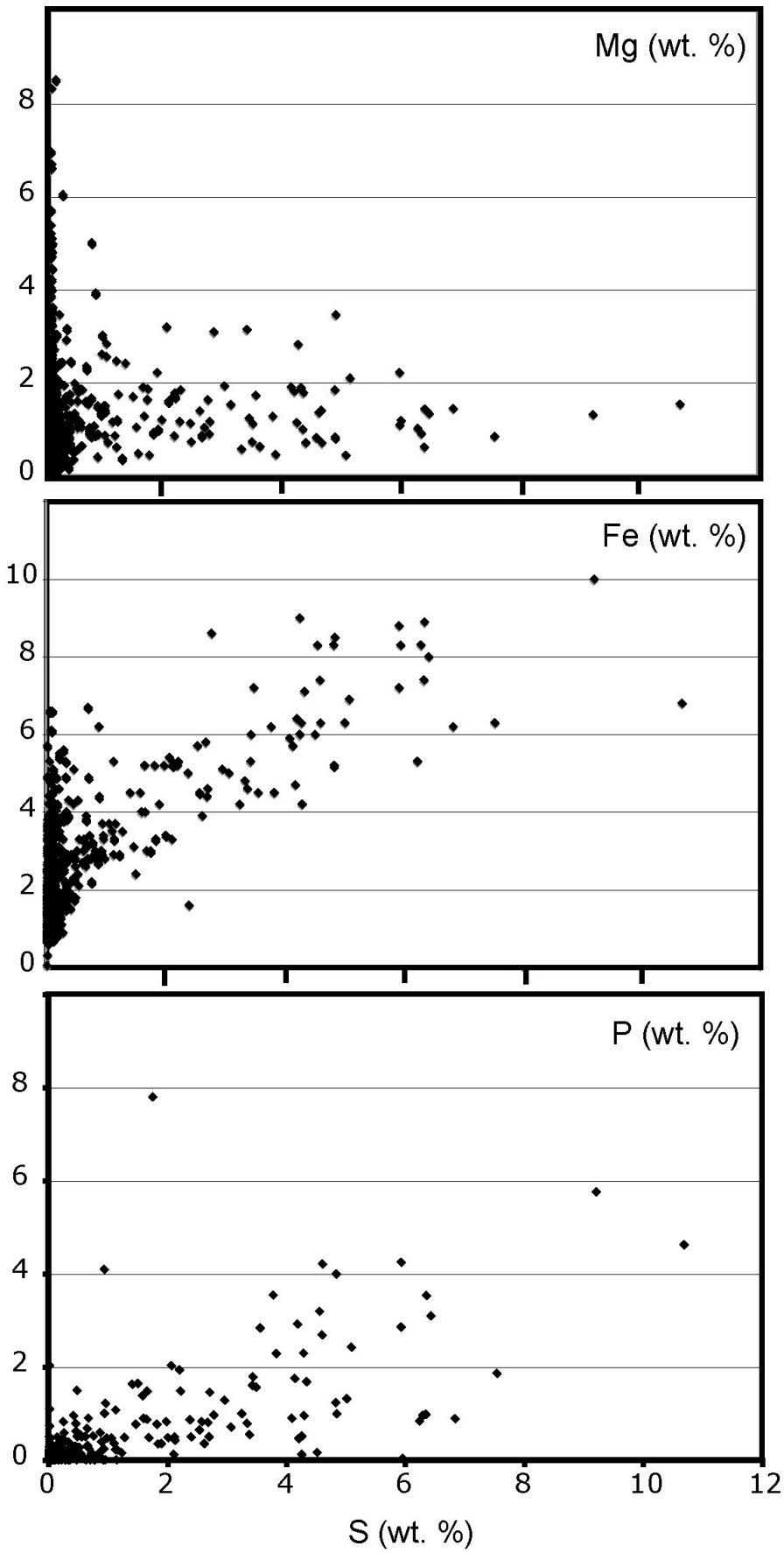

Figure 10. Plot of Mg, Fe and P contents versus S content for borehole FD45. Same data used in Figure 9.

Mineral Chemistry

Mineral analyses were performed on polished thin sections using a fully automated Cameca SX-50 Electron Microprobe at the Geosciences Institute, University of Brasília (Brazil). The wavelength dispersive (WDS) analyses were performed at an accelerating voltage of 15 kV and a beam current of 25 nA. Background counting time was set to half of the peak counting time. Both synthetic and natural mineral standards were used for the analyses and the same standards and procedure were retained throughout. Fe^{3+} contents were estimated using site and charge balance calculations on cation-normalised analyses. Routine analyses (WDS or EDS) were used to support petrographic studies. Systematic analyses were obtained for orthopyroxene (Table 2) and apatite (Table 3).

Systematic analyses of orthopyroxene crystals (opx) from orthopyroxenitites collected in different portions of the GT-34 prospect are very similar. En contents for orthopyroxene from the GT-34 vary from 68.0 to 77.5 % (Figure 11 and Table 2). Variation in En content shows no correlation with contents of TiO_2, Cr_2O_3, CaO and Al_2O_3 (Figure 11). Orthopyroxene compositions usually show up to 8 mol. % variations in the En content for the same sample. These variations in En content are mainly related to slightly higher En content of larger orthopyroxene crystals compared to crystals from fine-grained recrystallized aggregates. Distinct compositions of large and recrystallized orthopyroxene crystals (as shown in Figure 7C) for two different samples are illustrated in Figure 12. Lower En contents for fine-grained orthopyroxene crystals are not followed by systematic changes in contents of CaO and Al_2O_3 (Figure 12), as well as TiO_2 and Cr_2O_3. When compared to orthopyroxene with similar En content from orthopyroxenites from mafic-ultramafic layered intrusions, orthopyroxene crystals from the GT-34 show lower contents for TiO_2, Cr_2O_3, CaO and Al_2O_3 (Figure 11 and Table 2). These compositional features support the interpretation that orthopyroxenes in the GT-34 prospect are not magmatic, being originated by metasomatic processes. Low CaO and Al_2O_3 contents also indicate that orthopyroxenes from the GT-34 crystallized at relatively low temperature when compared with magmatic orthopyroxene, and low pressure when compared with high-grade metamorphic orthopyroxenes (Spier, 1993).

Table 2 – Representative microprobe analyses of orthopyroxene.

Sample		LSK29A	LSK29B	LSK30A	LSK30B	LSK32A	LSK32B	FD07A	FD07B	FD01A	FD01B
Comment		LC	LC	LC	SRC	LC	SRC	LC	SRC	LC	LC
SiO2	wt. %	55.08	54.32	53.51	53.29	54.81	54.15	54.77	53.52	53.17	54.15
TiO2	wt. %	0.03	0.01	0.07	0.04	0.04	0.03	0.04	0.01	0.04	0.03
Al2O3	wt. %	0.34	0.31	0.47	0.47	0.59	0.69	0.57	0.72	0.93	0.63
Cr2O3	wt. %	0.01	0.00	0.00	0.03	0.00	0.00	0.02	0.00	0.00	0.00
FeOT	wt. %	15.68	18.52	19.68	19.26	16.36	17.59	16.88	18.71	18.10	18.00
MnO	wt. %	0.17	0.22	0.24	0.20	0.16	0.19	0.17	0.20	0.31	0.21
MgO	wt. %	28.74	26.30	25.29	25.32	28.14	26.56	27.81	25.78	26.26	26.67
NiO	wt. %	0.04	0.18	0.11	0.11	0.08	0.01	0.07	0.05	0.13	0.11
CaO	wt. %	0.17	0.26	0.24	0.32	0.12	0.16	0.10	0.23	0.26	0.22
Na2O	wt. %	0.00	0.01	0.00	0.00	0.05	0.00	0.00	0.00	0.00	0.04
K2O	wt. %	0.00	0.00	0.01	0.00	0.02	0.02	0.02	0.00	0.01	0.02
TOTAL	wt. %	100.26	100.13	99.61	99.03	100.36	99.38	100.44	99.22	99.21	100.06
Number of cations per 6 oxygens.											
Si		1.977	1.981	1.974	1.974	1.972	1.979	1.974	1.972	1.958	1.971
Al		0.014	0.013	0.020	0.020	0.025	0.030	0.024	0.031	0.040	0.027
Ti		0.001	0.000	0.002	0.001	0.001	0.001	0.001	0.000	0.001	0.001
Cr		0.000	0.000	0.000	0.001	0.000	0.000	0.001	0.000	0.000	0.000
Fe		0.471	0.565	0.607	0.597	0.492	0.538	0.509	0.576	0.557	0.548
Mn		0.005	0.007	0.007	0.006	0.005	0.006	0.005	0.006	0.010	0.006
Mg		1.538	1.430	1.391	1.399	1.510	1.447	1.494	1.416	1.441	1.447
Ni		0.001	0.005	0.003	0.003	0.002	0.000	0.002	0.001	0.004	0.003
Ca		0.006	0.010	0.009	0.013	0.004	0.006	0.004	0.009	0.010	0.009
Na		0.000	0.001	0.000	0.000	0.003	0.000	0.000	0.000	0.000	0.002
K		0.000	0.000	0.001	0.000	0.001	0.001	0.001	0.000	0.001	0.001
T (Si+Al)		1.99	1.99	1.99	1.99	2.00	2.01	2.00	2.00	2.00	2.00
M1M2		2.02	2.02	2.02	2.02	2.02	2.00	2.02	2.01	2.02	2.02
En		76.14	71.09	69.03	69.44	75.05	72.47	74.27	70.53	71.41	72.00
Fs		23.54	28.42	30.50	29.93	24.73	27.22	25.54	29.02	28.08	27.57
Wo		0.32	0.50	0.47	0.63	0.22	0.32	0.19	0.46	0.51	0.43

LG = large crystal; SRC = small recrystallized crystal.

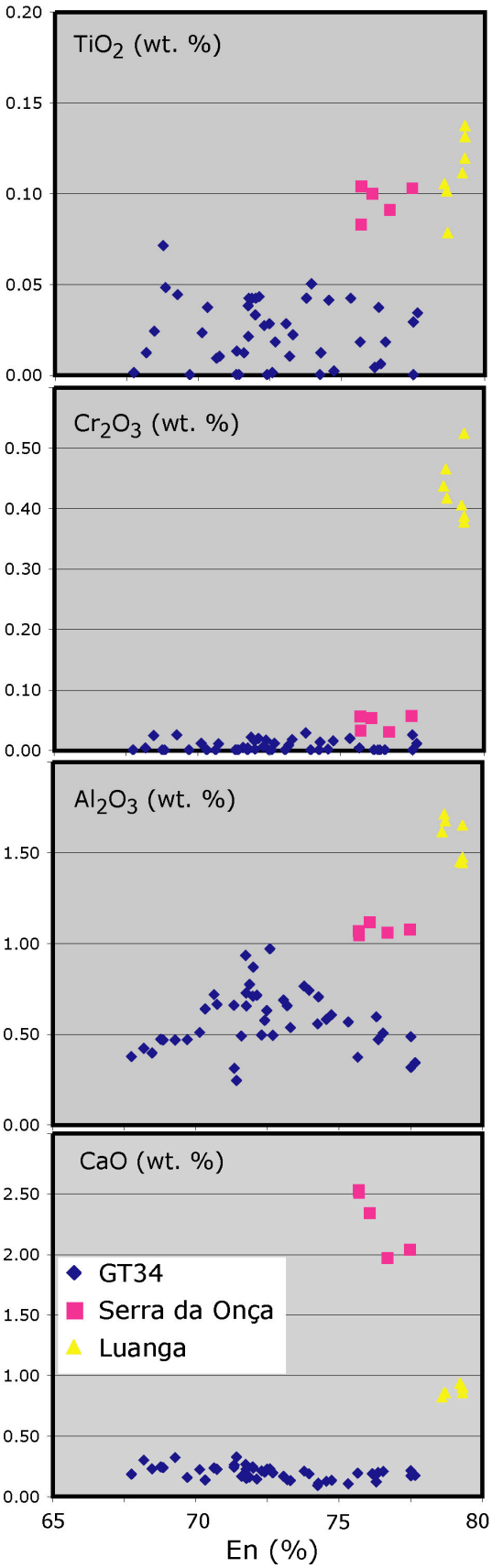

Figure 11. Plot of En content versus TiO_2, Cr_2O_3, CaO and Al_2O_3 contents for orthopyroxene compositions of orthopyroxenitites from the GT-34. Orthopyroxene compositions of othopyroxenites from the Serra da Onça Complex (Macambira and Ferreira Filho, 2002) and Luanga Complex (Ferreira Filho et al., 2007) were included for comparison.

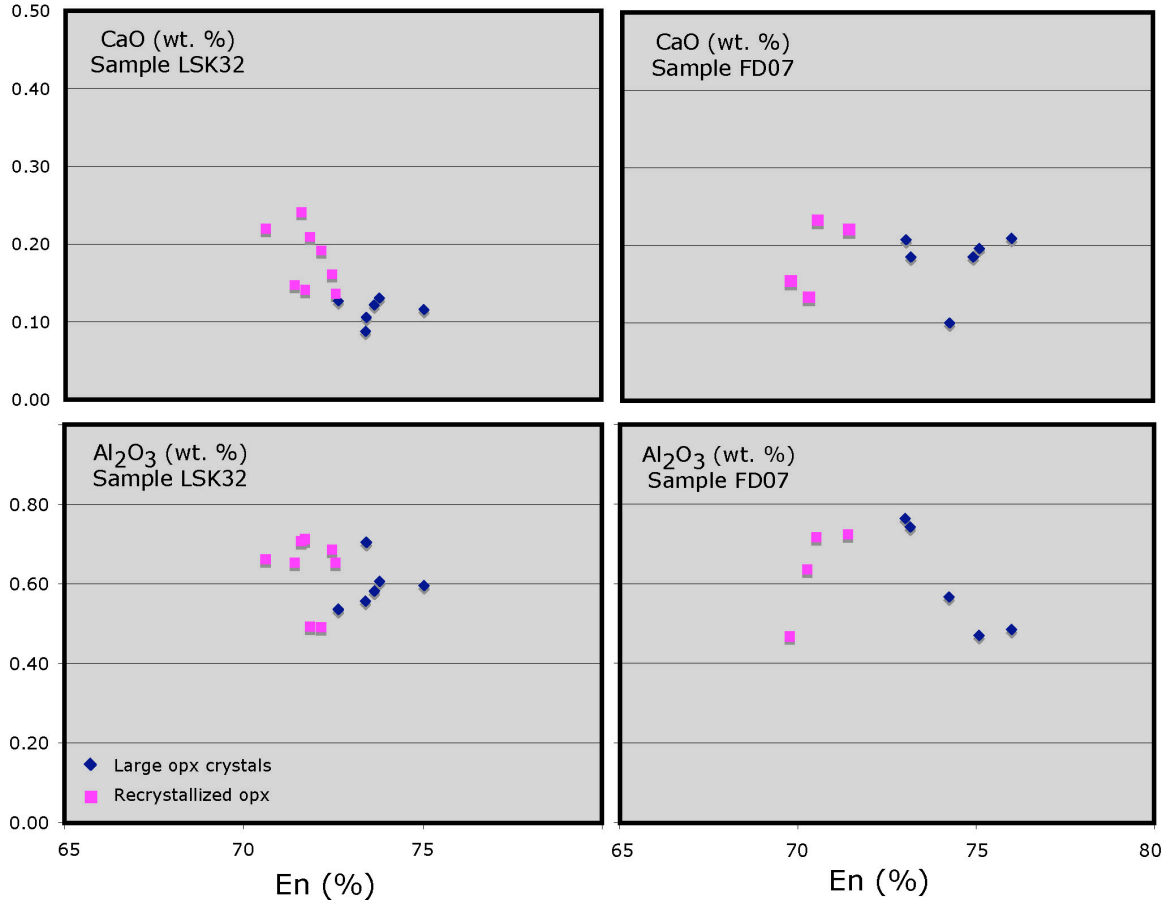

Figure 12. Plot of En content versus CaO and Al_2O_3 contents for orthopyroxene compositions of two selected samples of orthopyroxenitites from the GT-34. See text and figure 7C and 7D for petrographic features of large and recrystallized orthopyroxene crystals.

Amphibole occurs in amphibolitites, in some strings veins cutting orthopyroxenitites and in brecciated zones. All amphibole crystals assayed belong to calcic amphibole compositions (Leake et al., 1997). Ca contents range from 10.94 to 11.35 wt. % CaO, SiO_2 (up to 44.84 wt. %), Al_2O_3 (up to 13.50 wt. %), MgO (from 6.58 to 14.41 wt. %), Na_2O (up to 2.60 wt. %), K_2O (up to 1.96 wt. %), TiO_2 (up to 0.84 wt. %) and Cr (up to 0.47 wt. % Cr_2O_3).

Phlogopite occurs as accessory mineral in cross-cutting veins and as interstitial aggregates or lamellae of different sizes. Phlogopite crystals have mg# values in the range of 0.77 to 0.80. It also show Si content from 38.57 to 38.88 wt. % SiO_2, Fe_{total} (from 9.02 to 9.76 wt. %), MgO (from 18.98 to 20.24 wt. %), Al_2O_3 (up to 13.27 wt. %), TiO_2 (up to 2.29 wt. %), Na_2O (up to 0.56 wt. %), K_2O (up to 9.85 wt. %) and BaO (up to 0.09 wt. %).

Apatite assayed crystals (Table 3) occur in sulfide-rich veins and bodies, and present long axis sizes ranging from sub-mm to about 3cm. The apatite samples has Ca content from 51.87 to 54.67 wt. % CaO, P_2O_5 content from 41.13 to 42.89 wt. %, Fe_{total} (up to 0.30 wt. %), SrO (up to 0.20 wt. %), K_2O (up to 0.14 wt. %), and high Cl contends range from 3.27 to 6.58 wt. %. For this reason GT-34 apatites can be said as chloroapatites (Deer et al., 1992).

Scapolite occurs in scapolitites or as centimeter-scale aggregates with sub-mm granoblastic crystals. Scapolite assays has Na values ranging from 11.91 to 13.48 wt. %), Ca values ranging from 5.19 to 5.93 wt. % and Cl content range from 3.81 to 4.11 wt. %. GT-34 scapolite belongs to Na- and Cl-rich chloride marialite variety (Deer et al., 1992).

Table 3 – Representative microprobe analyses of apatite.

Sample		LSK28 F1-APAT 1	LSK28 F1-APAT 2	LSK28 F2-APAT 1.1-C	LSK28 F2-APAT 1.3-C	LSK28 F2-APAT 1.5-C	LSK28 F2-APAT 1.6-C	LSK28 APAT 1.7-C	LSK28 F2-APAT 1.8-C	LSK28 F2-APAT 1.9-C	LSK28 F2-APAT 1.11-C
SiO2	wt. %	0.00	0.01	0.05	0.10	0.12	0.07	0.07	0.05	0.10	0.12
Al2O3	wt. %	0.00	0.00	0.00	0.05	0.01	0.00	0.00	0.00	0.02	0.04
MgO	wt. %	0.00	0.00	0.00	0.00	0.00	0.00	0.00	0.00	0.00	0.00
P2O5	wt. %	42.02	42.08	42.17	41.13	41.33	41.91	42.16	41.57	42.21	42.42
CaO	wt. %	53.53	51.88	52.60	52.85	53.08	53.21	53.23	52.80	52.75	52.05
FeOT	wt. %	0.05	0.00	0.30	0.05	0.06	0.06	0.00	0.06	0.05	0.12
Na2O	wt. %	0.00	0.00	0.00	0.00	0.00	0.00	0.00	0.00	0.00	0.00
K2O	wt. %	0.00	0.00	0.01	0.02	0.00	0.01	0.00	0.01	0.01	0.14
BaO	wt. %	0.01	0.00	0.00	0.21	0.00	0.15	0.00	0.00	0.00	0.08
SrO	wt. %	0.00	0.08	0.13	0.06	0.01	0.12	0.07	0.18	0.12	0.05
Cl	wt. %	4.00	6.58	4.94	5.32	4.44	4.28	4.00	4.64	4.68	4.87
H2O	wt. %	0.70	0.00	0.45	0.32	0.56	0.62	0.70	0.51	0.52	0.47
TOTAL	wt. %	100.31	100.64	100.64	100.12	99.61	100.42	100.23	99.81	100.45	100.34
Number of cations per 26 oxygens.											
Si		0.000	0.002	0.008	0.005	0.021	0.012	0.012	0.010	0.018	0.022
Al		0.000	0.000	0.000	0.000	0.002	0.000	0.000	0.000	0.005	0.007
Fe		0.007	0.000	0.045	0.016	0.009	0.009	0.000	0.008	0.007	0.017
P		6.222	6.401	6.292	6.254	6.209	6.229	6.237	6.245	6.281	6.324
Mg		0.000	0.000	0.000	0.000	0.000	0.000	0.000	0.000	0.000	0.000
Ca		10.03	9.987	9.933	9.937	10.091	10.007	9.967	10.038	9.933	9.820
Na		0.000	0.000	0.000	0.000	0.000	0.000	0.000	0.000	0.000	0.000
K		0.000	0.000	0.002	0.004	0.000	0.001	0.000	0.002	0.001	0.030
Ba		0.001	0.000	0.000	0.001	0.000	0.01	0.000	0.000	0.000	0.006
Sr		0.000	0.009	0.013	0.015	0.001	0.012	0.007	0.018	0.012	0.005
Cl		-0.903	-1.485	-1.115	-0.949	-1.002	-0.965	-0.902	-1.046	-1.056	-1.099
H		0.000	0.000	0.000	0.000	0.000	0.000	0.000	0.000	0.000	0.000
Cations		15.357	14.914	15.178	15.283	15.331	15.315	15.321	15.275	15.201	15.132

Lithogeochemistry

Sample preparation and litogeochemistry analyses were performed at the ALS Chemex (Canada). A total of 33 representative samples from diamond drill holes of GT-34 deposit were analysed using three different procedures. These include the whole rock package plus LOI (ALS Chemex codes: ME-XRF06 and OA-GRA06), the 47 elements four acid ICP-MS package (ALS Chemex code: ME-MS61) and complete rare earth package (ALS Chemex code: ME-MS82). A complete description of analytical methods is available in the ALS Chemex Home Page (www.alsglobal.com).

Analysed samples (Tables 3) were arranged into five different groups representative of the main lithotypes. Granodioritic gneiss (4 samples) represents country rocks collected away from brecciation and/or metasomatic alteration. Orthopyroxenitite (9 samples) and sulfide-bearing orthopyroxenitite (6 samples) are rocks consisting mainly of orthopyroxenes, the latter showing mild to moderate sulfidization along fractures and veins. Sulfide-rich rocks (8 samples) are representative of brecciated sulfide-apatite-rich zones. Fine-grained mafic rocks (6 samples) represent mafic dikes with intergranular texture. The plots of major elements versus MgO (Figures 13 and 14) and chondrite-normalized REE patterns (Figure 15) illustrate the main characteristics of these five distinct groups.

Granodioritic Gneisses

Granodioritic gneisses are characterized by low MgO (0.52 to 2.62 wt. %) and Fe_2O_3 (2.57 to 5.60 wt. %) contents combined with high SiO_2 (62.46 to 70.66 wt. %), Al_2O_3 (13.91 to 15.37 wt. %), Na_2O (3.27 to 4.31 wt. %) and K_2O (2.22 to 4.76 wt. %). These compositional features reflect rocks consisting mainly of quartz, KF and plagioclase (rich in albite component). The plot of chondrite-normalized REE elements for different group of rocks is shown in Figure 15. Samples of granodioritic gneiss have very consistent trends with progressive enrichment toward LREE elements (Figure 15). These samples have chondrite-normalized Ce/Yb ratios between 45.8-110.1 and distinct Eu anomaly.

Orthopyroxenitites and Sulfide-bearing Orthopyroxenitites

Orthopyroxenitites are characterized by high MgO (23.91 to 27.58 wt. %) and total iron (19.48 to 22.94 wt. %) contents combined with low Al_2O_3 (0.55 to 1.52 wt. %), CaO (0.19 to 0.85 wt. %), Na_2O (0.13 to 0.36 wt. %) and K_2O (0.04 to 0.24 wt. %) contents. These compositional features reflect mainly monominerallic rocks consisting of orthopyroxene. Orthopyroxenitites have extremely low Cr_2O_3 (< 0.01 wt. %; or 22 to 71 ppm Cr) and TiO_2 (0.03 to 0.14 wt. %) contents, indicating distinctive compositional features when compared to orthopyroxenites of magmatic origin. Sulfide-bearing orthopyroxenitites follow the same compositional features described for orthopyroxenitites, except for higher sulphur (0.42 to 5.33 wt. %) and associated compositional changes related to interaction with sulfide-rich zones. Samples of orthopyroxenites have low REE contents, highly variable REE patterns (Figure 15) and low chondrite-normalized Ce/Yb ratios (between 0.83-4.03). Several REE values for orthopyroxenites are close to or below detection limits. Therefore, their highly variable REE patterns should be interpreted with discretion. These variations may result from relatively higher analytical uncertainities from analyses with low REE contents. Sulfide-bearing orthopyroxenitites have REE patterns similar to orthopyroxenitites, except for sample LSK29 (Figure 15). This sample has higher REE content and LREE enriched trend.

Sulfide-rich Rocks

Sulfide-rich rocks (S > 10 wt. %) have high total iron oxides (27.10 to 44.71 wt. %) and P_2O_5 (4.20 to 20.92 wt. %) contents, reflecting their abundance in Fe-sulfides (pyrrhotite, pyrite, chalcopyrite and pentlandite) and apatite. Compositional trends for orthopyroxenitites, sulfide-

bearing orthopyroxenitites and sulfide-rich rocks suggest that sulfide-bearing rocks result from mild to extensive replacement of orthopyroxene-bearing rocks. These compostional trends are shown for selected elements in Figure 14, together with compositional range for their most abundant minerals (orthopyroxene, apatite and Fe-bearing sulfides). Lithogeochemical data indicate that sulfide-rich zones evolved through progressive replacement of orthopyroxenites (orthopyroxene) by sulfide-apatite bearing veins. Samples LSK29, an orthopyroxenitite with abundant apatite-sulfide bearing veins, and LSK21, a brecciated apatite-sulfide rock with relicts of partially replaced orthopyroxene crystals or orthopyroxenitite fragments, point out the geochemical path followed duing this replacement process. Sulfide-rich samples are characterized by high REE contents and progressive enrichment toward LREE (Figure 15). These samples have strong negative Eu anomaly and chondrite-normalized Ce/Yb ratios between 13.43-45.73. Samples LSK29 and LSK21 have identical REE patterns and REE contents intermediate between orthopyroxenites and sulfide-rich rocks. These features reinforce their interpretation that samples LSK29 and LSK21 represent highly transformed orthopyroxenites, indicated by petrographic descriptions and major element contents. REE contents in sulfide-bearing rocks are correlated with the abundance of apatite. This correlation is illustrated by the plot of Ce versus P_2O_5 contents (Figure 16) for orthopyroxenitites, sulfide-bearing orthopyroxenitites and sulfide-rich rocks. Figure 16 also indicates that regional country rocks (granodioritic gneisses) are compositionally distinct of the trend defined by orthopyroxenites and sulfide-rich samples.

Mafic Rocks

Fine-grained mafic rocks form a highly variable group of mafic to intermediate (SiO_2 between 47.97-65.83 wt. %) igneous rocks. MgO contents (3.89-10.35 wt. %) and MgO/MgO+FeO ratios (< 0.46) indicate fractionated compositions. Poor correlation between major oxides and MgO, together with highly variable trace element contents (including Cr) suggests that dikes from different magmatic compostions were sampled. Samples of mafic-intermediate dikes have different chondrite-normalized REE patterns (Figure 15). Four samples of mafic dikes are characterized by mild progressive enrichment toward LREE (Figure 15), while two samples have flat pattern for HREE and mild progressive enrichment for the LREE. The first group of samples has higher chondrite-normalized Ce/Yb (3.80-7.58) and Gd/Yb (1.76-2.01) ratios, when compared to the second one (Ce/Yb = 1.90-2.82; Gd/Yb =1.10-1.18).

Table 4 – Chemical composition of GT-34 samples. Major elements and S (wt. %), trace elements and REE (ppm).

rock type	Sulfide-Rich Rocks								Sulfide-bearing Orthopyroxenitite						Orthopyroxenitite								
sample	LSK-005	LSK-008	LSK-012	LSK-020	LSK-021	LSK-023	LSK-027	LSK-028	LSK-007	LSK-013	LSK-017	LSK-018	LSK-019	LSK-029	LSK-010	LSK-015	LSK-016	LSK-025	LSK-030	LSK-031	LSK-032	LSK-033	LSK-034
SiO2	1.53	1.78	3.64	4.27	28.57	13.46	10.21	6.88	49.61	50.23	49.72	48.15	49.40	42.17	51.31	51.08	50.39	51.10	51.22	50.97	51.20	51.14	51.21
Al2O3	0.16	0.04	0.59	0.58	4.06	2.49	1.34	0.90	0.59	0.82	0.62	0.47	0.52	1.23	0.70	0.59	0.55	0.79	0.81	1.52	0.77	0.78	1.15
Fe2O3	44.71	39.00	36.86	35.57	27.10	31.64	15.26	38.86	23.09	21.98	22.53	24.52	23.37	24.67	20.80	20.90	21.34	21.76	22.94	20.21	20.34	21.05	19.48
CaO	12.37	15.72	17.40	18.80	8.23	14.83	29.96	16.87	0.21	0.24	0.33	0.21	0.20	3.04	0.20	0.19	0.45	0.66	0.49	0.85	0.19	0.27	0.50
MgO	0.66	0.81	1.44	1.19	8.68	4.88	3.01	3.34	25.75	25.89	25.55	24.56	25.55	21.00	26.19	27.31	26.11	25.10	23.91	25.32	27.58	26.20	27.05
Na2O	<0.01	<0.01	0.02	0.07	0.85	0.24	<0.01	0.11	0.15	0.17	0.12	0.07	0.19	0.11	0.23	0.19	0.20	0.18	0.23	0.36	0.19	0.13	0.27
K2O	0.04	0.02	0.06	0.05	0.36	0.25	0.06	0.10	0.09	0.23	0.06	0.05	0.07	0.15	0.10	0.06	0.06	0.04	0.24	0.24	0.13	0.13	0.13
Cr2O3	0.01	<0.01	0.01	<0.01	0.01	0.01	<0.01	<0.01	0.01	<0.01	<0.01	<0.01	<0.01	<0.01	0.01	<0.01	0.01	<0.01	<0.01	<0.01	0.01	0.01	<0.01
TiO2	0.03	0.02	0.04	0.05	0.18	0.21	0.04	0.07	0.05	0.06	0.05	0.06	0.03	0.10	0.07	0.03	0.09	0.05	0.13	0.10	0.11	0.05	0.14
MnO	0.04	0.05	0.06	0.06	0.11	0.09	0.13	0.09	0.25	0.23	0.24	0.22	0.23	0.20	0.22	0.24	0.25	0.25	0.24	0.22	0.22	0.24	0.20
P2O5	8.96	11.44	12.30	13.05	4.20	8.79	20.92	10.91	0.04	0.02	0.04	0.01	0.02	1.47	0.02	0.02	0.04	0.02	0.09	0.02	0.01	0.02	0.02
LOI	10.75	11.20	9.46	9.59	7.70	7.57	7.73	8.84	-0.25	-0.14	-0.02	0.43	-0.31	1.88	-0.38	-0.64	0.39	-0.13	-0.78	-0.02	-0.86	-0.67	-0.32
Total	79.27	80.08	81.88	83.28	90.08	84.48	88.68	86.99	99.59	99.74	99.27	98.76	99.28	96.03	99.49	99.98	99.90	99.82	99.53	99.79	99.92	99.34	99.84
S	>10	>10	>10	>10	>10	>10	>10	>10	1.07	0.65	0.42	2.48	1.11	5.33	0.06	0.01	0.15	0.03	0.09	0.02	0.01	0.01	0.13
Ag	na	na	na	na	na	na	na	na	na	na	na	na	na	na	0.05	0.03	0.05	0.12	0.03	0.04	0.03	0.04	0.02
As	5.8	<0.2	<0.2	<0.2	5.2	<0.2	43.0	<0.2	0.2	<0.2	<0.2	<0.2	<0.2	0.2	<0.2	<0.2	<0.2	0.2	<0.2	0.4	<0.2	<0.2	<0.2
Ba	10	10	10	10	100	60	10	20	50	50	40	20	30	30	40	20	40	10	60	50	40	40	30
Be	<0.05	<0.05	0.06	0.15	0.30	0.23	0.23	0.11	0.05	<0.05	<0.05	<0.05	<0.05	0.09	<0.05	<0.05	<0.05	0.06	0.05	0.09	<0.05	<0.05	0.06
Bi	0.08	0.03	0.03	<0.01	1.02	<0.01	3.83	<0.01	0.03	0.02	0.01	0.03	0.02	0.04	0.01	<0.01	0.01	0.01	0.01	0.02	0.01	0.02	0.01
Cd	<0.02	<0.02	<0.02	<0.02	<0.02	<0.02	<0.02	<0.02	0.10	0.04	0.04	0.07	0.10	0.06	0.06	0.02	0.04	0.06	0.03	0.02	0.03	0.03	0.06
Co	na	na	na	na	na	na	na	na	na	na	na	na	na	na	63.0	55.8	69.1	57.3	73.6	57.1	54.4	58.8	65.3
Cr	5	1	8	13	76	32	21	8	22	20	28	26	44	24	35	31	71	22	29	22	44	32	26
Cs	<0.05	<0.05	<0.05	<0.05	0.62	0.08	<0.05	<0.05	0.20	0.28	0.16	0.13	0.15	0.15	0.21	0.09	0.20	0.14	0.18	0.22	0.14	0.14	0.16
Cu	na	na	na	na	na	na	na	na	na	na	na	na	na	na	21.1	10.6	159.0	14.1	50.4	21.2	19.5	16.2	129.0
Ga	2.29	2.36	3.78	4.38	8.63	9.07	6.17	4.57	4.09	4.52	4.15	3.81	3.87	5.47	4.13	3.58	3.70	4.25	4.52	6.18	4.62	4.65	5.10
Ge	4.96	4.97	4.50	4.40	2.62	3.57	2.76	4.35	0.29	0.23	0.23	0.48	0.28	0.95	0.18	0.14	0.18	0.18	0.21	0.18	0.16	0.18	0.19
Hf	0.1	0.1	0.2	0.2	0.8	0.4	0.3	0.4	0.1	0.1	0.1	<0.1	<0.1	0.2	<0.1	<0.1	0.1	0.1	<0.1	0.1	<0.1	<0.1	0.3
In	<0.005	<0.005	<0.005	<0.005	<0.005	<0.005	<0.005	<0.005	<0.005	<0.005	0.01	<0.005	<0.005	0.01	<0.005	<0.005	<0.005	<0.005	<0.005	0.01	<0.005	<0.005	0.01
Li	1.2	1.6	3.4	1.7	10.5	4.10	5.5	3.0	2.9	4.5	3.8	3.4	3.7	4.7	2.2	1.6	3.6	4.0	4.3	3.5	3.0	2.8	3.7
Mn	104	99	115	125	554	288	291	229	1775	1650	1720	1625	1725	1305	1615	1670	1785	1735	1805	1515	1650	1765	1500
Mo	15.25	14.15	13.40	12.10	7.51	10.90	8.53	12.85	1.46	0.55	1.00	1.68	0.97	3.10	0.71	0.27	0.56	0.20	0.79	0.29	0.53	0.42	0.31
Nb	1.1	0.2	1.2	2.2	5.5	9.7	1.5	3.4	0.5	1.6	0.5	0.3	0.3	3.0	0.8	0.5	0.4	1.1	1.2	2.8	0.8	0.8	1.6
Ni	na	na	na	na	na	na	na	na	na	na	na	na	na	na	917	617	1420	719	1085	701	594	626	1195
P	>10000	>10000	>10000	>10000	>10000	>10000	>10000	>10000	90	160	110	10	20	7310	100	20	160	50	250	40	30	50	20
Pb	na	na	na	na	na	na	na	na	na	na	na	na	na	na	4.1	1.4	2.4	3.5	1.0	2.5	2.5	2.3	2.5
Rb	1.4	0.3	1.6	0.4	11.8	4.5	0.1	2.1	2.6	9.9	2.5	1.2	1.7	2.7	4.1	1.9	2.6	0.9	9.6	7.9	5.4	5.0	4.4

rock type	Sulfide-Rich Rocks								Sulfide-bearing Orthopyroxenitite						Orthopyroxenitite								
sample	LSK-005	LSK-008	LSK-012	LSK-020	LSK-021	LSK-023	LSK-027	LSK-028	LSK-007	LSK-013	LSK-017	LSK-018	LSK-019	LSK-029	LSK-010	LSK-015	LSK-016	LSK-025	LSK-030	LSK-031	LSK-032	LSK-033	LSK-034
Re	0.51	0.47	0.40	0.40	0.28	0.35	0.25	0.40	0.02	0.01	0.01	0.03	0.02	0.08	0.00	<0.002	0.00	<0.002	0.00	<0.002	<0.002	<0.002	0.00
Sb	0.30	0.12	0.06	0.05	0.08	<0.05	0.05	<0.05	0.05	<0.05	<0.05	<0.05	<0.05	<0.05	<0.05	<0.05	<0.05	<0.05	0.06	<0.05	<0.05	<0.05	<0.05
Se	105	106	102	99	60	75	50	84	5	4	3	11	5	20	1	1	2	2	2	2	1	1	2
Sn	1.8	0.8	0.8	1.3	2.0	3.3	1.3	1.6	0.3	0.2	0.2	<0.2	0.2	1.1	0.3	<0.2	0.2	0.4	0.2	0.8	0.3	0.2	0.6
Sr	167.0	222.0	212.0	171.5	130.5	189.0	219.0	221.0	7.7	3.9	4.9	3.7	4.4	38.4	5.4	3.9	5.1	4.1	7.4	7.3	5.2	5.1	5.6
Ta	0.05	<0.05	0.07	0.10	0.24	0.38	0.09	0.13	<0.05	0.06	<0.05	<0.05	<0.05	0.10	<0.05	<0.05	<0.05	0.05	0.07	0.11	<0.05	<0.05	0.07
Te	26.10	22.20	21.40	21.20	12.80	17.75	10.90	21.90	0.88	0.49	0.31	1.72	0.75	4.39	0.08	<0.05	0.14	<0.05	0.10	<0.05	<0.05	<0.05	0.10
Th	2.6	2.0	7.3	7.3	17.2	8.8	12.4	5.7	0.3	1.6	0.3	0.4	0.4	0.8	0.6	0.5	0.4	0.8	0.7	0.9	2.1	1.7	1.5
V	19	7	26	42	125	181	46	64	44	50	47	39	41	80	46	34	43	46	45	82	58	58	67
W	0.4	0.3	0.3	0.2	0.4	0.2	0.6	0.1	0.2	0.2	0.1	0.1	0.1	0.1	0.1	0.1	0.2	0.1	0.1	0.1	0.2	0.1	0.1
Zn	na	na	na	na	na	na	na	na	na	na	na	na	na	na	82	76	80	97	80	74	69	70	73
Zr	1.0	<0.5	2.9	3.3	24.9	7.3	6.5	8.6	2.1	2.9	1.8	<0.5	2.1	3.3	0.8	1.2	1.5	1.5	1.1	3.2	2.5	1.2	10.3
La	193.5	260.0	309.0	294.0	23.2	181.0	306.0	226.0	2.2	1.5	1.8	<0.5	0.9	39.8	1.6	0.9	3.4	1.4	2.0	1.8	1.0	0.9	1.8
Ce	428.0	565.0	665.0	645.0	53.2	414.0	762.0	497.0	4.6	3.7	4.3	0.6	1.9	95.8	3.5	1.5	5.8	4.4	4.3	7.5	2.1	1.9	5.4
Pr	50.4	66.6	76.7	79.1	6.7	51.4	97.7	59.5	0.5	0.5	0.5	0.1	0.2	12.0	0.4	0.1	0.5	0.8	0.5	1.6	0.2	0.2	1.0
Nd	189.5	255.0	289.0	305.0	27.2	204.0	382.0	228.0	1.9	2.3	1.8	<0.5	0.7	48.5	1.3	0.5	1.8	4.0	2.1	9.1	1.0	0.8	5.4
Sm	29.5	39.4	44.5	50.4	5.3	37.9	62.4	36.8	0.4	0.6	0.4	0.1	0.2	9.2	0.3	0.1	0.4	1.3	0.5	3.1	0.3	0.2	1.8
Eu	2.5	3.3	4.6	4.9	0.5	3.5	5.3	3.6	<0.1	0.1	0.1	<0.1	<0.1	1.0	<0.1	<0.1	0.1	0.2	0.1	0.4	<0.1	<0.1	0.2
Gd	25.3	35.5	40.3	43.3	4.8	33.9	53.0	32.8	0.4	0.6	0.4	0.1	0.1	8.4	0.2	0.1	0.3	1.2	0.5	3.2	0.3	0.2	1.8
Tb	2.7	3.9	4.4	4.8	0.6	4.3	5.8	3.7	0.1	0.1	0.1	<0.1	<0.1	1.1	<0.1	<0.1	0.1	0.2	0.1	0.5	0.1	<0.1	0.3
Dy	10.7	15.4	18.5	20.5	2.9	20.3	23.2	15.6	0.3	0.6	0.4	0.1	0.2	5.2	0.3	0.2	0.4	1.1	0.3	3.1	0.4	0.2	1.9
Ho	1.9	2.6	3.2	3.7	0.6	3.7	3.9	2.8	0.1	0.1	0.1	<0.1	<0.1	1.0	0.1	0.1	0.1	0.2	0.1	0.6	0.1	0.1	0.4
Er	5.1	7.2	8.9	10.0	1.6	10.2	10.9	7.6	0.3	0.4	0.3	0.1	0.2	2.7	0.2	0.2	0.3	0.6	0.2	1.8	0.4	0.3	1.2
Tm	0.5	0.7	0.9	1.1	0.2	1.2	1.1	0.8	0.1	0.1	0.1	<0.1	<0.1	0.3	<0.1	<0.1	0.1	0.1	<0.1	0.2	0.1	0.1	0.2
Yb	2.6	3.6	5.2	5.8	1.1	6.9	6.2	4.4	0.5	0.5	0.5	0.1	0.4	2.1	0.3	0.4	0.4	0.6	0.5	1.6	0.7	0.6	1.4
Lu	0.3	0.5	0.7	0.7	0.2	0.9	0.8	0.6	0.1	0.1	0.1	<0.1	0.1	0.3	0.1	0.1	0.1	0.1	0.1	0.2	0.1	0.1	0.2
Y	49.0	72.4	88.0	95.7	13.6	94.5	97.3	70.5	1.9	3.4	2.4	<0.5	1.3	24.1	1.4	1.3	2.2	5.2	2.1	15.5	2.7	1.7	9.6
Th	5	2	9	8	3	9	12	6	<1	2	<1	<1	<1	1	1	1	<1	1	1	1	2	2	2
U	<0.5	0.5	1.5	1.3	<0.5	1.0	2.1	0.7	<0.5	<0.5	<0.5	<0.5	<0.5	<0.5	<0.5	<0.5	<0.5	<0.5	<0.5	<0.5	<0.5	<0.5	<0.5

Table 4 – Chemical composition of GT-34 samples. Major elements and S (wt. %), trace elements and REE (ppm). (Cont.)

rock type	Fine-grained Mafic						Gneiss			
sample	LSK-014	LSK-035	LSK-036	LSK-037	LSK-038	LSK-024	LSK-001	LSK-002	LSK-003	LSK-004
SiO2	51.66	52.02	54.83	51.32	47.97	65.83	70.66	62.46	66.03	70.46
Al2O3	14.91	13.37	13.46	13.03	13.92	12.45	14.97	15.37	15.48	13.91
Fe2O3	14.02	11.15	9.18	12.13	13.76	5.38	2.57	4.87	5.60	2.88
CaO	6.88	5.60	9.70	5.70	10.60	4.59	1.67	5.38	3.11	2.52
MgO	5.82	9.05	3.98	10.35	7.04	3.89	0.52	2.62	1.43	1.22
Na2O	3.75	4.70	4.42	4.31	3.01	4.83	3.61	4.29	4.31	3.27
K2O	0.28	0.43	0.39	0.44	0.39	0.43	4.76	2.22	2.99	4.35
Cr2O3	<0.01	<0.01	<0.01	<0.01	0.03	0.03	<0.01	0.01	<0.01	<0.01
TiO2	1.02	1.82	1.99	1.94	1.49	0.31	0.26	0.58	0.46	0.30
MnO	0.16	0.14	0.07	0.11	0.13	0.08	0.03	0.08	0.08	0.06
P2O5	0.14	0.21	0.50	0.34	0.14	0.12	0.15	0.44	0.11	0.14
LOI	-0.15	-0.11	0.04	0.03	0.11	0.26	0.37	1.50	0.25	0.58
Total	98.56	98.42	98.62	99.74	98.64	98.25	99.81	99.97	99.99	99.92
S	0.10	0.02	0.03	0.01	0.10	0.18	0.01	0.54	0.03	0.09
Ag	na	na	na	na	na	na	na	na	na	na
As	<0.2	<0.2	<0.2	<0.2	<0.2	0.2	1.3	1.1	0.8	0.6
Ba	210	130	200	80	110	160	1750	700	910	1660
Be	0.44	1.09	1.18	0.84	0.43	1.21	0.97	1.63	1.72	1.42
Bi	0.01	0.06	<0.01	<0.01	<0.01	<0.01	0.05	0.08	0.07	0.04
Cd	0.04	0.15	0.04	<0.02	0.04	0.02	0.04	0.05	0.05	0.06
Co	43.9	31.5	27.5	37.0	46.0	27.9	3.9	14.3	10.2	9.0
Cr	47	35	15	26	167	189	10	47	37	11
Cs	0.13	0.25	0.31	0.12	0.21	0.17	1.22	1.62	1.66	0.64
Cu	228.0	9.8	76.9	2.9	172.0	26.1	7.5	<0.2	26.1	76.0
Ga	14.45	11.30	19.05	14.05	19.05	14.90	17.85	20.80	22.90	18.75
Ge	0.11	0.15	0.12	0.17	0.17	0.10	0.09	0.18	0.15	0.11
Hf	1.8	3.1	4.2	3.8	2.2	3.3	3.9	1.0	1.3	1.8
In	0.02	0.07	0.04	0.02	0.05	0.01	0.01	0.04	0.03	0.05
Li	5.4	4.0	5.7	3.9	8.0	3.4	10.5	11.7	6.6	5.6
Mn	1245	1070	482	766	957	631	155	636	563	383
Mo	1.04	0.50	0.28	0.38	0.67	1.51	0.39	1.02	1.76	0.37
Nb	3.9	14.2	10.1	16.2	4.6	3.2	3.1	5.4	6.6	3.9
Ni	179.5	381.0	264.0	502.0	289.0	1145.0	4.2	29.4	17.7	12.6
P	540	940	2300	1510	640	490	510	2050	440	650
Pb	1.4	6.7	3.0	2.9	2.9	4.5	17.2	10.4	14.8	16.7
Rb	5.9	4.0	7.1	2.5	6.5	3.0	149.0	83.0	113.5	127.0

rock type	Fine-grained Mafic						Gneiss			
Re	0.00	<0.002	<0.002	<0.002	<0.002	0.01	<0.002	<0.002	<0.002	0.00
Sb	0.07	0.06	<0.05	<0.05	0.05	0.05	0.20	0.14	0.17	0.07
Se	2	1	2	2	2	2	1	1	1	1
Sn	0.5	0.6	0.9	1.5	1.5	0.6	0.7	1.8	1.7	1.7
Sr	179.0	301.0	296.0	251.0	169.5	286.0	430.0	708.0	478.0	488.0
Ta	0.23	0.75	0.58	0.65	0.28	0.30	0.32	0.23	0.53	0.19
Te	<0.05	<0.05	<0.05	<0.05	<0.05	0.21	<0.05	<0.05	<0.05	<0.05
Th	1.3	6.9	6.9	9.7	0.8	14.9	18.1	9.4	23.3	13.2
V	245	128	362	194	296	39	26	75	69	36
W	0.1	0.1	0.1	0.1	0.1	0.1	0.1	0.3	0.2	0.1
Zn	44	70	22	30	35	26	38	82	94	56
Zr	69.2	123.0	159.5	145.0	73.6	106.5	135.0	30.4	37.7	56.7
La	8.7	8.2	21.4	11.7	8.4	9.5	85.0	88.6	92.4	65.1
Ce	18.3	19.0	48.3	32.8	22.6	19.1	158.5	190.0	185.0	132.0
Pr	2.3	2.4	6.2	5.0	3.1	2.2	16.1	23.3	20.0	14.6
Nd	9.6	9.8	24.8	23.0	13.8	9.0	50.5	87.0	65.8	49.7
Sm	2.2	1.8	5.0	5.8	3.4	1.9	5.6	12.1	8.1	7.3
Eu	0.8	0.5	1.3	1.1	1.3	0.5	0.9	2.0	1.1	1.0
Gd	2.4	1.7	5.1	5.7	4.7	1.7	4.6	9.2	6.8	5.9
Tb	0.4	0.2	0.8	0.9	0.9	0.2	0.4	0.9	0.7	0.6
Dy	2.6	1.1	4.2	4.9	5.5	1.4	1.1	3.2	2.3	2.4
Ho	0.6	0.2	0.8	0.9	1.2	0.3	0.2	0.5	0.4	0.4
Er	1.7	0.7	2.5	2.8	3.6	0.8	0.7	1.6	1.2	1.1
Tm	0.3	0.1	0.4	0.4	0.5	0.1	0.1	0.2	0.1	0.1
Yb	1.8	0.7	2.4	2.4	3.3	0.7	0.4	1.1	0.9	0.8
Lu	0.3	0.1	0.4	0.3	0.5	0.1	0.1	0.2	0.1	0.1
Y	14.0	5.9	21.2	23.5	29.1	6.7	4.6	13.9	9.9	9.7
Th	1	7	6	10	1	14	22	11	27	18
U	0.5	1.1	1.6	1.6	<0.5	2.9	1.1	0.7	1.5	0.7

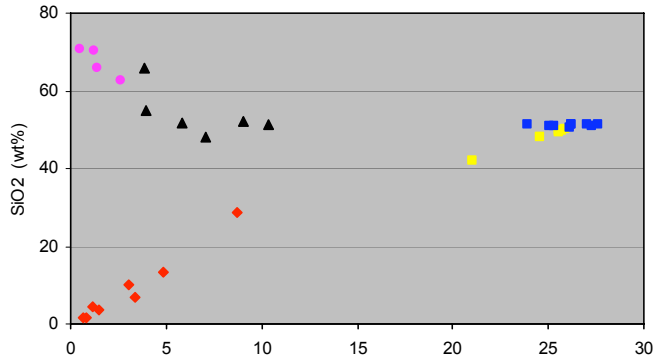
SiO2 (wt%)
80
60
40
20
0
0
5
10
15
20
25
30

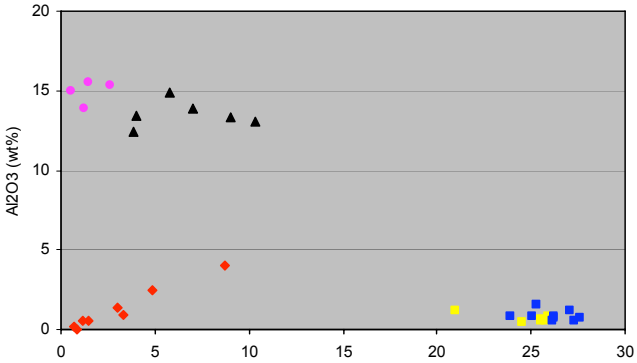
Al2O3 (wt%)
20
15
10
5
0
0
5
10
15
20
25
30

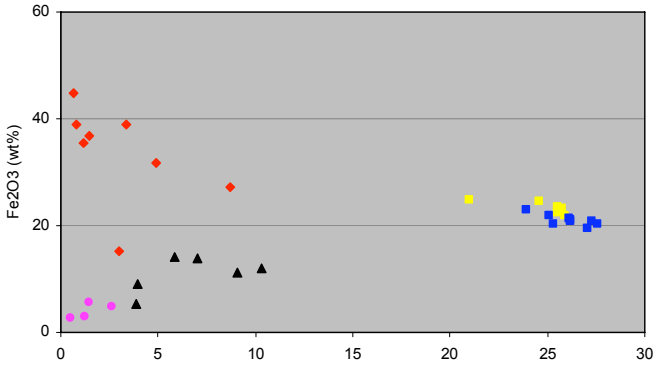
Fe2O3 (wt%)
60
40
20
0
0
5
10
15
20
25
30

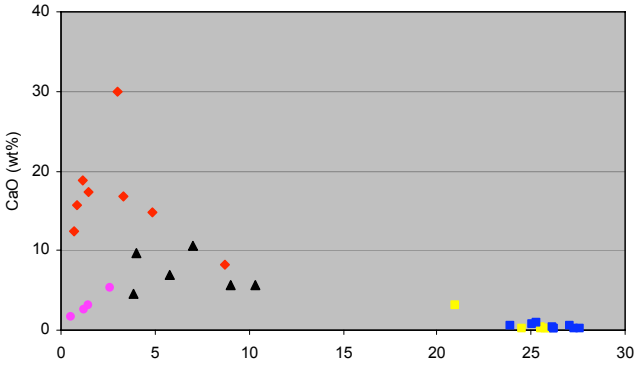
CaO (wt%)
40
30
20
10
0
0
5
10
15
20
25
30

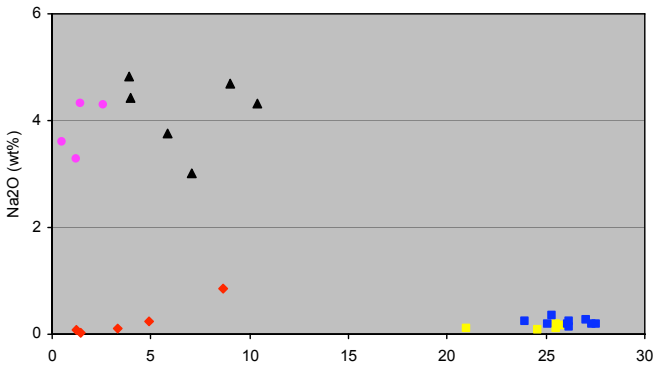
Na2O (wt%)
6
4
2
0
0
5
10
15
20
25
30

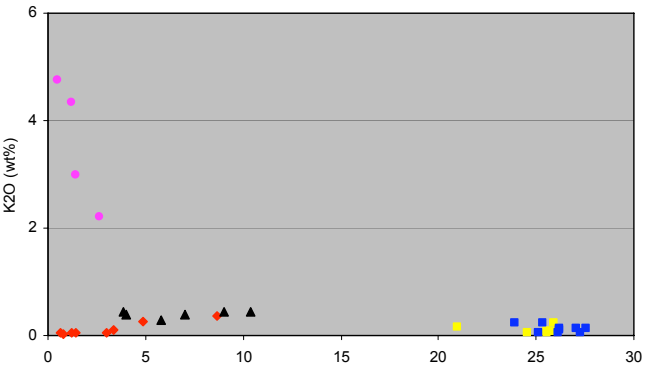
K2O (wt%)
6
4
2
0
0
5
10
15
20
25
30

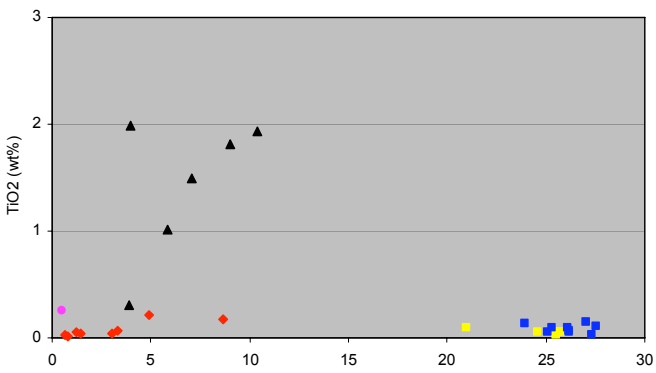
TiO2 (wt%)
3
2
1
0
0
5
10
15
20
25
30

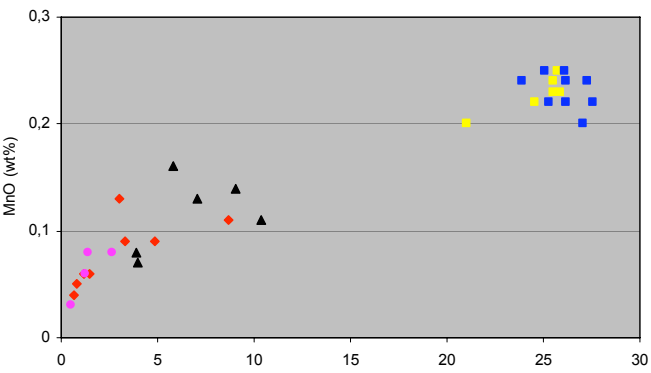
MnO (wt%)
0,3
0,2
0,1
0
0
5
10
15
20
25
30

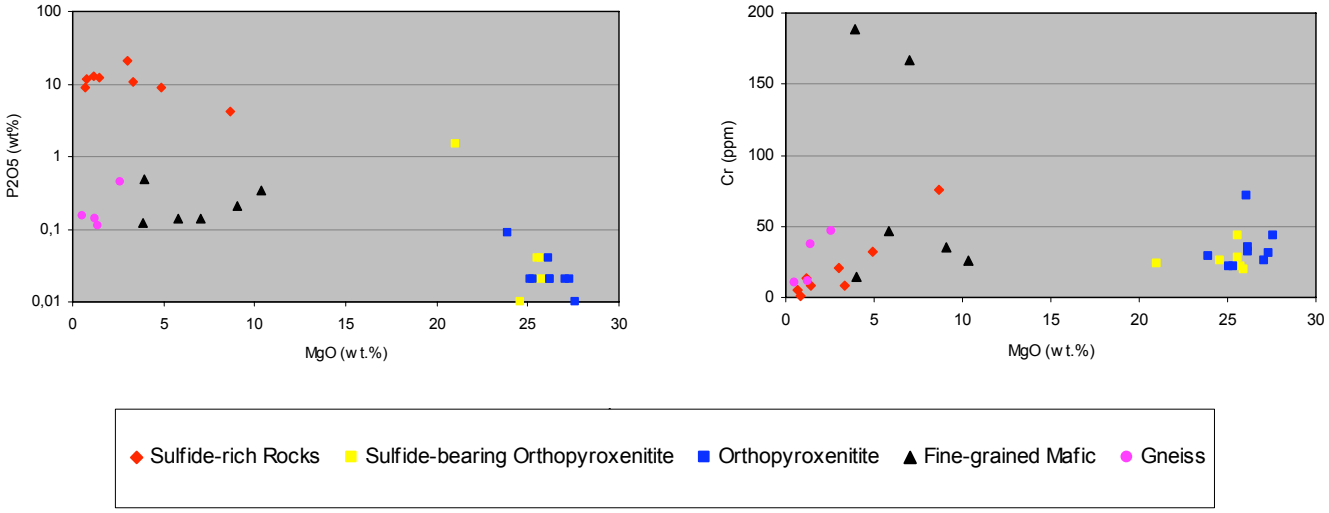

Figure 13. Plot of MgO content versus major oxides and Cr for different group of rocks of the GT-34 Prospect. See Table 4 for chemical analyses.

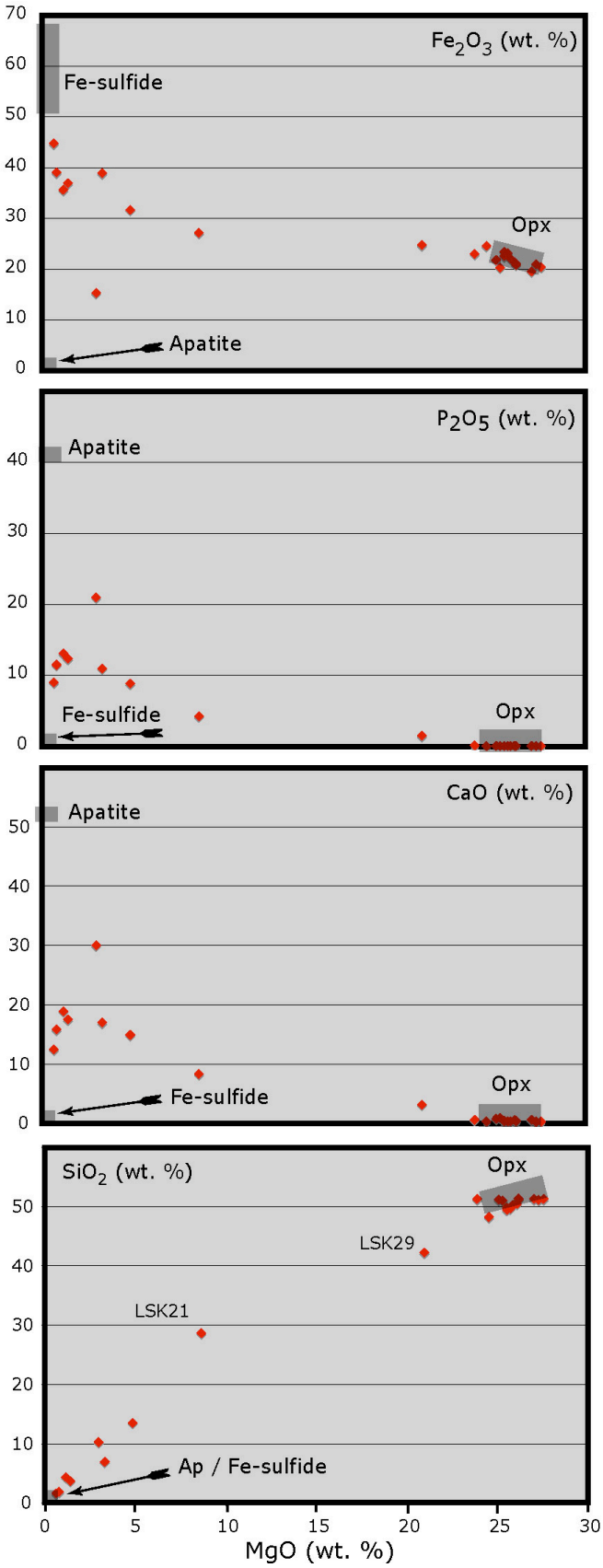

Figure 14. Plot of MgO content versus SiO_2, CaO, P_2O_5 and Fe_2O_3 (total iron calculated as Fe_2O_3) contents for orthopyroxenitite, sulfide-bearing orthopyroxenitite and sulfide-rich samples. The compostional trends of orthopyroxene and apatite (based on microprobe analyses), as well as the expected composition of the sulfide fraction (based on estimated modal compostion of the sulfide fraction), are included for comparison.

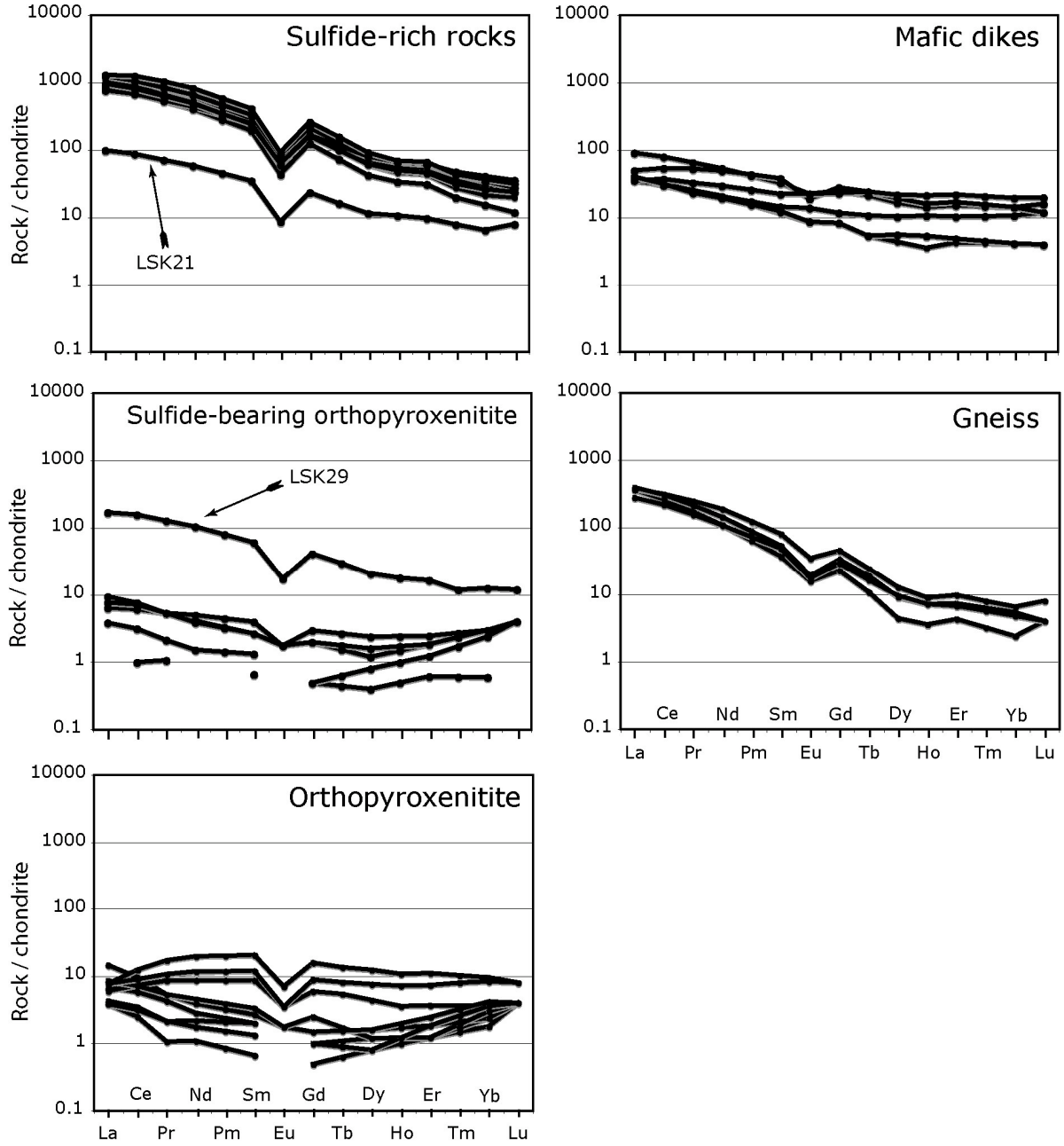

Figure 15. Chondrite-normalized REE patterns for different groups of rocks of the GT-34 Prospect. See Table 4 for chemical analyses. Normalization data from Sun and McDonough (1989).

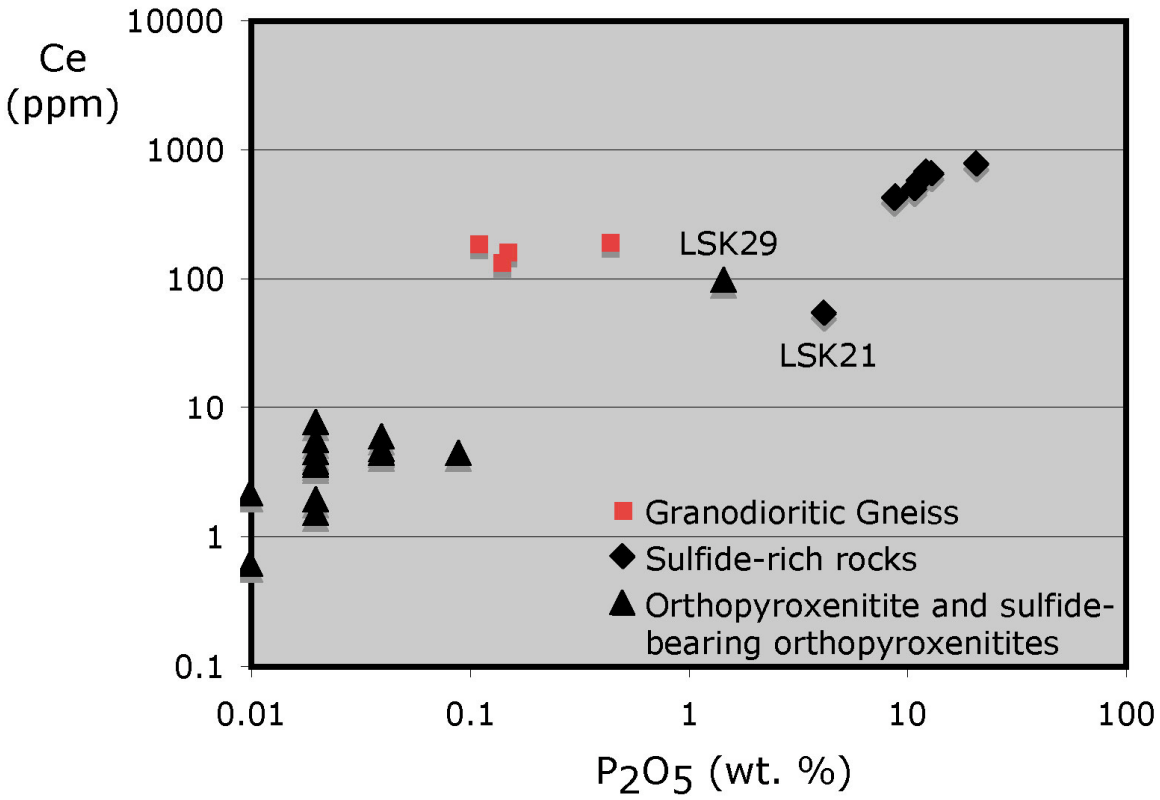

Figure 16. Plot of P_2O_5 versus Ce contents for orthopyroxenites, sulfide-bearing orthopyroxenites, sulfide-rich rocks and granodioritic gneisses. See Table 4 for chemical analyses.

Discussion

Field and petrologic-geochemical results obtained for the GT-34 Prospect indicate an unusual style of metasomatism. Rock types interpreted to result from alteration, as well as the sulfide assemblage, described in the GT-34 Prospect are distinctively different from previous descriptions of IOCG-type Cu-Au mineralizations in Carajás and worldwide. The GT-34 is also remarkably different from younger (1.8 Ga) granite-related Cu-Au mineralizations in Carajás, known to be enriched in granitophile elements such as W, Sn and Bi (Grainger et al. 2007). The following discussion will address three main questions regarding the GT-34 Prospect. How the GT-34 system evolved? How this system compare with typical 2.5 Ga Cu-Au mineralizations in Carajás? Does the GT-34 unveil an unexplored portion of regional scale IOCG-type systems?

It is worth mentioning that absolute age dating of the GT-34 Prospect metasomatic rocks is not available. The suggested correlation of the GT-34 Prospect with the widespread 2.5 Ga hydrothermal system of Carajás is based on spacial proximity with large scale matassomatic centers (Sossego and Cristalino Cu-Au deposits). It is also important to mention that robust 2.5 Ga ages for hydrothermal processes associated with IOCG-type deposits of Carajás is available just for few deposits (Bahia-Alemão and Salobo).

The GT-34 System

Interpretation of available data of the GT-34 Prospect suggests that high-temperature orthopyroxene-bearing metasomatic replacement bodies (Phase 1) developed within gneissic country rocks, followed by a late event of veining, brecciation and enrichemnt in sulfides (Phase 2). Table 5 summarizes the main features observed in the GT-34 Prospect, while Figure 17 gives the paragenetic association. The sequence of two distinct metasomatic events, the first developed prior to sulfide mineralization and the second concomitant, is characteristic of the GT-34 Prospect. These events carry several geological implications that will be addressed in the following discussion.

The indicated interpretation (Table 5) implies that orthopyroxenitites in the GT-34 are formed by metasomatism. Therefore, quartz-feldspathic gneisses (host rocks) were somehow replaced by orthopyroxenes with En contents averaging 73%, indicating significant Mg metasomatism (as well as extensive relative depletion in alkalis and Al_2O_3). Orthopyroxene is an unusual mineral in rocks formed by metasomatism and no report of metasomatic orthopyroxenitites exists in the literature. Monominerallic orthopyroxene-bearing rocks are common lithotypes in layered intrusions (an adcumulate orthopyroxenite), interpreted to result from magmatic crystallization in magma chambers. However, this interpretation is not supported by field, petrographic and geochemical data collected for the GT-34 Prospect. Orthopyroxene-bearing rocks of the GT-34 Prospect occur in irregular bodies or veins cross cutting gneissic rocks. Expected magmatic features in such irregular and small veins, including chilled margins, partially absorbed crustal xenoliths or trapped interstital liquids, are not observed in the GT-34 Prospect. Appropriate conditions for the development of adcumulate magmatic textures, typical of adcumulate-textured orthopyroxenites, demand extensive post-cumulus growth (Sparks et al., 1985; Hunter, 1996). This process demands sustained physical-chemical conditions of magmatic crystallization during post-cumulus growth, a process unlikely to occur in small scale cross cutting veins. Geological contacts of monominneralic orthopyroxenitites and host gneissic rocks usually consist of orthopyroxene-bearing rocks with variable amounts of hornblende and/or phlogopite. These rocks, including phlogopite amphibolitites, probably represent intermediate products of the metasomatic process. Orthopyroxenitites are thus considered to represent end-members of Mg±Fe metasomatism of gneissic rocks. Compositions of orthopyroxenitite indicate extremely low Cr contents, comparable with Cr contents of host gneisses. This feature results from extremely low Cr content in orthopyroxene crystals. Low Cr contents in orthopyroxene, as well as low TiO_2, CaO and Al_2O_3 contents, are incompatible with a magmatic origin for orthopyroxene crystals with En content between 68-77 % (Figure 11). Accepting that orthopyroxene in the GT-34 is not magmatic, and therefore results of a metasomatic process, implies constraints for the physical environment of this process. Orthopyroxenitites represent a chemical system consisting essentially of MgO-FeO-SiO_2 (MFS). Stability of orthopyroxene in the MFS system is favored by lower pressure and mainly anhydrous conditions (Spier, 1993). Under extreme condition (of low lithostatic pressure and low H_2O partial pressure) orthopyroxene may form at about 600°C (Spier, 1993). However, under geological conditions appropriated to sustain the extensive high-temperature metasomatic system described in the GT-34 Prospect (P > 0.5 Kb), orthopyroxene is not expected to be stable below 700 °C. Low CaO and Al_2O_3 contents also indicate that orthopyroxenes from the GT-34 crystallized at relatively low temperature, when compared with magmatic orthopyroxene, and low pressure when compared with orthopyroxenes originated under granulite facies of regional metamorphism (Spier, 1993).

The second Phase in the GT-34 system (Table 5 and Figure 17) consists of brecciation and veining of orthopyroxenitites and host gneisses, together with sulfide-apatite mineralization. This process involved the crystallization of significant amount of sulfides and apatite, thus promoting the concentration of a diverse range of elements (e.g. P, F, S, REE, Fe, Cu, Ni). Overprinting criteria indicates that sulfidization occurred during dilation and brecciation, mainly focused in the location of the most intense Mg metasomatism (Phase 1 in Tables 4 and Figure 17). Even though small sulfide-rich veins eventually cross cut host gneiss, sulfidization is always closely associated with orthopyroxenitites. The close spatial association suggests a genetic link between early alteration (Phase 1) and later sulfidization (Phase 2). However, relative enrichment and depletion of elements are distinctively different in these two events indicating that fluids associated with metasomatism, and/or physical conditions prevailing during alteration, were highly different during these events. No data (fluid inclusions, isotopes) are available to constraint the nature of the fluids and specific discussion regarding fluid compositions and causes of element concentrations would be speculative by now. Compositions of apatite and scapolite crystals indicate, however, significant abundance of Cl, suggesting that chloride complexes may have been an important component in fluids associted with sulfide-rich zones. These zones have abundant Fe-bearing sulfides (pyrrhotite, pyrite,

chalcopyrite, pentlandite) and no associated oxides. Crystallization of pyrrhotite and pyrite without Fe-oxides (magnetite or hematite) indicates conditions of high sulfur fugacity (fS_2) and low oxygen fugacity (fO_2). The temperature of crystallization is constrained by associated hornblende, suggesting temperatures above 500°C but below the stability limit of orthopyroxene (possibly < 700°C). Phase relations in the system Fe-S-O for temperatures of about 500°C (Holland, 1959) indicate appropriate fS_2 and fO_2 conditions for the sulfide assemblage of the GT-34 Prospect (Figure 18).

Table 5 - Summary of the characteristics associated with the main events of the GT-34 Prospect.

	Host Rock	**Phase 1** Mg Metasomatism Pre sulfide mineralization	**Phase 2** S-P metasomatism Syn sulfide mineralization
Dominant mineral assemblage	quartz-plagioclase- KF -amphibole	Orthopyroxene ± hornblende ± phlogopite	pyrrhotite-pyrite-apatite ±chalcopyrite ±pentlandite ±phlogopite ±hornblende ±scapolite
Main rock type	granodioritic gneiss	Orthopyroxenitite	Apatite-sulfide-rich breccias and veins.
Major components added.		Mg ± Fe	S-P-F-LREE ±Cu±Ni ±Ca
Evidence for timing		Veins cross cutting host rocks.	Brecciation and veining of orthopyroxenitites (as well as host country rocks).
Physical conditions		Temperature: >700°C Low $P(H_2O)$	Temperature: 500-700°C Low fO_2

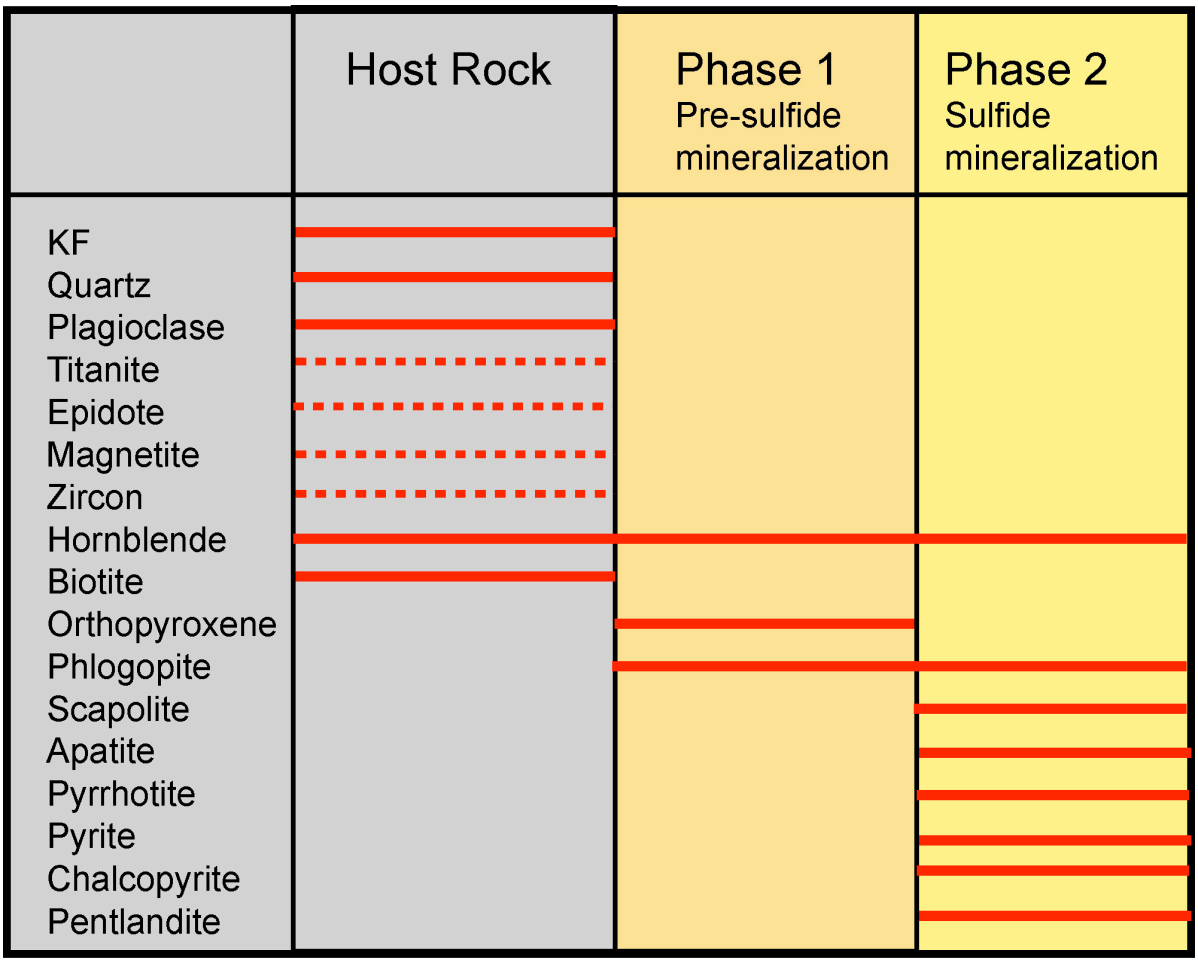

Figure 17. Mineral associations and paragenetic sequence in the GT-34 Prospect.

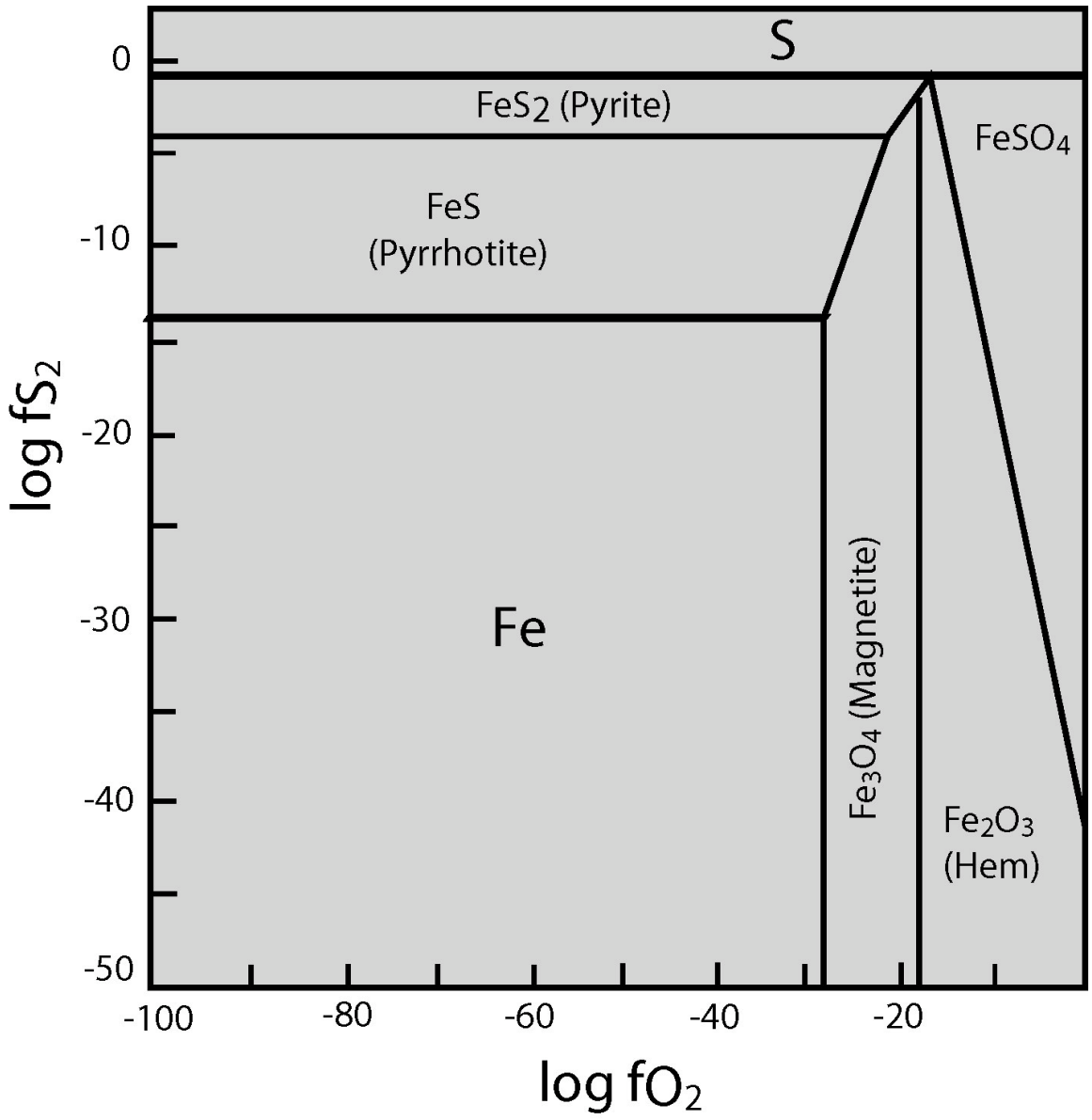

Figure 18. Phase relations of the iron sulfides and oxides at about 500°C (modified from Holland, 1959).

The GT-34 System Compared with Typical 2.5 Ga Cu-Au Mineralizations of Carajás

Table 6 summarizes some significant features of four Cu-Au deposits of Carajás and the GT-34 Prospect. This comparison is used to indicate the unusual characteristics of the GT-34 Prospect compared to Cu-Au mineralizations of Carajás.

IOCG-type deposits of Carajás are all considered to be associated with 2.7 Ga volcanic-sedimentary rocks of the Itacaiúnas Supergroup (Grainger et al., 2007). Country rocks of IOCG-type deposits in Carajás are typically low-temperature (greenschist facies) metamorphic rocks with primary structures and textures largely preserved. The Salobo host rocks are considered to have undergone metamorphism at higher grade (Lindenmayer, 1990). Fe-oxide Cu-Au deposits from Carajás show significant Fe-K±Na metasomatism expressed through different mineralogical assemblages for each deposit (Table 6). The association of different types of Fe-bearing silicates (e.g. grunerite, garnet, fayalite) and magnetite indicates the Fe metasomatism of these deposits (Table 6). Hydrothermal alteration is characterized by K metasomatism (Salobo, Bahia-Alemão) or K-Na metasomatism (Cristalino, Sossego-Sequeirinho). Ore mineralogy includes chalcopyrite associated with variable sulfides for different deposits (Table 6). Sulfides are frequently, but not

always (e.g. Sequeirinho Deposit, Monteiro, et al., 2008), associated with magnetite in the ore assemblage (Table 6). The deposits are characteristically enriched in LREE and U-Th, and ore is usually associated with uraninite, monazite and apatite (Table 6). U-Pb dating (SHRIMP II) for hydrothermal monazite of the Bahia-Alemão deposit gives and age of 2575±12 Ma (Tallarico et al., 2005). This age confirms the epigenetic nature of the mineralization, developed in Archean (2.7 Ga) country rocks. All these features are typical of deposits of the Fe-oxide Cu-Au group (Hitzman et al., 1992; 2000), suggesting the existence of a 2.57 Ga regional scale hydrothermal system in Carajás.

Metasomatism and sulfide mineralization of the GT-34 is located within older basement gneissic-migmatitic rocks of the Xingu Complex, probably implying a much deeper crustal level for the metasomatic system. Fe-K-Na metasomatism, typical of IOCG-type deposits (Hitzman et al., 1992; 2000), does not occur in the GT-34 Prospect. Even though scapolite-rich rocks associated with sulfide-apatite zones indicate enrichment in Na, and phlogopite-rich samples indicate enrichment in K, their occurrence are localized and do not characterize an extensive metasomatic event. Their restricted occurrence does not compare with typical K-Na metasomatism of IOCG-type deposits. The GT34 prospect has an extensive early alteration (Mg metasomatism) followed by widespread later sulfidization. Mg metasomatism is indicated by orthopyroxenitites (orthopyroxene with En content averaging 73 %) replacing quartz-feldspathic gneiss. Orthopyroxene-bearing assemblages indicate high temperature for metasomatism, possibly above 700°C. The later sulfidization produces sulfide-apatite bearing rocks. These rocks have abundant Fe-bearing sulfides (pyrrhotite, pyrite, chalcopyrite, pentlandite) without associated oxides. Crystallization of pyrrhotite and pyrite without Fe-oxides (magnetite or hematite) indicates conditions of high sulfur fugacity (fS_2) and low oxygen fugacity (fO_2) for the GT-34 Prospect at the indicated temperature (Figure 18). It is worth mentioning that phase relations of the iron sulfides and oxides change with temperature, implying that iron oxides (hematite and magnetite) are stable at lower fO_2 with decreasing temperature (Holland, 1959). Comparison of the sulfide assemblage of the GT34 Prospect with sulfide-oxide assemblages of different IOCG-type deposits in Carajás, as indicated in Table 6, does not suggest, however, that temperature alone may explain such differences.

Characteristics of the GT-34 Prospect suggest that metasomatism occurred under higher temperature and lower fO_2 conditions, compared to Cu-Au deposits in Carajás. These features possibly indicate that metasomatism and sulfidization of the GT-34 Prospect represent deep zones (e.g. deeper crustal level) of the regional 2.5 Ga Cu-Au ore-forming system of Carajás.

Table 6 - Comparison of IOCG-type deposits in Carajás and the GT-34 Prospect.

Deposit	Bahia-Alemão	Salobo	Sossego-Sequeirinho	Cristalino	GT-34
Country Rock	Itacaiúnas Spg (2.7 Ga)	Itacaiúnas Spg (2.7 Ga)	Itacaiúnas Spg (2.7 Ga)	Itacaiúnas Spg (2.7 Ga)	Xingu Complex (~ 2.9 Ga)
Age	2.57 Ga	2.57 Ga	(?)	(?)	(?)
Size	219 Mt	789 Mt	355 Mt	~ 500 Mt	na
Grade	1.4%Cu, 0.86 g/t Au	0.95%Cu, 0.52 g/t Au	1.1%Cu, 0.28 g/t Au	1.0%Cu, 0.3 g/t Au	na
Metasomatism	Fe-K±Na	Fe-K	K-Na	Fe-K-Na	Mg
Sulfide Association	Cp±Py±Bn	Cp-Bn-Cs	Cp±Py	Cp±Py	Po-Py-Cp-Pn
Fe silicate/oxide	Grunerite-Mag	Grunerite-Fayalite-Grt-Mag	Grunerite-Mag	Magnetite	None
REE-P minerals	Allanite-monazite-Apatite	Allanite-Apatite	Monazite-Allanite	Allanite-Apatite	Apatite
U-Th minerals	Uraninite, thorite	Uraninite	Uraninite	Uraninite	None
References	Grainger et al. (2007) Tallarico et al. (2005)	Lindenmayer (1990) Réquia et al. (2003) Grainger et al. (2007)	Monteiro et al. (2008)	Huhn et al. (1999, 2000) Grainger et al. (2007).	This study.

The GT-34 System and IOCG-type Deposits

Iron oxide-copper-gold (IOCG) deposits comprise a wide range of epigenetic mineralizations, including several world-class Cu-Au deposits (Hitzman et al., 1992; 2000). Even though IOCG deposits are now considered a well-recognized style of mineralization, our understanding of the genesis and evolution of the ore-forming system is controversial. A review of the main point of contential (e.g. role(s) of coeval intrusions, origin of fluids, sources of metals, sulphur and ligands in the ore-forming fluids, among others) is beyond the scope of this study.

The close association of iron oxides and Cu-Au in IOCG-type deposits provides a successful exploration guide being used worldwide. Targetting criteria use combined geological, geophysical and geochemical characteristics derived from the intimate relationship of iron oxides and ore. Even though IOCG-type deposits exhibit a wide range of mineralogical and chemical association, they are usually defined in terms of two main end-members, the hematite-rich and the magnetite-rich types (Hitzman, 2000). These types were considered to form the end-members of a continuum ore-forming system (Hitzman et al., 1992), ranging from deeper level magnetite-rich environment to shallow oxidizing hematite environment. Our study of the GT-34 Prospect provides data suggesting the existence of a deeper high-temperature and low fO_2 zones for the Cu-Au mineralizing system in Carajás. These inferred deep zones have distinctively different geological features, indicated by Mg metasomatism (orthopyroxenitites), pyrrhotite-pyrite sulfide assemblages and none associated iron-oxides. Robust geochronological age dating of the GT-34 metasomatism is neccessary to conciliate this process with regional hydrothermal activities in Carajás. Similar ages will create new insights to understand IOCG-type metalogenesis in Carajás and worlwide.

Conclusion

This study did not aimed to give a comprehensive final model for the origin of the GT-34 Prospect, but rather to unveil a new type of metasomatic alteration in the Carajás Mineral Province. The GT-34 Prospect is likely to represent a small portion of a much larger system. Therefore, our data set constrains for the physical and chemical conditions prevailing during metasomatic alteration at this site. Our study of the GT-34 Prospect provided data suggesting the existence of a deeper high-temperature and low fO_2 zones for the Cu-Au mineralizing system in Carajás. The style of metasomatic alteration of the GT-34 Prospect is distinctively different from typical IOCG-type Cu-Au mineralizations in Carajás. The rocks formed by metasomatism in the GT-34 are not Fe-enriched, are free of iron oxides (magnetite and/or hematite), include abundant orthopyroxene-bearing metasomatic rocks (orthopyroxenitite) and have abundant pyrrhotite and pyrite in the sulfide assemblage. These characteristics suggest that alteration in the GT-34 occurred under high-temperature and low fO_2 conditions, possibly representing deep zones of the regional 2.5 Ga ore-forming system of Carajás.

The Carajás region is well known for hosting several world-class deposits, standing as one of the richest mineral provinces in the world. Recent studies of mineral deposits in Carajás indicate some unique characteristics for their mineralizations. These features have challenged widely accepted concepts for the origin of mineral deposits, opening new opportunities for academic research and mineral exploration. Recent studies indicating that world-class iron deposits of Carajás are related to extensive hydrothermal alteration derived from Paleoproterozoic intrusions (Lobato et al., 2005), challenged the notion that they formed together with the Archean volcanic-sedimentary sequence. The recent discovery in Carajás of PGE mineralizations hosted by gabbronorite without associated immiscible sulfides and/or chromitites (Ferreira Filho et al., 2007), have also challenged the generally accepted concept for the origin of PGE deposits. The unique characteristics described for the GT-34 Prospect in this study, may provide new insights to improve the still controvertial models for the origin of

IOCG-type deposits.

Acknowledgments

This study was partially supported by VALE. The company's Exploration Manager for Brazil (Dr. Noevaldo Teixeira) is acknowledged for providing access for drill cores as well as available geological, geophysical and geochemical exploration data. C.F. Ferreira Filho is grateful to the Brazilian Research Council (CNPq) for continuous support to research activities and for research grants.

References

Araújo, O.J.B., Maia, R.G.N., João, X.S.J., and Costa, J.B.S., 1988, A megaestruturação arqueana da Folha Serra dos Carajás: in Congresso Latino Americano de Geologia, Anais, Belém-Brasil, v. 1, p. 324-338.

Araújo, O.J.B., and Maia, R.G.N., 1991, Projeto especial mapas de recursos minerais, de solos e de vegetação para a área do Programa Grande Carajás; Subprojeto Recursos Minerais; Folha SB.22-Z-A Serra dos Carajás - Estado do Pará: DNPM/CPRM, Brasilia, 136 p.

Avelar, V.G., Lafon, J.M., Correia JR., F.C., and Macambira, E.M.B., 1999, O magmatismo arqueano da região de Tucumã-Provínica Mineral de Carajás: Novos dados geocronológicos: Revista Brasileira de Geociências, v. 29, p. 453-460.

Barros, C.E.M., Sardinha, A.S., Barbosa, J.P.O., Krimski, R., and Macambira, M.J.B., 2001, Pb–Pb and U–Pb zircon ages of Archean syntectonic granites of the Carajás metallogenic province, northern Brazil: in South American Symposium on Isotopic Geology, 3, Proceedings, p. 94-97.

Barros, C.E.M., Barbey, P., and Boullier, A.M., 2001, Role of magma pressure, tectonic stress and crystallization progress in the emplacement of syntectonic granites. The A-type Estrela Granite Complex (Carajás mineral province, Brazil): Tectonophysics, v. 343, p. 93-109.

Carvalho, E.R., Xavier, R.P., Monteiro, L.V.S., and Souza Filho, C.R., 2005, Geology and hydrothermal alteration of the Sossego iron oxide-copper-gold deposit, Carajás Mineral Province, Brazil: in I Simpósio Brasileiro Metalogenia: 1, 1, ISBN: CD-ROM.

Costa, J.B.S., Araújo, O.J.B., Santos, A., João, X.S.J., Macambira, M.J.B. and Lafon, J.M., 1995, A Província Mineral de Carajás: aspectos tectono estruturais, estratigráficos e geocronológicos: Boletim do Museu Paraense Emílio Goeldi, Série Ciências da Terra, v. 7. p. 199-235.

CVRD-Companhia Vale do Rio Doce, 2006, Relatório de pesquisa do alvo GT-34: Relatório Interno-CVRD, Carajás-PA (inédito), 154 p.

Dall'Ágnol, R., Souza, Z.S., Althoff, F.J., Barros, C.E.M., Leite, A.A.S., and João, X.S.J., 1997, General aspects of the granitogenesis of the Carajás metallogenetic province: in Proceedings of the International Symposium on Granites and Associated Mineralizations, Salvador, Excursion Guide, p. 135-161.

Dardenne, M.A., Ferreira Filho, C.F., and Meirelles, M.R., 1988, The role of shoshonitic and calc-alkaline suites in the tectonic evolution of the Carajás District, Brazil: Journal of South American Earth Science, v. 1, p. 363-372.

Deer, W.A., Howie, R.A. and Zussman, J., 1992, An introduction to the rock-forming minerals: Longman Longman, London. 2nd ed., Essex., 696 p.

Dias, G.S., Macambira, M.J.B., Dall'Agnol, R., Soares, A.D.V., and Barros, C.E.M., 1996, Datação de zircões de Sill de metagabro: Comprovação da idade arqueana da Formação Águas Claras, Carajás, Pará: Simpósio de Geologia da Amazônia, V, Belém, Sociedade Brasileira de Geologia, Extended Abstracts Bulletin, p. 376-379.

Docegeo, 1988, Revisão litoestratigráfica da Província Mineral de Carajás, in SBG, 35° Congresso Brasileiro de Geologia, Belém, PA, Anexo dos Anais, Província Mineral de Carajás-Litoestratigrafia e principais depósitos minerais, p. 11–54.

Dreher, A.M., Xavier, R.P., Taylor, B.E., and Martini, S. L., 2008, New geologic, fluid inclusion and stable isotope studies on the controversial Igarapé Bahia Cu–Au deposit, Carajás Province, Brazil: Mineralium Deposita v. 43, p. 161-184.

Faraco, M.T.L., Carvalho, J.M.A., Klein, E.L., 1996, Carta metalogenética da Província Carajás-SE do Estado do Pará, Folha Araguaia (SB–22): Nota explicativa, Belém, CPRM.

Ferreira Filho, C.F., Cançado, F., Correa, C., Macambira, E.M.B., Siepierski, L., and Brod, T.C.J., 2007, Mineralizações estratiformes de EGP-Ni associadas a complexos acamadados em Carajás: os exemplos de Luanga e Serra da Onça: in Contribuições à Geologia da Amazônia, Sociedade Brasileira de Geologia - Núcleo Norte, v. 5, p. 01-14.

Figueiredo e Silva, R.C., Lobato, L.M., Rosière, C.A., Zucchetti, M., Hagemann, S.H., Baars, F.J., Morais, R., and Andrade, I., 2008, A hydrothermal origin for the jaspilite-hosted, giant iron ore of the Serra Norte deposits in the Carajás Province, Pará State, Brazil, in Hagemann, S.G., Rosière, C.A., Gutzmer, J., and Beukes, N.J., eds., BIF-related high-grade iron mineralization: Reviews in Economic Geology, v. 15, in press.

Gibbs, A.K., Wirth, K.R., Hirata, W.K., and Olszewski Jr., W.J., 1986, Age and composition of the Grão Pará Group volcanics, Serra dos Carajás: Revista Brasileira de Geociências, v. 16, p. 201-211.

Grainger, C.J., Groves, D.I., Tallarico, F.H.B., and Fletcher, I.R., In Press, Metallogenesis of the Carajás Mineral Province, Southern Amazon Craton, Brazil: Varying styles of Archean through Paleoproterozoic to Neoproterozoic base- and precious-metal mineralization: Ore Geology Reviews, 39 p., Available online 12 March 2007.

Hirata, W.K., Rigon, J.C., Kadekaru, K., Cordeiro, A.A.C., Meireles, E.A., 1982, Geologia Regional da Província Mineral de Carajás: in Simpósio Geologia da Amazônia, 1, Belém, Anais Belém, SBG/NO, v. 1, p. 100-110.

Hitzman, M.W., Oreskes, N., and Einaudi, M.T., 1992, Geological characteristics and tectonic setting of Proterozoic iron oxide (Cu-U-Au-REE) deposits: Precambrian Research, v. 58, p. 241-287.

Hitzman, M.W., 2000, Iron oxide-Cu-Au deposits: What, where, when, and why: in Porter,

T.M. ed., Hydrothermal iron oxide-copper-gold and related deposits: A global perspective: Adelaide, Australia, Australian Mineral Foundation, p. 9-25.

Holdsworth, R.E., and Pinheiro, R.V.L., 2000, The anatomy of shallow-crustal transpressional structures: insights from the Archean Carajás fault zone, Amazon, Brazil: Journal Structural Geology, v. 22, p. 1105-1123.

Holland, H.D., 1959, Some applications of thermodynamic data to poblems of ore deposits. I. Stability relations among the oxides, sulfides, sulfates and carbonates of ore and gangue minerals: Economic Geology, v. 54, p. 184-233.

Huhn, S.R.B., Santos, A.B.S., Amaral, A.F., Ledsham, E.J., Gouveia, J.L., Martins, L.P.B., Montalvão, R.M.G., and Costa, V.C., 1988, O terreno granito-greenstone da região de Rio Maria-Sul do Pará: in Congresso Brasileiro de Geologia, 35, Anais, Sociedade Brasileira de Geologia, v. 3, p. 1438-1452.

Huhn, S.R.B., Macambira, M.J.B., and Dall'Agnol, R., 1999, Geologia e Geocronologia Pb/Pb do Granito Alcalino Arqueano Planalto, Região da Serra do Rabo, Carajás-PA: in Simpósio de Geologia da Amazônia, 6. Manaus, Anais, Sociedade Brasileira de Geologia - Núcleo Norte, v. 1, p. 463-466.

Huhn, S.R.B., Soares, A.D.V., Souza, C.I.J., Albuquerque, M.A.C., Leal, E.D., Vieira, E.A.P., Masotti, F.S., Brustolin, V., 2000, The Cristalino copper–gold deposit, Serra dos Carajás, Pará: in 31th International Geological Congress, Rio de Janeiro, Brazil, Extended Abstracts, CD-ROM.

Hunter, R.H., 1996, Texture development in cumulate rocks: in Developments in Petrology 15 (Layered Intrusions), R. G. Cawthorn (editor). Elsevier, p. 77-101.

Leake, B.E., Woolley, A.R., Arps, C.E.S., Birch, W.D., Gilbert, M.C., Grice, J.D., Hawthorne, F.C., Kato, A., Kisch, H.J., Krivovichev, V.G., Linthout, K., Laird, J., Mandarino, J.A., Maresch, W.V., Nickel, E.H., Rock, N.M.S., Schumacher, J.C., Smith, D.C., Stephenson, N.C.N., Ungaretti, L., Whittaker, E.J.W., and YOUZHI, G., 1997, Nomenclature of amphiboles: Report of the Subcommittee on Amphiboles of the International Mineralogical Association, Commission on New Minerals and Minerals Names: The Canadian Mineralogist, v. 35, p. 219-246.

Leveille, R.A., and Marschik, R., 2000, Iron oxide copper-gold deposits in South América: in 31th International Geological Congress, Rio de Janeiro, Brazil, Extended Abstracts, CD-ROM.

Lindenmayer, Z.G., 1990, Salobo Sequence, Carajás, Brazil: Geology, Geochemistry and Metamorphism: Unpublished Ph.D. thesis, University of Western Ontario, Canadá, 407 p.

Lobato, L.M., Figueiredo e Silva, R.C., Rosière, C.A., Zucchetti, M., Baars, F.J., Seoane, J.C.S., Rios, F.J. and Monteiro, A.M., 2005, Hydrothermal origin for the iron mineralisation, Carajás province, Pará State, Brazil: in Proceedings Iron Ore 2005. The Australian Institute of Mining and Metallurgy, Publication Series No 8, p. 99-110.

Lobato, L.M., Rosière, C.A., Figueiredo e Silva, R.C., Zucchetti, M., Baars, F.J., Seoane, J.C.S., Rios, F.J., Pimentel, M.M., Mendes, G., e Monteiro, A.M., 2005b, A mineralização hidrotermal de ferro da Província Mineral de Carajás, controle estrutural e contexto na

evolução metalogenética da província: in O J Marini; E T de Queiroz; B W Ramos. (Org.). Caracterização de depósitos minerais em distritos mineiros da Amazônia. 1 ed. Brasília, DNPM/FINEP/ADIMB, v. 1, p. 21-92.

Macambira, E.M.B. and Vale, A.G., 1997, Programa de Levantamentos Geológicos Básicos do Brasil, Programa Grande Carajás: Folha SB-22-Y-B, São Félix do Xingu, Estado do Para: Convenio DNPM/CPRM, 344 p.

Macambira, M.J.B., and Lancelot, J.R., 1996, Time constraints for the formation of the Archean Rio Maria crust, Southeastern Amazonian Craton, Brazil: International Geology Review, v. 38, p. 1134-1142.

Macambira, E.M.B. and Ferreira Filho, C.F., 2002, Fracionamento magmático dos corpos máfico-ultramáficos da Suíte Intrusiva Cateté, Sul do Pará: implicações geotectônicas e metalogenéticas: in Simpósio de Geologia da Amazônia, 7, Belém, Anais, Sociedade Brasileira de Geologia - Núcleo Norte, v. 3, p. 105-114.

Machado, W., Lindenmayer, Z.G., Krogh, T.E., and Lindenmayer, D., 1991, U-Pb geochronology of Archean magmatism and basement reactivation in the Carajás área, Amazon shield, Brazil: Precambrian Research, v. 49, p. 329-354.

Mark, G. and Crookes, R.A., 1999, Epigenetic alteration at the Ernest Henry Fe-oxide-(Cu-Au) deposit Australia: in Stanley et al. eds., Proceedings of the Fifth biennial SGA meeting and the Tenth Quadrennial IAGOD Symposium: Mineral deposits: processes to processing, v. 5, p. 185-188.

Marschik, R., Leveille, R.A., and Martin, W., 2000, La Candelaria and the Punta del Cobre district, Chile: early Cretaceous iron-oxide Cu–Au(–Zn–Ag) mineralization: in Porter, T.M. ed., Hydrothermal iron oxide copper-gold and related deposits: A global perspective: Adelaide, Australia, Australian Mineral Foundation, p. 163-176.

Marschik R., Spangenberg J.E., Leveille R.A., and de Almeida A.J., 2003, The Sossego iron oxide Cu-Au deposit, Carajas, Brazil: in Mineral Exploration and Sustainable Development, Eliopolous et al. (eds), p. 331-334.

Meireles, E.M., Hirata, W.K., Amaral, A.F., Medeiros Filho, C.A., Gato, W.C., 1984, Geologia das Folhas Carajás e Rio Verde, Província Mineral de Carajás, Estado do Pará: in SBG, Congresso Brasrasileiro de Geologia, 34, Rio de Janeiro, Anais, v. 5, p. 2163-2174.

Monteiro, L.V.S., Xavier, R.P., Johnson, C.A., Hitzman, M.W., Carvalho, E.R., and Souza Filho, C.R., 2005, The Sossego iron oxide-copper-gold deposit, Carajás Mineral Province, Brazil: stable isotope constraints on the genesis and hydrothermal system evolution: in I Simpósio Brasileiro Metalogenia: 1, 1, ISBN: CD-ROM.

Monteiro, L.V.S., Xavier, R.P., Carvalho, E.R., Hitzman, M.W., Johnson, C.A., Souza Filho, C.R., and Torresi, I., 2008, Spatial and temporal zoning of hydrothermal alteration and mineralization in the Sossego iron oxide–copper–gold deposit, Carajás Mineral Province, Brazil: paragenesis and stable isotope constraints: Mineralium Deposita v. 43, p. 129-159.

Nogueira, A.C.R., Truckenbrod, W., Costa, J.B.S., and Pinheiro, R.V.L., 1994, Análise faciológica e estrutural da Formação Águas Claras, Pré-Cambriano da Serra dos Carajás [ext. abs.]: Simpósio de Geologia da Amazônia, 4, Belém, Sociedade Brasileira de

Geologia, Resumos Expandidos, p. 363-364.

Nogueira, A.C.R., Truckenbrod, W., and Pinheiro, R.V.L., 2000, Storm and tide-dominated siliciclastic deposits of the Archean Águas Claras Formation, Serra dos Carajás, Brazil: in 31th International Geological Congress, Rio de Janeiro, Brazil, Extended Abstracts, CD-ROM.

Olszewski, W.J., Wirth, K.R., Gibbs, A.K., and Gaudette, H.E., 1989, The age, origin, and tectonics of the Grão Pará Group and associated rocks, Serra dos Carajás, Brazil: Archean continental vulcanism and rifting: Precambrian Research, v. 42, p. 229-254.

Oreskes, N., and Einaudi, M.T., 1992, Origin of hydrothermal fluids at Olympic Dam: preliminary results from fluid inclusions and stable isotopes: Economic Geology, v. 87, p. 64-90.

Pidgeon, R.T., Macambira, M.J.B., and Lafon, J.M., 2000, Th-U-Pb isotopic systems and internal structures of complex zircons from na enderbite from the Pium Complex, Carajás Province, Brazil: evidence for the ages of granulite facies metamorphism and the protolith of the enderbite: Chemical Geology, v. 166, p. 159-171.

Pinheiro, R.V.L., and Holdsworth, R.E., 1995, Significado tectônico da clivagem transversa (transecting cleavage) em dobras na Mina de Serra Pelada, Pará: Boletim do Museu Paraense Emílio Goeldi, Série Ciências da Terra, v. 7, p. 259-278.

Pinheiro, R.V.L., and Holdsworth, R.E., 1997, Reactivation of Archaean strike-slip fault systems, Amazon region, Brazil: Journal of the Geological Society, London, v. 154, p. 99-103.

Pinheiro, R.V.L., and Holdsworth, R.E., 2000, Evolução Tectonoestratigráfica dos Sistemas Transcorrentes Carajás e Cinzento, Cinturão Itacaiúnas, na borda leste do Cráton Amazônico, Pará: Revista Brasileira de Geociências, v. 30, p. 597-606.

Pollard, P.J., 2000, Evidence of a magmatic fluid and metal source for Fe-Oxide Cu-Au mineralization: in Porter, T.M. ed., Hydrothermal iron oxidecopper-gold and related deposits: A global perspective: Adelaide, Australia, Australian Mineral Foundation, p. 27-42.

Requia, K., and Fontboté, L., 1999, Hydrothermal alkali metasomatism in the Salobo iron oxide Cu (-Au) deposit, Carajás Mineral Province, northern Brazil: in C.J. Stanley et al. eds., Mineral deposits: processes to processing, Balkema, Amsterdam, p. 1025-1028.

Requia, K., and Fontboté, L., 2000, The Salobo iron oxide copper-gold deposit, Carajás, northern Brazil: in Porter, T.M. ed., Hydrothermal iron oxide-copper-gold and related deposits: A global perspective: Adelaide, Australia, Australian Mineral Foundation, p. 225-236.

Requia, K., Stein, H., Fontboté, L., and Chiaradia, M., 2003, Re-Os and Pb-Pb geochronology of the Archean Salobo iron oxide copper-gold deposit, Carajás mineral province, northern Brazil: Mineralium Deposita, v. 38, p. 727-738.

Ronze, P.C., Soares, A.D.V., dos Santos D.G.V., and Barreira C.F., 2000, Alemão copper-gold (U-REE) deposit, Carajás, Brazil: in Porter, T.M. ed., Hydrothermal iron oxide-copper-

gold and related deposits: A global perspective: Adelaide, Australia, Australian Mineral Foundation, p. 191-202.

Santos, J.O.S., Groves, D.I., Hartmann, L.A., Moura, M.A., and Mc-Naughton, N.J., 2001, Gold deposits of the Tapajós and Alta Floresta domains, Tapajós-Parima orogenic belt, Amazon craton, Brazil: Mineralium Deposita, v. 36, p. 278–299.

Sillitoe, R.H., 2003, Iron oxide-copper-gold deposits: an Andean view: Mineralium Deposita, v. 38, p. 787-812.

Souza, S.R.B., Macambira, M.J.B., and Sheller, T., 1996, Novos dados geocronológicos para os granitos deformados do Rio Itacaiúnas (Serra dos Carajás, PA), implicações estratigráficas: in Simpósio de Geologia da Amazônia, 5, Belém, Anais, Sociedade Brasileira de Geologia, p. 380-383.

Souza, L.J., and Vieira, E.A., 2000, Salobo 3 Alpha deposit: geology and mineralization: in Porter, T.M. ed., Hydrothermal iron oxide-copper-gold and related deposits: A global perspective: Adelaide, Australia, Australian Mineral Foundation, p. 213–224.

Soares, A.D.V., Santos, A.B., Vieira, E.A., Bella, V.M., and Martins, L.P.B., 1994, Área Águas Claras: Contexto geológico e mineralizações: Simpósio de Geologia da Amazônia, 4, Belém, Anais, Sociedade Brasileira de Geologia, p. 379–382.

Sparks, R.S.J., Huppert, H.E., Kerr, R.C., McKeinzie, D.P., and Tait, S.R., 1985, Post-cumulus processes in layered intrusions: Geological Magazine, v. 122, p. 555-568.

Spier, S.F., 1993, Metamorphic Phase Equilibria and Pressure-Temperature-Time Path: Mineralogical Society of America, Monograph Series, Washington, 799 p.

Sun, S.S. and McDonough, W.F., 1989, Chemical and isotopic systematics of oceanic basalts: implications for mantle composition and processes: in Saunders, A. D., Norry, M.J. (eds), Magmatism in Ocean Basins. Geol. Soc. London Spec. Publ. v. 42. p. 313-345.

Tallarico, F.H.B., Figueiredo, B.R., Groves, D.I., Kositcin, N., McNaughton, J., Fletcher, I.R., and Rego, J.L., 2005, Geology and SHRIMP U-Pb geochronology of the Igarapé Bahia deposit, Carajás copper-gold belt, Brazil: An Archean (2.57 Ga) example of iron-oxide Cu-Au mineralization: Economic Geology, v. 100, p. 7–28.

Tazava, E., and de Oliveira, C.G., 2000, The Igarape Bahia Au-Cu-(REE-U) deposit, Carajás mineral province, northern Brazil: in Porter, T.M. ed., Hydrothermal iron oxide-copper-gold and related deposits: A global perspective: Adelaide, Australia, Australian Mineral Foundation, p. 203–212.

Teixeira, J.B.G., and Eggler, D.H., 1994, Petrology, Geochemistry, and Tectonic Setting of Archaean Basaltic and Dioritic Rocks from the N4 Iron Deposit, Serra dos Carajás, Pará, Brazil: Acta Geologica Leopoldensia, v. 17, p. 71-114.

Trendall, A.F., Basei, M.A.S., De Laeter, J.R., and Nelson, D.R., 1998, SHRIMP zircon U-Pb constraints on the age of the Carajás Formation, Grão Pará Group, Amazon Craton: Journal of South American Earth Sciences, v. 11, p. 265-277.

Villas, R.N., and Santos, M.D., 2001, Gold deposits of the Carajás mineral province: Deposit types and metallogenesis: Mineralium Deposita, v. 36, p. 300-331.

Zucchetti, M., 2007, Rochas máficas do Grupo Grão Pará e sua relação com a mineralização de ferro dos depósitos N4 e N5, Carajás, PA: Tese de Doutorado, Belo Horizonte, Instituto de Geociências,UFMG, 116 p.

Zucchetti, M., Lobato, L.M., and Hagemann, S., 2007, Hydrothermal alteration of basalts that host the giant Northern Range Carajás iron deposits, Brazil: in C.J. Andrew et al. (eds.), Proceedings of 9th Biennial SGA Meeting, Dublin, p. 1231-1234.

CONCLUSÕES

Um sumário das principais conclusões obtidas no presente estudo sobre as feições peculiares do Prospecto GT-34 são apresentadas a seguir.

1- As rochas metassomáticas do GT-34 apresentam paragêneses enriquecidas em Mg e não contém óxidos de Fe (hematite e magnetite), sendo abundantes litotipos ricos em ortopiroxênio (ortopiroxenititos).

2- Apresenta pirrotita e pirita como paragênese sulfetada dominante.

3- O estilo de alteração metassomática do GT-34 é distintamente diferente daqueles presentes nos sistemas Cu-Au tipo IOCG observados na região de Carajás.

4- A interpretação dos dados obtidos sugere que as condições físicas e químicas presentes durante a alteração metassomática no GT-34 ocorreram em profundidade, a altas temperaturas e sob baixa fO_2.

5- O Prospecto GT-34 representaria parte de um sistema bem maior, considerado aqui como relacionado a zonas profundas do sistema mineralizante Cu-Au, de idade 2.5 Ga, marcadamente presente na região de Carajás.

Estudos recentes indicam que os mega depósitos de hematite maciça de Carajás estão relacionados a alteração hidrotermal derivada de intrusões Paleoproterozóicas (Lobato et al. 2005), desafiando a noção de que teriam sido formados exclusivamente a partir de sedimentos quimicos Arqueanos. A recente descoberta em Carajás de mineralizações de EGP hospedadas em gabronoritos, sem sulfetos imiscíveis e/ou cromititos associados (Ferreira Filho et al. 2007), também contrapõem-se ao conceito mundialmente aceito sobre a origem dos depósitos de EGP. Portanto, as características apresentadas no presente estudo sobre o GT-34 podem trazer novas perspectivas, contribuindo para ampliar o conhecimento sobre a origem dos depósitos tipo IOCG.

ANEXOS

Tabela 1A – Resultados Analíticos de Microssonda em Ortopiroxênios

Tabela 2A – Resultados Analíticos de Microssonda em Anfibólios

Tabela 3A – Resultados Analíticos de Microssonda em Flogopitas

Tabela 4A – Resultados Analíticos de Microssonda em Apatitas

Tabela 1A – Resultados Analíticos de Microssonda em Ortopiroxênios

	LSK29 OPXLG 1.1	LSK29 OPXLG 1.2	LSK29 OPXLG 1.3	LSK29 OPXLG 1.4	LSK29 OPXLG 2.1	LSK29 OPXLG 2.2	LSK29 OPXLG 2.3	LSK29 OPXLG 3.1	LSK29 OPXLG 3.2	LSK29 OPXLG 1.5	LSK30 OPXLG 1.1	LSK30 OPXLG 1.2	LSK30 OPXLG 1.3	LSK30 OPXLG 1.4	LSK30 OPXSM 2.1	LSK30 OPXSM 2.3	LSK32 OPXSM 1.1	LSK32 OPXSM 1.2	LSK32 OPXLG 1.1	LSK32 OPXLG 1.2	LSK32 OPXLG 1.3	LSK32 OPXLG 1.4
SiO2	53.81	54.37	55.08	55.51	53.69	53.92	54.32	53.33	53.48	54.77	53.51	53.89	54.01	53.88	53.29	53.04	52.08	52.15	53.41	54.11	53.34	54.81
TiO2	0.00	0.02	0.03	0.00	0.02	0.00	0.01	0.01	0.00	0.02	0.07	0.05	0.01	0.02	0.04	0.00	0.04	0.04	0.00	0.00	0.02	0.04
Al2O3	0.97	0.37	0.34	0.32	0.51	0.24	0.31	0.49	0.66	0.50	0.47	0.47	0.42	0.39	0.47	0.37	0.71	0.65	0.55	0.60	0.53	0.59
Cr2O3	0.00	0.00	0.01	0.03	0.01	0.00	0.00	0.00	0.00	0.00	0.00	0.00	0.00	0.02	0.03	0.00	0.02	0.00	0.00	0.02	0.02	0.00
FeOT	17.91	16.32	15.68	15.71	18.99	18.42	18.52	17.92	18.37	15.86	19.68	19.34	19.79	19.73	19.26	20.09	17.56	17.72	16.85	16.70	17.63	16.36
MnO	0.13	0.10	0.17	0.20	0.22	0.17	0.22	0.29	0.19	0.20	0.24	0.27	0.35	0.20	0.20	0.23	0.24	0.21	0.16	0.21	0.25	0.16
MgO	26.55	27.36	28.74	28.68	25.67	26.28	26.30	25.66	26.00	27.83	25.29	24.98	25.10	24.99	25.32	24.74	25.57	25.42	26.53	27.00	26.89	28.14
NiO	0.08	0.10	0.04	0.10	0.08	0.11	0.18	0.03	0.14	0.09	0.11	0.14	0.05	0.08	0.11	0.09	0.08	0.00	0.01	0.03	0.05	0.08
CaO	0.22	0.19	0.17	0.17	0.22	0.32	0.26	0.16	0.24	0.20	0.24	0.24	0.30	0.22	0.32	0.18	0.14	0.15	0.09	0.13	0.13	0.12
Na2O	0.09	0.04	0.00	0.00	0.00	0.00	0.01	0.00	0.00	0.00	0.00	0.00	0.00	0.00	0.00	0.00	0.00	0.05	0.00	0.00	0.00	0.05
K2O	0.00	0.02	0.00	0.00	0.01	0.01	0.00	0.01	0.00	0.00	0.01	0.01	0.01	0.00	0.00	0.01	0.00	0.00	0.01	0.01	0.01	0.02
TOTAL	99.76	98.89	100.26	100.71	99.44	99.46	100.13	97.91	99.06	99.47	99.61	99.37	100.04	99.54	99.03	98.76	96.45	96.40	97.61	98.82	98.87	100.36
Cations on basis of 6 oxygens																						
Si	1.96	1.99	1.98	1.98	1.98	1.98	1.98	1.98	1.97	1.98	1.97	1.99	1.98	1.99	1.97	1.98	1.97	1.97	1.98	1.98	1.96	1.97
Al	0.04	0.02	0.01	0.01	0.02	0.01	0.01	0.02	0.03	0.02	0.02	0.02	0.02	0.02	0.02	0.02	0.03	0.03	0.02	0.03	0.02	0.03
Ti	0.00	0.00	0.00	0.00	0.00	0.00	0.00	0.00	0.00	0.00	0.00	0.00	0.00	0.00	0.00	0.00	0.00	0.00	0.00	0.00	0.00	0.00
Cr	0.00	0.00	0.00	0.00	0.00	0.00	0.00	0.00	0.00	0.00	0.00	0.00	0.00	0.00	0.00	0.00	0.00	0.00	0.00	0.00	0.00	0.00
Fe	0.55	0.50	0.47	0.47	0.58	0.57	0.56	0.56	0.57	0.48	0.61	0.60	0.61	0.61	0.60	0.63	0.56	0.56	0.52	0.51	0.54	0.49
Mn	0.00	0.00	0.01	0.01	0.01	0.01	0.01	0.01	0.01	0.01	0.01	0.01	0.01	0.01	0.01	0.01	0.01	0.01	0.00	0.01	0.01	0.00
Mg	1.44	1.49	1.54	1.53	1.41	1.44	1.43	1.42	1.43	1.50	1.39	1.37	1.37	1.37	1.40	1.38	1.44	1.43	1.47	1.47	1.48	1.51
Ni	0.00	0.00	0.00	0.00	0.00	0.00	0.01	0.00	0.00	0.00	0.00	0.00	0.00	0.00	0.00	0.00	0.00	0.00	0.00	0.00	0.00	0.00
Ca	0.01	0.01	0.01	0.01	0.01	0.01	0.01	0.01	0.01	0.01	0.01	0.01	0.01	0.01	0.01	0.01	0.01	0.01	0.00	0.01	0.00	0.00
Na	0.01	0.00	0.00	0.00	0.00	0.00	0.00	0.00	0.00	0.00	0.00	0.00	0.00	0.00	0.00	0.00	0.00	0.00	0.00	0.00	0.00	0.00
K	0.00	0.00	0.00	0.00	0.00	0.00	0.00	0.00	0.00	0.00	0.00	0.00	0.00	0.00	0.00	0.00	0.00	0.00	0.00	0.00	0.00	0.00
Si+Al	2.01	2.00	1.99	2.00	2.00	1.99	1.99	2.01	2.00	2.01	1.99	2.01	2.00	2.00	1.99	1.99	2.00	2.00	2.01	2.01	1.99	2.00
M1M2	2.01	2.01	2.02	2.01	2.01	2.03	2.02	2.00	2.01	2.00	2.02	1.99	2.01	2.00	2.02	2.02	2.01	2.01	2.00	2.00	2.04	2.02
En	72.08	74.54	76.14	76.02	70.12	71.15	71.09	71.29	71.08	75.25	69.03	69.10	68.56	68.79	69.44	68.22	71.72	71.43	73.42	73.81	72.66	75.05
Fs	27.48	25.09	23.54	23.66	29.45	28.23	28.42	28.39	28.46	24.36	30.50	30.43	30.85	30.77	29.93	31.42	28.00	28.28	26.41	25.94	27.10	24.73
Wo	0.44	0.37	0.32	0.32	0.43	0.62	0.50	0.32	0.47	0.39	0.47	0.47	0.58	0.44	0.63	0.36	0.28	0.30	0.17	0.26	0.24	0.22

Tabela 1A – Resultados Analíticos de Microssonda em Ortopiroxênios (continuação).

	LSK32 OPXSM 2.1	LSK32 OPXSM 2.2	LSK32 OPXSM 3.2	LSK32 OPXLG 2.2	LSK32 OPXLG 2.2	LSK32 OPXSM 3.1	LSK32 OPXSM 3.2	LSK32 OPXSM 4.1	FD07 OPXLG 1.1	FD07 OPXLG 1.2	FD07 OPXLG 1.3	FD07 OPXLG 1.4	FD07 OPXSM 2.1	FD07 OPXSM 2.2	FD07 OPXSM 3.1	FD07 OPXSM 3.2	FD07 OPXLG 2.1	FD07 OPXLG 2.2	FD01 OPXLG 1.1	FD01 OPXLG 1.2	FD01 OPXLG 2.1	FD01 OPXLG 2.2	FD01 OPXLG 2.3
SiO2	53.88	54.15	54.10	54.16	54.16	53.49	53.87	53.59	54.07	54.48	54.27	54.77	53.52	53.83	53.58	53.11	54.30	53.65	53.17	53.54	54.15	53.51	54.04
TiO2	0.01	0.03	0.03	0.04	0.01	0.03	0.02	0.01	0.01	0.03	0.00	0.04	0.01	0.02	0.04	0.00	0.05	0.04	0.04	0.04	0.03	0.00	0.04
Al2O3	0.65	0.69	0.71	0.58	0.70	0.49	0.49	0.66	0.47	0.48	1.12	0.57	0.72	0.72	0.64	0.47	0.74	0.76	0.93	0.87	0.63	0.57	0.77
Cr2O3	0.01	0.00	0.02	0.00	0.01	0.01	0.01	0.01	0.00	0.00	0.00	0.02	0.00	0.00	0.00	0.00	0.00	0.03	0.00	0.00	0.00	0.02	0.02
FeOT	17.47	17.59	17.87	16.93	16.87	17.90	17.96	18.72	15.92	15.42	16.03	16.88	18.71	18.16	19.11	18.96	17.05	17.22	18.10	17.91	18.00	17.63	18.38
MnO	0.19	0.19	0.25	0.23	0.24	0.27	0.20	0.28	0.17	0.19	0.20	0.17	0.20	0.21	0.21	0.22	0.27	0.17	0.31	0.20	0.21	0.21	0.24
MgO	26.47	26.56	26.08	27.17	26.75	26.42	26.77	25.99	27.65	28.23	27.62	27.81	25.78	26.14	25.84	25.09	26.87	26.82	26.26	26.05	26.67	26.02	26.50
NiO	0.02	0.01	0.09	0.06	0.03	0.08	0.12	0.11	0.00	0.06	0.07	0.07	0.05	0.02	0.07	0.12	0.11	0.08	0.13	0.08	0.11	0.12	0.10
CaO	0.14	0.16	0.24	0.12	0.11	0.21	0.19	0.22	0.20	0.21	0.18	0.10	0.23	0.22	0.13	0.15	0.18	0.21	0.26	0.23	0.22	0.20	0.16
Na2O	0.00	0.00	0.00	0.00	0.01	0.00	0.00	0.00	0.02	0.00	0.01	0.00	0.00	0.00	0.10	0.04	0.01	0.00	0.00	0.00	0.04	0.08	0.00
K2O	0.00	0.02	0.00	0.00	0.02	0.02	0.01	0.00	0.01	0.02	0.00	0.02	0.00	0.00	0.00	0.00	0.01	0.00	0.01	0.00	0.02	0.00	0.00
TOTAL	98.85	99.38	99.39	99.30	98.90	98.92	99.64	99.59	98.50	99.10	99.49	100.44	99.22	99.32	99.70	98.16	99.60	98.98	99.21	98.92	100.06	98.36	100.25
Cations on basis of 6 oxygens																							
Si	1.98	1.98	1.98	1.98	1.98	1.97	1.97	1.97	1.98	1.98	1.97	1.97	1.97	1.97	1.97	1.98	1.98	1.97	1.96	1.97	1.97	1.98	1.97
Al	0.03	0.03	0.03	0.02	0.03	0.02	0.02	0.03	0.02	0.02	0.05	0.02	0.03	0.03	0.03	0.02	0.03	0.03	0.04	0.04	0.03	0.02	0.03
Ti	0.00	0.00	0.00	0.00	0.00	0.00	0.00	0.00	0.00	0.00	0.00	0.00	0.00	0.00	0.00	0.00	0.00	0.00	0.00	0.00	0.00	0.00	0.00
Cr	0.00	0.00	0.00	0.00	0.00	0.00	0.00	0.00	0.00	0.00	0.00	0.00	0.00	0.00	0.00	0.00	0.00	0.00	0.00	0.00	0.00	0.00	0.00
Fe	0.54	0.54	0.55	0.52	0.52	0.55	0.55	0.58	0.49	0.47	0.49	0.51	0.58	0.56	0.59	0.59	0.52	0.53	0.56	0.55	0.55	0.55	0.56
Mn	0.01	0.01	0.01	0.01	0.01	0.01	0.01	0.01	0.01	0.01	0.01	0.01	0.01	0.01	0.01	0.01	0.01	0.01	0.01	0.01	0.01	0.01	0.01
Mg	1.45	1.45	1.42	1.48	1.46	1.45	1.46	1.42	1.51	1.53	1.49	1.49	1.42	1.43	1.42	1.40	1.46	1.47	1.44	1.43	1.45	1.44	1.44
Ni	0.00	0.00	0.00	0.00	0.00	0.00	0.00	0.00	0.00	0.00	0.00	0.00	0.00	0.00	0.00	0.00	0.00	0.00	0.00	0.00	0.00	0.00	0.00
Ca	0.01	0.01	0.01	0.00	0.00	0.01	0.01	0.01	0.01	0.01	0.01	0.00	0.01	0.01	0.01	0.01	0.01	0.01	0.01	0.01	0.01	0.01	0.01
Na	0.00	0.00	0.00	0.00	0.00	0.00	0.00	0.00	0.00	0.00	0.00	0.00	0.00	0.00	0.01	0.00	0.00	0.00	0.00	0.00	0.00	0.01	0.00
K	0.00	0.00	0.00	0.00	0.00	0.00	0.00	0.00	0.00	0.00	0.00	0.00	0.00	0.00	0.00	0.00	0.00	0.00	0.00	0.00	0.00	0.00	0.00
Si+Al	2.01	2.01	2.01	2.00	2.01	1.99	1.99	2.00	2.00	2.00	2.01	2.00	2.00	2.01	2.00	2.00	2.01	2.00	2.00	2.01	2.00	2.00	2.00
M1M2	2.00	2.00	1.99	2.01	1.99	2.02	2.03	2.02	2.01	2.01	1.99	2.02	2.01	2.00	2.02	2.01	2.00	2.01	2.02	2.00	2.02	2.01	2.02
En	72.57	72.47	71.61	73.66	73.44	71.86	72.16	70.61	75.11	76.02	74.94	74.27	70.53	71.41	70.27	69.77	73.17	73.04	71.41	71.62	72.00	71.93	71.52
Fs	27.16	27.22	27.92	26.10	26.35	27.73	27.46	28.96	24.51	23.58	24.70	25.54	29.02	28.16	29.47	29.92	26.47	26.56	28.08	27.92	27.57	27.67	28.18
Wo	0.27	0.32	0.48	0.24	0.21	0.41	0.37	0.43	0.38	0.40	0.36	0.19	0.46	0.43	0.26	0.31	0.36	0.40	0.51	0.45	0.43	0.39	0.30

Tabela 2A – Resultados Analíticos de Microssonda em Anfibólios

	DDH1-239.15 F2-HORN1	DDH1-239.15 F2-HORN1.2	DDH1-239.15 F2-HORN2	DDH1-239.15 F1-HORN1	DDH1-239.15 F3-HORN1	DDH1-239.15 F3-HORN1.2	LSK28 F2-HORN1	LSK28 F3-HORN2
SiO2	39.13	40.22	38.26	36.69	38.05	38.90	44.84	44.39
TiO2	0.75	0.73	0.75	0.76	0.51	0.85	0.83	0.79
Al2O3	11.72	11.10	12.07	13.50	11.59	11.81	10.55	10.17
Cr2O3	0.43	0.34	0.40	0.44	0.40	0.48	0.00	0.01
FeO	19.20	18.82	20.87	20.35	20.87	19.00	11.91	12.41
MnO	0.01	0.06	0.05	0.10	0.00	0.04	0.11	0.01
MgO	8.53	8.35	7.42	6.07	6.58	7.79	14.42	13.91
CaO	11.07	11.21	11.11	11.06	10.94	11.00	11.17	11.35
Na2O	2.05	2.61	2.06	2.21	1.63	2.40	2.48	2.58
K2O	1.51	1.54	1.88	1.97	1.91	1.58	0.85	0.76
H2O	1.88	1.89	1.87	1.83	1.82	1.87	2.03	2.01
TOTAL	96.28	96.87	96.73	94.97	94.31	95.71	99.18	98.40
Cations basis of 24 oxygens								
Si	6.24	6.37	6.15	6.02	6.27	6.25	6.61	6.62
Al	2.20	2.07	2.29	2.61	2.25	2.24	1.83	1.79
Ti	0.09	0.09	0.09	0.09	0.06	0.10	0.09	0.09
Cr	0.05	0.04	0.05	0.06	0.05	0.06	0.00	0.00
Fe	2.56	2.49	2.81	2.79	2.87	2.55	1.47	1.55
Mn	0.00	0.01	0.01	0.01	0.00	0.01	0.01	0.00
Mg	2.03	1.97	1.78	1.48	1.62	1.86	3.17	3.09
Ca	1.89	1.90	1.91	1.94	1.93	1.89	1.76	1.81
Na	0.63	0.80	0.64	0.70	0.52	0.75	0.71	0.75
K	0.31	0.31	0.38	0.41	0.40	0.32	0.16	0.14
H	0.00	0.00	0.00	0.01	0.00	0.00	0.00	0.00
cations	16.01	16.05	16.11	16.13	15.98	16.04	15.81	15.84
Si+Al	8.44	8.44	8.44	8.62	8.52	8.49	8.44	8.41
Al+Mg+Ti+Fe+Mn+Cr	5.45	5.30	5.44	5.34	5.31	5.38	5.46	5.40
Na+K+Ca	2.83	3.01	2.94	3.06	2.85	2.97	2.63	2.71

Tabela 3A – Resultados Analíticos de Microssonda em Flogopitas

	LSK28 F1-PHLOG1	LSK28 F4-PHLOG2	LSK28 F4-PHLOG3
SiO2	39.54	38.57	39.88
TiO2	2.29	1.85	1.56
Al2O3	13.27	13.26	12.61
FeO	9.50	9.77	9.02
MnO	0.01	0.01	0.05
MgO	19.83	18.99	20.24
CaO	0.00	0.00	0.00
Na2O	0.07	0.56	0.36
K2O	9.59	9.74	9.86
BaO	0.09	0.05	0.08
SrO	0.00	0.00	0.00
Cl	0.91	1.03	0.97
H2O	3.83	3.71	3.79
TOTAL	98.92	97.54	98.42
Cations basis of 24 oxygens			
Si	5.84	5.82	5.93
Al	2.31	2.36	2.21
Ti	0.25	0.21	0.18
Fe	1.17	1.23	1.12
Mn	0.00	0.00	0.01
Mg	4.37	4.27	4.49
Ca	0.00	0.00	0.00
Na	0.02	0.16	0.11
K	1.81	1.88	1.87
Ba	0.01	0.00	0.01
Sr	0.00	0.00	0.00
Cl	-0.20	-0.23	-0.22
H	0.00	0.00	0.00
Cations	15.57	15.71	15.69
Si+Al	8.11	8.14	8.09
Ti+Fe2++Mn+Mg	6.63	6.45	6.37
Ca+Na+K+Ba	1.83	2.03	1.97
OH+Cl	3.98	3.98	3.98

Tabela 4A – Resultados Analíticos de Microssonda em Apatitas

	LSK28 F1-APAT 1	LSK28 F1-APAT 2	LSK28 F1-APAT 3	LSK28 F2-APAT 1.1-C	LSK28 F2-APAT 1.2-C	LSK28 F2-APAT 1.3-C	LSK28 F2-APAT 1.4-C	LSK28 F2-APAT 1.5-C	LSK28 F2-APAT 1.6-C	LSK28 APAT 1.7-C	LSK28 F2-APAT 1.8-C	LSK28 F2-APAT 1.9-C	LSK28 F2-APAT 1.10-C	LSK28 F2-APAT 1.11-C	LSK28 F2-APAT 1.12-C	LSK28 F2-APAT 5	LSK28 F3-APAT 6	LSK28 F4-APAT 7	LSK28 F5-APAT 8	LSK28 F5-APAT 9	LSK28 F5-APAT 10
SiO2	0.00	0.01	0.07	0.05	0.03	0.10	0.03	0.12	0.07	0.07	0.05	0.10	0.04	0.12	0.13	0.05	0.01	0.03	0.06	0.10	0.08
Al2O3	0.00	0.00	0.00	0.00	0.00	0.05	0.02	0.01	0.00	0.00	0.00	0.02	0.00	0.04	0.02	0.01	0.00	0.00	0.02	0.00	0.00
MgO	0.00	0.00	0.00	0.00	0.00	0.00	0.00	0.00	0.00	0.00	0.00	0.00	0.00	0.00	0.00	0.00	0.00	0.00	0.00	0.00	0.00
P2O5	42.02	42.08	41.99	42.17	42.80	41.13	42.18	41.33	41.91	42.16	41.57	42.21	41.54	42.42	41.62	42.30	42.89	41.75	40.27	41.91	41.71
CaO	53.53	51.88	53.13	52.60	53.74	52.85	53.06	53.08	53.21	53.23	52.80	52.75	52.10	52.05	52.71	54.29	54.67	53.91	52.65	52.05	53.80
FeO	0.05	0.00	0.12	0.30	0.11	0.05	0.08	0.06	0.06	0.00	0.06	0.05	0.02	0.12	0.05	0.05	0.10	0.10	0.07	0.05	0.03
Na2O	0.00	0.00	0.00	0.00	0.00	0.00	0.00	0.00	0.00	0.00	0.00	0.00	0.00	0.00	0.00	0.00	0.00	0.00	0.00	0.00	0.00
K2O	0.00	0.00	0.00	0.01	0.02	0.02	0.00	0.00	0.01	0.00	0.01	0.01	0.00	0.14	0.00	0.01	0.03	0.00	0.00	0.00	0.01
BaO	0.01	0.00	0.00	0.00	0.01	0.21	0.11	0.00	0.15	0.00	0.00	0.00	0.00	0.08	0.04	0.00	0.12	0.00	0.00	0.00	0.00
SrO	0.00	0.08	0.07	0.13	0.15	0.06	0.10	0.01	0.12	0.07	0.18	0.12	0.09	0.05	0.20	0.04	0.09	0.06	0.02	0.08	0.21
Cl	4.00	6.58	6.57	4.94	4.20	5.32	5.14	4.44	4.28	4.00	4.64	4.68	5.25	4.87	5.07	3.85	3.28	3.70	6.20	6.32	4.38
H2O	0.70	0.00	0.02	0.45	0.67	0.32	0.40	0.56	0.62	0.70	0.51	0.52	0.34	0.47	0.40	0.76	0.93	0.78	0.06	0.07	0.60
TOTAL	100.31	100.64	101.97	100.64	101.73	100.12	101.12	99.61	100.42	100.23	99.81	100.45	99.39	100.34	100.23	101.35	102.12	100.32	99.35	100.56	100.80
Cations basis of 26 oxygens																					
Si	0.00	0.00	0.01	0.01	0.01	0.02	0.01	0.02	0.01	0.01	0.01	0.02	0.01	0.02	0.02	0.01	0.00	0.01	0.01	0.02	0.01
Al	0.00	0.00	0.00	0.00	0.00	0.01	0.00	0.00	0.00	0.00	0.00	0.01	0.00	0.01	0.00	0.00	0.00	0.00	0.01	0.00	0.00
Fe	0.01	0.00	0.02	0.05	0.02	0.01	0.01	0.01	0.01	0.00	0.01	0.01	0.00	0.02	0.01	0.01	0.02	0.01	0.01	0.01	0.00
P	6.22	6.40	6.33	6.29	6.25	6.24	6.29	6.21	6.23	6.24	6.25	6.28	6.30	6.32	6.26	6.19	6.18	6.17	6.24	6.36	6.20
Mg	0.00	0.00	0.00	0.00	0.00	0.00	0.00	0.00	0.00	0.00	0.00	0.00	0.00	0.00	0.00	0.00	0.00	0.00	0.00	0.00	0.00
Ca	10.03	9.99	10.13	9.93	9.94	10.14	10.01	10.09	10.01	9.97	10.04	9.93	10.01	9.82	10.03	10.06	9.98	10.09	10.32	10.00	10.11
Na	0.00	0.00	0.00	0.00	0.00	0.00	0.00	0.00	0.00	0.00	0.00	0.00	0.00	0.00	0.00	0.00	0.00	0.00	0.00	0.00	0.00
K	0.00	0.00	0.00	0.00	0.00	0.01	0.00	0.00	0.00	0.00	0.00	0.00	0.00	0.03	0.00	0.00	0.01	0.00	0.00	0.00	0.00
Ba	0.00	0.00	0.00	0.00	0.00	0.02	0.01	0.00	0.01	0.00	0.00	0.00	0.00	0.01	0.00	0.00	0.01	0.00	0.00	0.00	0.00
Sr	0.00	0.01	0.01	0.01	0.02	0.01	0.01	0.00	0.01	0.01	0.02	0.01	0.01	0.01	0.02	0.00	0.01	0.01	0.00	0.01	0.02
Cl	-0.90	-1.49	-1.48	-1.12	-0.95	-1.20	-1.16	-1.00	-0.97	-0.90	-1.05	-1.06	-1.18	-1.10	-1.14	-0.87	-0.74	-0.83	-1.40	-1.43	-0.99
H	0.00	0.00	0.00	0.00	0.00	0.00	0.00	0.00	0.00	0.00	0.00	0.00	0.00	0.00	0.00	0.00	0.00	0.00	0.00	0.00	0.00
Cations	15.36	14.91	15.01	15.18	15.28	15.23	15.17	15.33	15.32	15.32	15.28	15.20	15.15	15.13	15.21	15.40	15.46	15.45	15.19	14.97	15.36